U.PORTO

FEUP FACULDADE DE ENGENHARIA
UNIVERSIDADE DO PORTO

Master Dissertation in Mechanical Engineering

NUMERICAL ANALYSIS OF AN ELECTRICAL URBAN MOTORCYCLE'S FRAME

Ana Sofia Bernardo Silva

Supervisor: Professor José Luís Soares Esteves
Second Supervisor: Professor Marco Paulo Lages Parente
Company Supervisor: Eng. Miguel Ângelo Nogueira da Costa Oliveira

Faculty of Engineering of University of Porto

October 31, 2022

"Progress is not a straight line."

Dr. An Wang

Resumo

Esta dissertação tem como objectivo o design e a análise numérica de um chassis de uma scooter, que pertence a um novo projeto no qual a AJP Motos está envolvida. Este projeto foca-se na criação de uma scooter citadina, de forma a entrar no mundo dos veiculos partilhados. Um dos pontos fulcrais para o desenvolvimento das várias soluções de frame apresentadas foi a estrutura exterior que a AJP forneceu. Através do corpo da scooter e dos componentes já definidos para o projeto, foram desenhadas várias soluções para o chassis da scooter. Algumas soluções foram desenvolvidas antes de informações cruciais para o projeto, tendo então perdido a validade.

Vários aspetos foram considerados durante o desenvolvimento das soluções, desde o armazenamento das baterias e do capacete à qual a forma de ligação mais correta e estruturalmente melhor para conectar o frame à coluna de direção. As soluções apresentadas nesta dissertação foram desenvolvidas no software SolidWorks.

De seguida, três soluções foram selecionadas para avançarem para uma análise numérica, utilizando o software Abaqus. Para as simulações foi necessário definir o material, as condições de fronteira do problema e as forças aplicadas. Para esta análise estática foi considerado um caso de estudo de um condutor de 75 kg e um passageiro de 50 kg.

Após análise dos resultados obtidos foi necessário efectuar várias modificações aos chassis em estudo, de forma a diminuir as tensões obtidas. Uma das soluções foi a utilização de reforços estruturias que têm como objetivo fornecer mais rigidez ao chassis. Várias iterações foram desenvolvidas para chegar aos reforços estruturais finais.

Relativamente ao software Abaqus foi possível constatar que, além da conversão entre SolidWorks e Abaqus apresentar vários problemas, o software é muito sensível aos detalhes do desenho.

Após análise dos resultados obtidos foram obtidos pontos positivos e negativos de cada solução, estando agora na mão da AJP de escolher o que melhor se adequa na visão da empresa para o projeto.

Palavras-chave: Design de produto, Análise estrutural, Chassis de motociclo, Scooter

Abstract

This dissertation aims to design and develop the numerical analysis of a scooter' chassis, that is a part of a new project in which AJP Motorcycle is involved. This project focuses on the production of a city scooter in order to enter the world of sharing vehicles. One of the key points for the development of the various frame solutions presented, was the exterior structure that AJP provided. Through the scooter' body and the components already defined for the project, several solutions were designed for the chassis. Some solutions were developed prior to crucial information for the project, and then lost their validity.

Several aspects had to be considered during the development of the solutions, from the storage of the batteries and the helmet to what was the most correct and structurally best way to connect the frame to the steering column. The solutions presented in this dissertation were developed in SolidWorks software.

Then, three solutions were selected to proceed to the numerical analysis using the Abaqus software. For the simulations it was necessary to define the material, the boundary conditions of the problem and the applied forces. For this static analysis a case study of a 75 kg driver and a 50 kg passenger was considered.

From the results obtained it was necessary to make some modifications to the chassis under study, in order to reduce the stresses obtained. One of the solutions was the use of structural reinforcements which aim to give more rigidity to the frame. Several iterations were developed to reach the final structural reinforcements.

Regarding the Abaqus software, it was possible to verify that besides the conversion between SolidWorks and Abaqus presenting several problems and requiring reworking, the software is very sensitive to design details.

After the analysis of the simulations results, positive and negative points of each solution were highlighted, leaving it up to AJP to choose the solution that best fits their vision for the project.

Keywords: Product design, Structural Analysis, Motorcycle Frame, Scooter

Acknowledgements

All the work presented in this dissertation resulted from several months of research, analysis and learning. It required a great effort of time organisation, concentration and resilience. However, this document was only achieved with the help and support of several people whom I thank in advance and take this opportunity to mention below.

To professor José Luis Esteves, for all his effort in giving all the possible availability and support in any question. The success of this dissertation is also due to the teacher's passion for the motorbike world and how he can transmit the knowledge and passion he has in the area.

To the teacher Marco Parente, I thank all the help and availability, especially for the tips on numerical analysis and computational resources that he put at my disposal unconditionally.

To AJP Company, which welcomed me for five months, and particularly to Engineer Miguel Oliveira, for all the knowledge sharing and for having integrated me into this new project, that can take AJP to new markets.

To Professor Luis Galamba, who embraced my project from the first moment I presented it, despite all the priorities he had in his own career. He shared all the experience and knowledge he had to give without any hesitation.

To my parents and brother, who taught me to grow and always ensured that I had every possible opportunity open to me, always giving me unconditional support and strength to overcome any obstacles.

To my partner Ricardo Seca, who has always been a pillar in the toughest moments, always finding ways to give me the courage and the strength to face all challenges. He has become an example to follow, mainly for his ability to never give up what he really wants.

Finally, to all my friends and colleagues, with whom I am proud to have shared these last five years of such an important stage of our lives. From laughter to tears, every moment I keep in my heart.

Contents

1 Introduction **1**

1.1 Framework and motivation . . . 1
1.2 AJP Motorcycle . . . 1
1.3 Sharing World . . . 2
1.4 MobiNext . . . 3
1.4.1 Consortium . . . 4
1.4.2 Objectives . . . 4
1.4.3 Activities . . . 4
1.5 Objectives . . . 5
1.6 Outline of the thesis . . . 6

2 Market Analysis **7**

2.1 Project requirements . . . 7
2.2 Aspect Comparison . . . 8
2.2.1 Power of the motor . . . 10
2.2.2 Batteries . . . 11
2.2.3 Suspension . . . 12
2.2.3.1 Front suspension . . . 13
2.2.3.2 Rear suspension . . . 13
2.2.4 Dimensions . . . 15
2.2.5 Weight . . . 17
2.2.6 Tyres . . . 18
2.2.7 Frame . . . 19

3 Frame structure **25**

3.1 Methodology . . . 25
3.2 Initial Frame . . . 25
3.3 First Draft . . . 30
3.4 First Solution . . . 32

3.5 Second Solution . . . 36
3.5.1 Storage Box and static prototype . . . 36
3.5.2 Second Solution Frame . . . 38
3.6 Third Solution . . . 40
3.7 Fourth Solution . . . 43
3.8 Fifth Solution . . . 45
3.9 Sixth, seventh and eighth Solutions . . . 46
3.10 Extra Solution . . . 49

4 FEM Analysis **51**
4.1 Methodology . . . 51
4.2 Material . . . 52
4.3 Selected solutions . . . 53
4.4 Partitions and mesh . . . 55
4.5 Boundary conditions . . . 57
4.6 Loads . . . 59
4.6.1 Weight Distribution . . . 60
4.6.2 Forces applied by the shock absorber . . . 61
4.6.3 Final forces . . . 63

5 Results and discussion **65**
5.1 Results with shell elements . . . 65
5.2 Structural reinforcements in solution six . . . 79
5.2.1 Zone 1 . . . 80
5.2.2 Zone 2 . . . 94
5.2.3 New design SolidWorks . . . 96
5.2.4 Extra zone . . . 103
5.2.5 Zone 3 - Modification on Boundary Conditions . . . 104
5.2.6 Final Mesh . . . 107
5.3 Structural reinforcements in solution seven . . . 109
5.3.1 Zone 3 . . . 114
5.4 Structural reinforcements in solution eight . . . 120
5.5 Weight Requirement . . . 125

6 Conclusions and Future Works **127**
6.1 Conclusions . . . 127
6.2 Future Work . . . 128

Bibliography **131**

7 Attachments **133**

7.1 Technical specifications of PR7 [5] 133
7.2 Technical specifications of PCx electric of Honda [16] 134
7.3 Technical specifications of LX08 of Lexmoto [17] 135
7.4 Technical specifications of LX06 of Lexmoto [18] 136
7.5 Technical specifications of Yadea G5S of Lexmoto [19] 137
7.6 Technical specifications and battery details of EK3 of Horwin [20] 138
7.7 Technical specifications of CPx of Super Soco [21] 140
7.8 Technical specifications of Muvi of Torrot [22] 141
7.9 Properties of S235 Steel [36] 142
7.10 Properties of S355 Steel [36] 144

List of Figures

1.1 Motorcycle PR7, designed by AJP motorcycles [5]. 2
1.2 Forms of transportation used in the sharing systems. 3

2.1 Scooter PCX Eletric from Honda [16]; 8
2.2 Lexmoto with the LX08 model [17]; 8
2.3 Lexmoto with the LX06 model [18]; 9
2.4 Scooter Yadea G5S form Lexmoto [19]; 9
2.5 Motorcycle EK3 of Horwin [20]; 9
2.6 Scooter CPx from Super Soco [21]; 10
2.7 Torrot with the model Muvi [22]. 10
2.8 Conventional (classic) and inverted telescopic forks[26]. 13
2.9 Zoom in on the connection between the rear suspension and the swingarm of the Muvi scooter [22]. 14
2.10 Main parameters of the motorcycle geometry [26]. 15
2.11 Classical frame of a scooter [24]. 20
2.12 Monocoque frame of a Vespa's scooter[31]. 20
2.13 The spine frame of an standard motorcycle [33]. 21
2.14 Two type of cradle frames. 21
2.15 Frame of PCx electric of Honda [16]. 22
2.16 Several frames of the Lexmoto brand. 22
2.17 Frame of EK3 from Horwin [20]. 23
2.18 Frame of CPx from Super Soco [21], ... 23
2.19 Frame of Muvi from Torrot [22], ... 23

3.1 Initial project, provided by AJP, in several views. 26
3.2 External design of the scooter, provided by AJP, in several views. 27
3.3 Initial frame, provided by AJP, in several views. 27
3.4 Design errors between the chassis tubes, with zoom in views. 28
3.5 Design error between the chassis and the exterior design. 29
3.6 Design error between the chassis tubes and front fork. 29

3.7 More design errors of initial project. 29
3.8 First draft of the chassis, in several views. 30
3.9 Assembly between the main components of the scooter and the first draft. . . 31
3.10 Final result of the corrections done. 31
3.11 Swing arm and eyebolt corrections on the frame. 32
3.12 Simplified drawing of a helmet, in several views. 32
3.13 Battery support box. 33
3.14 Helmet support box. 33
3.15 First solution for the scooter's frame. 33
3.16 Assembly between the first solution, the storage boxes, the batteries and the helmet. 34
3.17 Assembly between the first solution and the exterior design. 35
3.18 Footrest connection eyebolts. 35
3.19 Storage box, provided by AJP, in different views. 36
3.20 Construction of the static prototype. 37
3.21 Prototype's structure. 37
3.22 Prototype of the storage box. 37
3.23 First prototype of the scooter, in Expomoto. 38
3.24 Second solution for the scooter's frame. 38
3.25 Assembly of the second solution. 39
3.26 Zoom in view of the new support. 39
3.27 Support, of the second solution, with the storage box. 39
3.28 Error between the steering column and the main frame tubes corrected. 40
3.29 Scooter available in DEMEC's laboratories. 41
3.30 Frame of the third solution. 41
3.31 Combination of the new solution with the rest of the scooter components. . . . 42
3.32 Connection between the main and intermediate tubes. 42
3.33 Frame of the fourth solution. 43
3.34 Connection between two tubes of different diameters. 44
3.35 Rear frame assembly with the storage box. 44
3.36 Assembly between the fourth solution and main components. 45
3.37 Frame of the fifth solution. 46
3.38 Right view of the assembly between the fifth solution and the main components of the scooter. 46
3.39 Frame of the sixth solution. 47

3.40 Frame of the seventh solution. 48
3.41 Frame of the eighth solution. 48
3.42 Possible configuration for the batteries. 49
3.43 Direction of the battery grips. 50

4.1 Solution six in multiple views. 53
4.2 Solution seven in several views. 54
4.3 Solution eight in multiple views. 54
4.4 Solution sixth with only half of the structure, to simplify the analysis. 55
4.5 Scheme of the main features used in Abaqus software. 56
4.6 Mesh parameters used. 57
4.7 Regions with constraints. 58
4.8 Solution seven with boundary conditions imposed. 58
4.9 Areas of the structure for application of forces. 59
4.10 Force application diagram. 61
4.11 Angle ratio between the shock absorber and the swingarm. 61
4.12 Diagram of the forces between shock absorber and swingarm. 62
4.13 Solution six with the applied forces. 63
4.14 Solution six with boundary conditions and forces applied. 64

5.1 Part of the solution six, in Abaqus. 66
5.2 Detail of the steering column, ... 66
5.3 von Mises stress of the first simulation of solution six [Pa]. 67
5.4 Detail between the end of the support and the rest of the structure [Pa]. . . . 67
5.5 Frame of the six solution with a division between the front edge of the support and the rest of the structure. 68
5.6 von Mises stress of the second simulation of solution six, with the detail fixed [Pa]. 68
5.7 Details of the most stressed areas, ... 69
5.8 von Mises stress of the correction made to the connection between the two parts [Pa]. 69
5.9 Frame of the seventh solution with the several constituent parts. 70
5.10 Detail of the tie constraint. 70
5.11 Detail of the boundary condition on the tube edges. 71
5.12 von Mises stress of the first simulation of solution seven [Pa]. 71
5.13 Details of the most stressed areas in solution seven, ... 72

5.14 Frame of the eight solution with the several constituent parts. 72
5.15 Tie constraint between the two parts. 73
5.16 Detail of the boundary condition on the tube edges. 73
5.17 Detail of the area associated with the application of the driver's feet force. . . 74
5.18 von Mises stress of the first simulation of solution eight [Pa]. 74
5.19 Details of the most stressed areas, ... 75
5.20 Solution six with a 60mm diameter on the main tubes. 75
5.21 Solution six with a 50 mm diameter on the main tubes. 76
5.22 von Mises stress of the frame simulation, with the modification of 60 mm for the diameter [Pa]. 77
5.23 von Mises stress for the frame simulation, with the modification of 50 mm for the diameter [Pa]. 77
5.24 Frame of the seven solution. 78
5.25 von Mises stress of the solution seven, after some modifications [Pa]. 79
5.26 Solution six with the main areas highlighted. 80
5.27 View of the middle plate reinforcement. 80
5.28 von Mises stress of the simulation with a sheet of 5mm [Pa]. 81
5.29 von Mises stress of the simulation with a sheet of 3mm [Pa]. 81
5.30 Several views of the double plate reinforcement. 82
5.31 von Mises stress of the simulation with the double plate reinforcement [Pa]. . . 83
5.32 Different views for the external reinforcement, ... 83
5.33 von Mises stress of the simulations with the several designs for the external plate reinforcement [Pa]. 84
5.35 First design of the hole. 85
5.37 Second design of the hole. 85
5.39 Third design of the hole. 85
5.41 Different design with two holes. 85
5.42 von Mises stress of the simulation with the first design [Pa]. 85
5.43 von Mises stress of the simulation with the second design [Pa]. 85
5.44 von Mises stress of the simulation with the third design [Pa]. 86
5.45 von Mises stress of the simulation with the two holes design [Pa]. 86
5.46 Reinforcement with the hole at the top. 86
5.47 von Mises stress of the simulation with the hole at the top design [Pa]. 87
5.49 First design of the strip reinforcement. 87
5.51 Second design of the strip reinforcement. 87

5.53 Third design of the strip reinforcement. 88
5.54 von Mises stress obtained from the first design of the reinforcement [Pa]. . . . 88
5.55 von Mises stress obtained from the second design of the reinforcement [Pa]. . . 88
5.56 von Mises stress obtained from the third design of the reinforcement [Pa]. . . . 88
5.57 Extension of the sheet reinforcement. 89
5.58 Reinforcement with no connection to the curve. 89
5.59 von Mises stress obtained with the extension of the plate [Pa]. 89
5.60 von Mises stress obtained with the design with no connection to the curve [Pa]. 89
5.61 Longer reinforcement in zone 1, ... 90
5.62 von Mises stress obtained with the longer reinforcement [Pa], ... 90
5.63 Several views of the reinforcement created, ... 91
5.64 von Mises stress obtained with the new reinforcement [Pa]. 92
5.65 Reinforcement without the lateral plates, in zone 1. 92
5.66 von Mises stress obtained by the simulation with the reinforcement without the lateral plates [Pa]. 93
5.67 General von Mises stress obtained by the simulation with the reinforcement in zone 1 [Pa]. 94
5.68 von Mises stress of the simulation with the increase of the tube diameter [Pa]. 95
5.69 Detail section with thickness visible. 95
5.70 von Mises stress obtained with the addition of the reinforcement plate, in zone 2 [Pa]. 96
5.71 Frame part of solution six with the new modifications. 97
5.72 von Mises stress of the solution six without any reinforcements [Pa]. 97
5.73 Frame part of the sixth solution with the main reinforcements. 98
5.74 von Mises stress obtained with the simulation with the main reinforcements applied [Pa]. 99
5.75 Reinforcement with the lateral plates. 99
5.76 von Mises stress obtained by the simulation with the change in the reinforcement [Pa]. 100
5.77 New design of the reinforcement in zone 1. 100
5.78 von Mises stress obtained with the new design of the reinforcement in zone 1 [Pa]. 101
5.79 Detail added to the reinforcement. 101
5.80 von Mises stress obtained with the change of the reinforcement [Pa]. 102
5.81 Final results of von Mises stress of the zone 1 with the reinforcement design improved [Pa]. 102

5.82 Detail in the results obtained in the last simulation [Pa]. 103
5.83 von Mises stress obtained with the improvement in the intermediate tube [Pa]. 104
5.84 Tie constraints, ... 105
5.85 Tie constraint between the reference point and the inner edges of the eyebolts. 105
5.86 von Mises stress obtained by the simulation with the new boundary conditions [Pa]. 106
5.87 von Mises stress of solution six with the reinforcements applied [Pa]. 107
5.88 Colour code used by Abaqus software to identify that the surfaces that is able to create a structured mesh. 108
5.89 von Mises stress of the simulation of the solution six with a structured mesh [Pa]. 108
5.90 Displacement results, in meters of the sixth solution simulation. 109
5.91 New modifications intersect the external body of the scooter. 110
5.92 Frame of the seventh solution with new the modifications. 111
5.93 von Mises stress of the simulation of the seven solution, without any reinforcement [Pa]. 111
5.94 Reinforcement of the zone 1, ... 112
5.95 Reinforcement of the zone 2. 112
5.96 von Mises stress of the simulation with the reinforcements applied [Pa]. 113
5.97 Reinforcement of the zone 3 of the solution seven. 114
5.98 von Mises stress of the solution seven with the added reinforcement in zone 2 [Pa]. 115
5.99 View of the tubes that suffered a change in the thickness. 115
5.100von Mises stress of the simulation with the change of thickness in the main tube [Pa]. 116
5.101Final result of von Mises stress of the solution seven with the reinforcements in zone 2 [Pa]. 117
5.102New iteration of the reinforcement on zone 2. 117
5.103von Mises stress of the new iteration of the reinforcement on zone 2 [Pa]. . . . 118
5.104General result of von Mises stress of the new iteration of the reinforcement on zone 2 [Pa]. 119
5.105Displacement results, in meters, of the simulation of the solution seven. 120
5.106Frame part of solution eight with the new modifications. 121
5.107von Mises stress of the solution eight without any reinforcements [Pa]. 122
5.108Reinforcement of the zone 1 in the solution eight, ... 123
5.109Reinforcement of the zone 3 in the solution eight. 123

5.110von Mises stress obtained with the simulation of the solution eight with all the reinforcement applied [Pa]. 124
5.111Displacement results, in meters, of the eighth solution simulation. 125

List of Tables

2.1 Dimensions required by the consortium 7
2.2 Comparison of the nominal and maximal power of the electric motors in the market, in kW 11
2.3 Comparison of the type of batteries used in the market 12
2.4 Comparison between the number of shock absorbers used by the models in review 15
2.5 Comparison of various scooter dimensions, in mm 16
2.6 Comparison of the models' masses, in kg 17
2.7 Comparison between the tyres used in the market 18

4.1 Main properties of S235 steel [36] 52
4.2 Main properties of S355 steel [36] 52
4.3 Table of the forces applied to the structure 64

5.1 Table of the masses of the principal components of the scooter 126
5.2 Table with each frame' mass and the total mass of the scooter for each solution 126

Nomenclature

kg	kilogram
kW	kilowatt
mm	millimetre
Pa	Pascal
V	Volts

Chapter 1

Introduction

1.1 Framework and motivation

The present thesis represents the final dissertation of the author's Master's Degree in Mechanical Engineering, in machine design specialisation, conducted by the Engineering Faculty of the University of Porto.

This dissertation is integrated into a current project of the company AJP Motos, where in consortium with four other companies, they aim to design an urban scooter to enter the world of sharing vehicles. This transportation sector is already very developed in certain countries, with various types of transport such as bicycles and stand-up scooters. In Portugal, the sharing of scooters is not yet developed compared to this sector in some eastern countries.

The motorcycle world has evolved exponentially in the last century. Initially, the first motorbike was just a bicycle mounted with an engine and was called the "motor bicycle". Since then, the field of motorcycles has developed in multiple aspects, from geometry to the type of engine used, from price and comfort to ergonomics and riding posture. There are thousands of models on the motorcycle market, from city riding models to models designed for the mountains and track racing [1].

In certain countries, scooters are models widely manufactured and developed due to their various advantages, like their low price compared to cars to their high capacity to be handled by traffic and easily parked. Despite their popularity mainly in highly populated countries, the emissions of polluting gases emitted by scooters have led to research and studies to improve their environmental footprint. One of the solutions to this problem was converting from combustion engines to electric motors, making the electric scooter the new green transportation technology in the 21st century [2] [3].

1.2 AJP Motorcycle

AJP Motorcycle is a portuguese company, founded in 1987 and is currently the only company, in Portugal, that manufactures motorcycles. The company was founded by shareholders António Pinto and Jorge Pinto and its production is mainly focused on development,

manufacture and marketing off-road motorcycles. Enduro, Adventure, and Supermoto are the three main types of motorcycles created by AJP, which are designed mainly for riding in the mountains and on racing tracks. Over the years, AJP has participated in several motorcycle competitions, with its own motorcycles produced in the factory [4].

The latest model released by AJP is an evolution of the PR7, originally introduced to the market in 2017. In the picture below, we can see the PR7 motorcycle, which consists of a 600 cc single-cylinder engine and a 6-speed gearbox. It features a super light chassis composed of aluminium and steel parts, and a front suspension, capable of handling any kind of jump, with a travel of 300 mm. The main specifications of PR7 are presented in attachment 7.1 [5].



Figure 1.1: Motorcycle PR7, designed by AJP motorcycles [5].

AJP is recognised for specific details of its motorcycle models, as casting aluminium swingarms in one piece, rather than welding several components together, which is time-consuming and expensive. Another peculiarity of several AJP models is the use of the fuel tank as a structural component of the motorcycles, with the tank being located under the rider's seat [5] [6].

1.3 Sharing World

The world of sharing has been growing exponentially, particular in the last decade. The figure 1.2 presents the wide range of transportation means that this service offers, such as bicycles, stand-up scooters, motorcycle scooters and even cars. It consists in sharing forms of transportation without the need to own them. It is usually associated with a temporary product rental application, where the information required to utilise the service is minimal compared to the needed to acquire one.



(a) Bicycles [7].



(b) Stand-up Scooters [8].



(c) Electric scooters [9].



(d) Cars [10].

Figure 1.2: Forms of transportation used in the sharing systems.

This type of solution is being explored all over the world, mainly as a mobility solution that contributes to a sustainable and environmentally-friendly society. In many means of transportation in the sharing world, either no engines are used, as in bicycles, or electric motors are used, which replace traditional motors and lead to lower carbon emissions. In addition, it also allows the reduction of the use of personal transport for commuting and the decrease of traffic congestion. After several years of evolution, studies show that the average travel distance is between 2 and 3 kilometres and that these services are mainly used for short trips, tourism, shopping, and entertainment [11] [12] [13].

Studies show the impact that these solutions can have, for example, when integrated into a city like Shanghai. The need to improve the city's health and climate conditions led to the integration of the sharing world, resulting in changes in the city's sustainability as well as its commercial and industrial levels [14].

1.4 MobiNext

The project MobiNext, is a project founded in 2020 and guided by a consortium of 5 companies, being AJP Motorcycle the responsible one. The consortium also includes CEIIA,

Alma Design, CiTNM and Wyze Mobility. The project is funded by Compete 2020, Portugal 2020 and the European Union's European Regional Development Fund [15][6].

1.4.1 Consortium

The consortium is composed of five companies, with AJP, already presented in subchapter 1.2 is one of them.

CEIIA is a Centre of Engineering and Product Development, which connects industry, cities, and universities in order to develop new technologies, products, and services, always with a mindset of developing a society more sustainable.

Almadesign is a company that focuses more on the user's perspective and experience in order to best create a product or service. In this project, Almadesign will contribute with its experience in managing the processes that must be followed throughout the creation of a new design or concept to this project.

The CiTNM Center for Innovation and Technology N. Mahalingam is an association, linked to the automotive, metallurgical and foundry sector. It has two main goals, which are to connect specialised training, such as universities, with industry projects and to focus on developing projects that promote the improvement of businesses, such as improving competitiveness and increasing skilled employment.

Finally, Wyze Mobility is a startup focused on the development of a more innovative and technological society, introducing 100 percent electric mobility solutions. At MobiNext, the company will ensure that the new product is integrated into its service, commercially exploring the final product [6].

1.4.2 Objectives

MobiNext is a project that was created to address a variety of mobility problems in society. The increased population density in cities causes issues such as overuse of personal transportation, increased carbon emissions, and public transportation insufficiency in the face of high demand. As a result, the project's objectives are organised into four simple concepts. The product, which is the design and development of an electric scooter aimed specifically for the shared vehicle market. The adaptability to different city conditions and usage. And the connectivity and interactivity, since the goal is that the user's connection with the vehicle is through a digital service management platform, with an intuitive and interactive design [6].

1.4.3 Activities

The project is divided into several phases:

1. "Technological surveillance and specification of scooters and sharing systems" - Preliminary studies phase, where a review of the concepts and specifications necessary for the development of the project is conducted;

2. "Scooter concept study, structure and software" - Phase divided into two objectives: the development of alternative solutions for the design of the scooter, taking into account the studies carried out and the development of the interface that makes the connection between the user, the vehicle and the management system;

3. "Scooter development, structure, connectivity and software": Development of the main components of the scooter, such as the design, the structure and the mobility management platform;

4. "Prototype building and integration" - Construction of two prototypes of the scooter in order to validate the designed concept. The static prototype. The static prototype was built during this dissertation, and it is referred to in subchapter 3.5.1;

5. "Prototype testing and validation" - Performing structural tests on the prototypes as well as testing them outdoors;

6. "Promotion and disclosure" - Dissemination of project progress and outcomes at technical and scientific fairs and conferences, as well as on the website and through social media [6].

The last two objectives of the MobiNext project were not achieved while this dissertation was being developed.

1.5 Objectives

The major goal of this dissertation is to develop a frame for an electric urban scooter and use FEM analysis to validate its structure. To ensure that this goal is achieved, the following intermediate goals were established from the beginning:

- Literature review of current scooter frame designs, taking into account the different specifications of each motorcycle;
- Understanding the connections and constraints of the frames;
- Analyse the 3D drawings provided by the company, of the current model;
- Develop alternative solutions to the current model, taking into consideration the company's demands;

- Perform numerical analysis and structural study of the solutions, using FEM software;
- Define and comprehend which parameters are indicated for the numerical simulations, such as the mesh size, the type of element to use and singularities that may exist;
- Analyse the simulation results, comprehending and commenting on them;
- Examine the critical points identified and propose ways to avoid them.

1.6 Outline of the thesis

This dissertation is divided into 6 chapters whose content is briefly explained in the following points:

- Introduction: Serves as a brief introduction to the subject of the dissertation and presents its objective, outline and a description of the company associated with this project;
- Market Analysis: Includes an analysis of the current market and a comparison of some of the main aspects of a scooter;
- Frame Structure: Presents the alternative solutions designed for the scooter frame and their errors. This solutions were develop using SolidWorks software;
- FEM Analysis: Contains a presentation of the material used and a description of all parameters required for the numerical analysis, using the Abaqus software. Exposition of the boundary conditions and connections considered and the forces applied to the frame;
- Results and Discussion: Presentation of the results obtained from the structural studies of the selected frame solutions. Modifications made are presented as a optimisation of the frame's critical points.
- Conclusions and Future works: Final reviews of the project are presented as well as suggestions and recommendations for the future of the project.

Chapter 2

Market Analysis

2.1 Project requirements

In order to enter the world of trip sharing, MobiNext project was created and the main goal is to produce a scooter for city navigation. After some considerations, they decided to design an electric scooter, with a motor mounted directly on the rear wheel and with two removable batteries of lithium-ion, that can be accessible through the compartment under the driver's seat. Besides batteries, the storage also has room for a small helmet and for another helmet is necessary the use of a top case. The chosen batteries have a value of 69 V of voltage and 2,2 kWh of capacity.

For the suspension of the scooter, in the front requires a telescopic fork and in the back is used a double swingarm with a single shock absorber and coil spring. As this set of suspension will be mentioned several times throughout the report, the term shock absorber will be used to refer to the assembly.

In order to hide the shock absorber from the outside, it is mounted on the front of the rear wheel, connected to the swingarm and the frame of the scooter, by an eyebolt. The motor power of the scooter is 4 kW, with a peak power of 5,5 kW, but the speed is going to be limited to 45 km/h.

In order to simplify the process of transporting the scooters between the respective parks, the desired mass of the scooter is 80 kg, including the mass of the batteries, which in total is 25 kg.

In addition, there are also some base dimensions, desired by the consortium, that are listed in the table 2.1:

Table 2.1: Dimensions required by the consortium

Description	Dimensions
Wheelbase	1350 mm
Seat height	750 mm
Ground clearance	160 mm

Finally, the required front and rear wheels are the same and type 130/70 and R17 (130 mm width and 17 inch rim radius).

2.2 Aspect Comparison

In this chapter, a study of the electric scooter market worldwide is presented. The power of the motors has been taken into account, so that it can be compared with the power of the motor being used. Therefore only scooters with electrical engines between 3 kW and 6 kW were considered.

The brands and models of the motorcycles analysed in the chapter are as follows: (The main specifications of the different motorcycles models are presented from attachment 7.2 to 7.8.)

1. From Honda, the evolution of the traditional PCX with an electric motor, released in 2020.



Figure 2.1: Scooter PCX Eletric from Honda [16];

2. From the Lexmoto brand, the LX08 model.



Figure 2.2: Lexmoto with the LX08 model [17];

3. Also from Lexmoto, the LX06 model.



Figure 2.3: Lexmoto with the LX06 model [18];

4. Also from Lexmoto, the Yadea G5S model. 7.5.



Figure 2.4: Scooter Yadea G5S form Lexmoto [19];

5. From the brand Horwin, the EK3 model.



Figure 2.5: Motorcycle EK3 of Horwin [20];

6. From the Super Soco brand, the model CPx, launched in 2020.



Figure 2.6: Scooter CPx from Super Soco [21];

7. Finally, from the Spanish brand Torrot, the model Muvi, launched in 2017.



Figure 2.7: Torrot with the model Muvi [22].

2.2.1 Power of the motor

A motorcycle engine is like the heart of a human being. Several types of motors are used on the market, ranging from internal combustion engines, such as two-stroke and four-stroke engines, to electric motors. These have been explored over the past few years, mostly due to their ability to convert energy, without the emission of pollutant gases. In the scooter market, it is still more usual to find scooters with combustion engines, but several models, such as those indicated in the previous subchapter, already use electric motors as their power producers [23].

When comparing motorcycles with combustion engines and electric motors, it is possible to verify that when electric motors are used, the presence of a fuel tank is not necessary, but rather the use of batteries and that the transmission of movement is simpler. The electric motor can offer instant torque after starting, allowing the use of only one gear without needing

a very complex gearbox. Moreover, transmission can be avoided when the motor is mounted directly on the wheel, as required by AJP [1] [24].

One of the most important aspects to compare engine performance is the output power. In the table 2.2, it is possible to compare the nominal and maximal power of each model presented. The nominal, or also known as continuous power, sets a particular output at a particular speed for a set of time, while the maximum power is the maximum amount delivered at a particular speed [25].

Table 2.2: Comparison of the nominal and maximal power of the electric motors in the market, in kW

Brand	Model	Nominal Power	Maximum Power
AJP	MobiNext	4	5,5
Honda	PCx Eletric	-	4,2
	Lx08	-	4
Lexmoto	Lx06	-	4
	Yadea G5S	-	4,1
Horwin	EK3	3,5	6,2
Super Soco	CPx	4	4,8
Torrot	Muvi	3	-

As it is possible to verify, the engine required by AJP has a nominal power of 4 kW and a maximum power of 5,5 kW. Of the models to compare, it is possible to say that the most similar to the MobiNext motor is the engine used by Super Soco, this because it has the same nominal power and a maximum power of 4,8 kW. All the other models either have a nominal power lower than 4 kW, or a maximum power lower than the 5,5 kW like the one used by AJP.

2.2.2 Batteries

As already mentioned, using electric motors leads to the need for batteries since they are the energy source for the engines. This component is a significant aspect to be compared between motorcycles, not only because it determines the autonomy of the motorcycle, but also because it is necessary to have a balance between weight, size, and energy storage capacity. One of the disadvantages of using batteries is their low power density, whose units are Watts per kilo. This means that a battery of outstanding performance and storage will be a battery of significant volume and weight [1].

Regarding the batteries used in the market, it is possible to say that all models are equipped with two removable batteries, so they can be charged outside the scooter. In

addition, the batteries are all located under the driver's seat, as requested in the MobiNext project.

In order to compare the batteries used in the market, in table 2.3, it is presented the type of batteries and more two parameters: the voltage and capacity of the battery.

The voltage (V) is the nominal voltage at which the batteries work, and the unit used is Volts. The capacity of the batteries was compared by amp-hours (Ah), which represents how many amps the battery can deliver in an hour. Some brands presented the voltage and the watt-hours of the batteries, so to have a term of comparison, this information was converted to amp-hours, by the following equation [25]:

$$Amphours = \frac{Watts}{Voltage} \tag{2.1}$$

Table 2.3: Comparison of the type of batteries used in the market

Brand	Model	Type	Voltage / V	Capacity / Ah
AJP	MobiNext	Lithium-Ion	69	31,9
Honda	PCx Eletric	Lithium-Ion	50,4	20,8
	Lx08	Lithium	60	32
Lexmoto	Lx06	Lithium	60	32
	Yadea GS5	Lithium	-	-
Horwin	EK3	Lithium-Ion	72	40
Super Soco	CPx	Lithium	60	46
Torrot	Muvi	Lithium-Ion	48	31,9

Comparing the information in the table, we can see that the type of batteries is divided into lithium and ion-lithium batteries, and the usage is evenly distributed.

As noted, the battery with the highest voltage is the EK3 model use, with 72 V, and the most common value is 60 V. The battery chosen by AJP is within an expected value.

Regarding the capacity, the range between the lowest and highest value is relatively small, with a value of 31,9 Ah, a relatively common capacity in the market.

2.2.3 Suspension

The motorcycle's suspension is a dynamic system whose main function is to connect the wheels to the ground, always trying to absorb the irregularities of the road as much as possible. This system is essential for a comfortable and safe ride and protects the motorbike components from vibrations caused by the road [1][25].

2.2.3.1 Front suspension

After analysing the solutions used for the front suspension and comparing them with those used by the models under review, it can be concluded that telescopic forks are the most widely used. All models use classic telescopic forks, which consists of two telescopic legs, each with a piston that moves along a casting called a slider. The cylinder is filled with a special type of oil, called shock absorber fluid, whose resistance allows the piston movement to slow down when there is an irregularity in the floor [25][26].

In the figure 2.8 shows the difference between "conventional" and inverted telescopic forks:

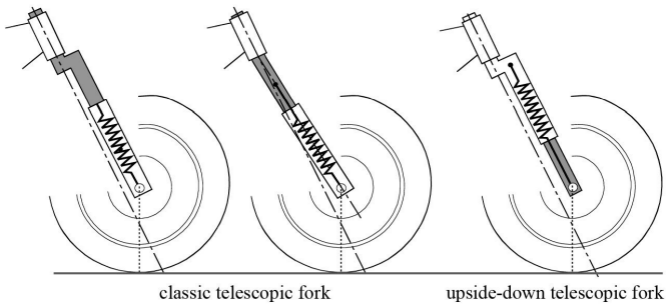


Figure 2.8: Conventional (classic) and inverted telescopic forks[26].

As it is possible to see in the conventional solution, the two forks tubes are fixed to the lower end, and the two telescopic sliders are fixed on the steering head. In contrast, the inverted solution is presented the other way round. The telescopic forks are characterised by low inertia around the steering head's axis. The inverted solution normally presents more bending capacity and large torsional stiffness and are often used in sport motorcycles. Despite the several advantages of the telescopic forks, they are not yet the perfect solution for the front suspension, nor the cheapest, less need of maintenance, or less complex solution. There is a need to seek a balance between the suspension's performance during braking and acceleration, its ability to transmit forces, and the best way to ensure a better and safer ride [26] [1].

2.2.3.2 Rear suspension

For many years, motorcycles had only front suspension, with the rear wheel mounted directly to the motorcycle's chassis. Later, the rear suspension was then added. This component has varied greatly over the years, not in concept, but by how it connects with other components, which varies the influence it has on the structure. In terms of concept, the most used solution is an assembly composed of a shock absorber with a coil spring fitted around. This spring is normally made from round section spring steel and offers a large amount of

suspension movement and lightness. The shock absorber has the function of damping the spring's action and reaction, and it is usually filled with gas or oil. Over the years, what has really been tested and applied is a modification of the connection of the shock absorber assembly to the swingarm and frame. From varying the distance where the suspension is connected to the swingarm, to using rockers or connection roads. Another variation is using two assemblies, one on each side of the wheel or just one. Each change has its advantages and disadvantages, and the best choice is the one that uses the minimum number of joints in the system and presents the best structural and space-saving results [25][27][26][28].

After analysing the models under study, it was possible to see that they all have a direct connection between the suspension and the swingarm, without any extra linking component. The places where these connections are made are all very similar to what is shown in figure 2.9. What varies between the models is the use of duo or mono shock absorber and, in the table 2.4, it is possible to compare this aspect.

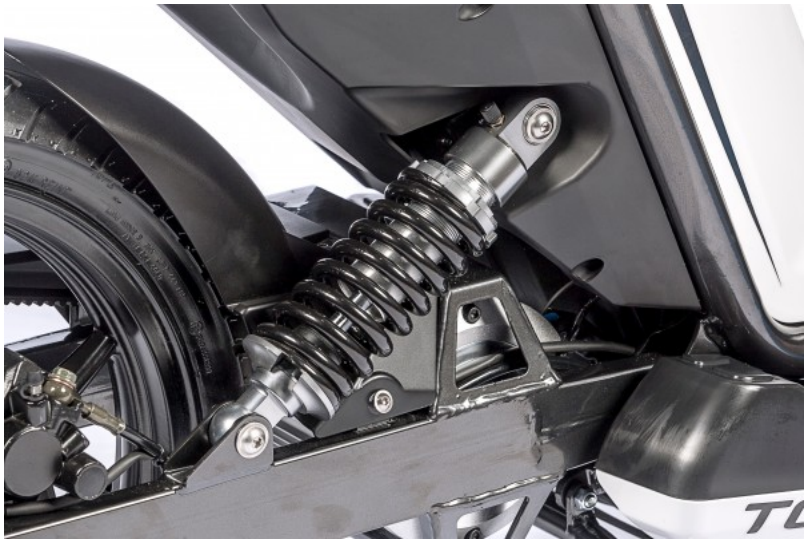


Figure 2.9: Zoom in on the connection between the rear suspension and the swingarm of the Muvi scooter [22].

Table 2.4: Comparison between the number of shock absorbers used by the models in review

Brand	Model	Quantity
AJP	MobiNext	1
Honda	PCx Eletric	2
	Lx08	2
Lexmoto	Lx06	2
	Yadea G5S	2
Horwin	EK3	2
Super Soco	CPx	1
Torrot	Muvi	1

In the table above, it is possible to note that manufacturers' most chosen solution is using a set of two shock absorbers for the rear suspension. Regarding the MobiNext model, one of the features that most differentiates this scooter from the rest of the market is that, besides using only one central shock absorber, this suspension is hidden from the outside, being connected to the central front side of the swingarm. This assembly will be presented in detail in the next chapter.

2.2.4 Dimensions

In order to define more easily the dynamics of the motorcycle, usually, the following geometrical parameters are used: the trail, the caster angle and the wheelbase. The figure 2.10 serves to simplify the understanding of the distances that the parameters represent.

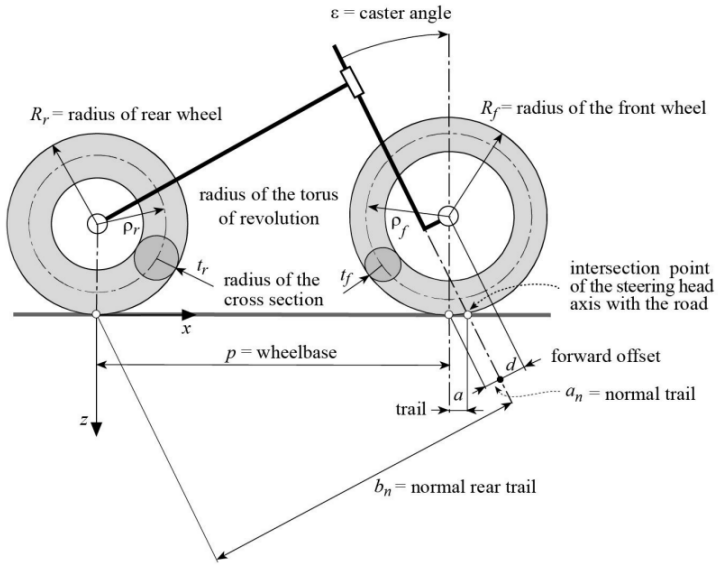


Figure 2.10: Main parameters of the motorcycle geometry [26].

The caster angle, also known as rake, is the angle between the vertical axis and the headstock, the front rotation axis. The trail is the distance, at ground level, between the front wheel and the intersection point of the steering head axis with the road. Finally, the wheelbase is the distance between the contact points of the tires on the road, and it varies according to the type of motorcycle. The values range from 1200mm for small scooters to 1600mm for touring motorcycles. In general, the increase of the wheelbase has several advantages and disadvantages, from the increase of the directional stability of the motorcycle to the rise of flexional and torsional deformability of the frame [27][1][24][26].

In this report, only the wheelbase parameter was analysed since the other two parameters are not usually supplied by the brands, being extremely complicated to get the values to make a serious comparison. In table 2.5, it is presented the values of the base dimensions of each model, such as the height of the seat and the wheelbase.

Table 2.5: Comparison of various scooter dimensions, in mm

Brand	**Model**	**Overall Length**	**Overall Width**	**Overall Height**	**Seat Height**	**Wheel Base**
AJP	MobiNext	-	-	-	750	1350
Honda	PCx Eletric	1960	740	1095	760	1380
	Lx08	1895	700	1180	-	1345
Lexmoto	Lx06	1865	700	1113	-	1350
	Yadea G5S	1825	700	1150	-	1290
Horwin	EK3	1900	690	1130	780	1320
Super Soco	CPx	1975	720	1132	760	1365
Torrot	Muvi	1855	-	1025	810	1290

Regarding the basic dimensions of the models, we can see that they all have similar dimensions. The intervals between the minimum and maximum values of each parameter are relatively short, with the overall length between 1825 mm and 1960 mm, the overall width between 690 and 740 mm, and, finally, the overall height between 1025 mm and 1150 mm. Values for the MobiNext scooter were not presented, but considering that the project aims to enter the world of shared vehicles, it is expected that the base dimensions are as small as possible to ease parking and transportation.

Analysing the values of the seat height, we can observe that the values are in the range of seven hundred and eight hundred mm. This parameter can have a lot of influence on the ergonomics of the scooter. Therefore, it is important to always analyse the dimensions of the scooter in order to guarantee a good ergonomic factor, which can be verified by the riding comfort and the driver's driving posture [29].

Finally, analysing the wheelbase, it can be seen that the values vary between 1290 and 1380 mm and that the value of 1350 mm proposed by MobiNext is within the range normally used.

2.2.5 Weight

Weight is one of the most critical factors in any vehicle. On motorcycles, the weight is distributed between the front and rear wheels, significantly influencing the bike's manoeuvrability and handling. Furthermore, the weight distribution in combination with aspects such as the suspension, the wheelbase and the centre of gravity plays an essential role in the balance of the motorbike. A good balance can be achieved with low weight and low centre of gravity, but these conditions are not always possible. In the current scooter design, by MobiNext, there are two main aspects that strongly influence the weight distribution: the fact that it is a scooter and the fact that it is electric.

There is a big difference in weight and distribution between a conventional and an electric motorcycle, since the electrical one does not have a fuel tank but rather batteries. As already mentioned in subchapter 2.2.2, a battery with excellent performance will most likely have a substantial weight and volume. Normally, the total weight of an electric motor and its batteries is higher than a conventional motor and its tank. Therefore, it is already possible to conclude that the scooter can be heavier than a scooter with a combustion engine.

Furthermore, and also as mentioned in subchapter 2.2.2, the batteries in scooters are generally located under the driver's seat. Due to the typical design of scooters, the lower part of the bike, where the rider places his feet, is usually not used for the storage of the batteries. This leads to the batteries being placed in a very high position, thus raising the centre of gravity and impairing the balance of the scooter [27][1][24].

In the table 2.6, the masses of the models to be compared are presented, with detail if that mass includes the masses of the batteries and how many. This detail had to be included as the brands sometimes do not provide more information about the individual mass of both the scooters and the batteries. Also, in the same table is included the information on the maximal capacity mass of each model.

Table 2.6: Comparison of the models' masses, in kg

Brand	Model	Mass	Details	Maximal Capacity Mass
AJP	MobiNext	80	With 2 batteries	-
Honda	PCx Eletric	144	With 2 batteries	-
Lexmoto	Lx08	84	With 2 batteries	255
	Lx06	90	With 2 batteries	261
	Yadea G5S	81	With 2 batteries	264
Horwin	EK3	95	With no batteries	284
Super Soco	CPx	115	With 1 battery	-
Torrot	Muvi	93	With 2 batteries	235

As it is possible to analyse, only two models, besides MobiNext, present a mass below

ninety kilograms, including the mass of two batteries. Moreover, comparing the maximum capacities, it is possible to verify that the values are around 260 kilograms. Relatively to the MobiNext, there is not a defined maximum value. In the present report, it will be considered as a study case, the set of a 75 kg driver with a 50 kg passenger, preferring 125 kg, significantly below the values presented by the market.

2.2.6 Tyres

As common knowledge, the function of tyres is to support the weight of the machine by transmitting the forces applied to it to the ground. However, tyres are a fundamental element when it comes to suspension. For comfortable driving and road holding, the pneumatic tyres used in the market act like a spring, and the rubber acts as a damper when it flexes. Tyres are distinguished by their main dimensions and are usually classified with three numbers. The first stands for the width, in millimetre, of the tyre cross-section. The second is the aspect ratio, which represents the ratio between the height of the sidewall and the width of the cross-section. And finally, the last one represents the dimension of the rim and is presented in inches.

The following table 2.7 shows the tyres used by the models to be compared:

Table 2.7: Comparison between the tyres used in the market

Brand	Model	Front		Rear	
		Tyre	Rim Radius	Tyre	Rim Radius
AJP	MobiNext	130/70	13”	130/70	13”
Honda	PCx Eletric	100/80	14”	120/70	14’
Lexmoto	Lx08	120/70	12”	120/70	12”
	Lx06	120/70	12”	120/70	12”
	Yadea GS5	90/90	12”	100/80	12”
Horwin	EK3	100/80	14”	110/70	13”
Super Soco	CPx	100/80	16”	110/80	14”
Torrot	Muvi	90/80	16”	90/80	16”

As it is possible to see, the model that presents the largest width is the AJP model, that also presents the same type of tyre on both wheels. Other models vary in width from ninety to one hundred and twenty mm, with only a few having the same width for both tyres. Analysing now aspect ratio values, these vary between seventy and ninety, being more common a value of eighty in the front and a value of seventy in the back. Comparing the tyre’s inner rim diameters, these ranged between twelve and sixteen inches. The MobiNext model, uses a value of rim radius within the normal range.

2.2.7 Frame

The frame is the skeleton of the whole motorcycle, one of the most complex elements in a bike. It must support the rider and all the motorcycle components, such as the engine and suspension, always providing a secure ride in all conditions.

Over the years, the chassis technology has evolved, always associated with the development of the engines, as the frame has to be able to support the new and more powerful engines. The main objective of chassis evolution is to achieve a lightweight chassis without compromising structural stability, so achieving a balance between weight, stiffness and strength is necessary. Stiffness is associated with the structure's temporary deformation when loaded and unloaded. However, strength is the measure of the load that can be applied before the structure breaks or deforms permanently. One of the main principles to evaluate the efficiency of structures is the stiffness/weight ratio. However, in mass production, as the weight is connected to the cost, it is customary to use a ratio between stiffness to cost [24][1][27].

The role of the chassis is divided into two main categories: static and dynamic. The role of the frame in static terms is to support the weights of all the different components of the bike and the rider. In dynamic terms, this component significantly influences steering precision, road holding and comfort. Steering precision is the ability to keep the steering axles in the same plane as the rear wheel, so that the geometry of the motorbike remains unaffected. To achieve this, the frame must have torsional and bending strength. Finally, the chassis should also sustain fatigue, caused by continual stress reversal, for a long time, so that little maintenance is required [24][1][27].

After years of evolution, nowadays, the chassis used by ordinary users are classic chassis, used for years. Major evolutions, such as the application of new materials or the manufacture by new industrial processes, are mainly incorporated into motorcycles of high-end brands or competitions. In this subchapter, the various types of chassis present on the market will be presented, as well as the frames used on the models compared in this chapter [24][1][27].

The classical scooter frame, as the one presented in figure 2.11, has a characteristic shape, like the flat platform between the seat and the handlebar. This type of chassis can be very complicated, and it can be challenging to balance between good mechanical properties and the frame's weight. It is usually made of steel tubes, like the solutions that will be developed in the next chapter for the MobiNext scooter [24][1][27].



Figure 2.11: Classical frame of a scooter [24].

Still, on scooter models' most dominant chassis types, there is available the monocoque frame and the steel trellis frames. These models have to have certain features to be considered as scooter models, such as the fact that there is a flat platform in the centre of the scooter. However, in order to be easier to understand the type of frame solution, the pictures presented will be of standard motorcycle models [28].

Regarding the monocoque, presented in figure 2.12, this type of frame comprises two large parts, which are pressed and stamped to shape and then welded together, along the centre line of the scooter. Several opinions are made regarding this type of frame as far as its production is concerned. On the one hand, it reduces the number of individual parts needed for the frame and can be simplified so that it can quickly be produced on machines, reducing the production time. On the other hand, the monocoque can be a very complex type of frame, in which components like the seat and the fuel tank have to be structural and which is not easily accessible for maintenance. Usually, they are built in pressed steel for scooters, but for motorcycles, they were initially built in aluminium. However, with the use of composite materials, like carbon fibre, they have very high structural efficiencies [24][28][30].

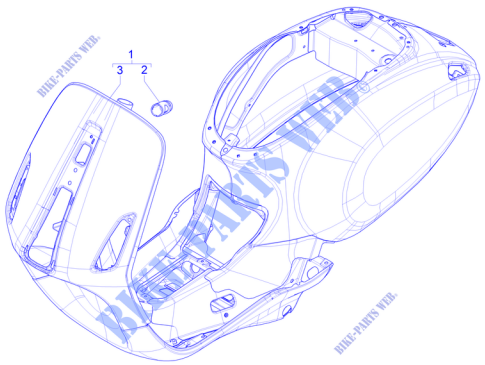


Figure 2.12: Monocoque frame of a Vespa's scooter[31].

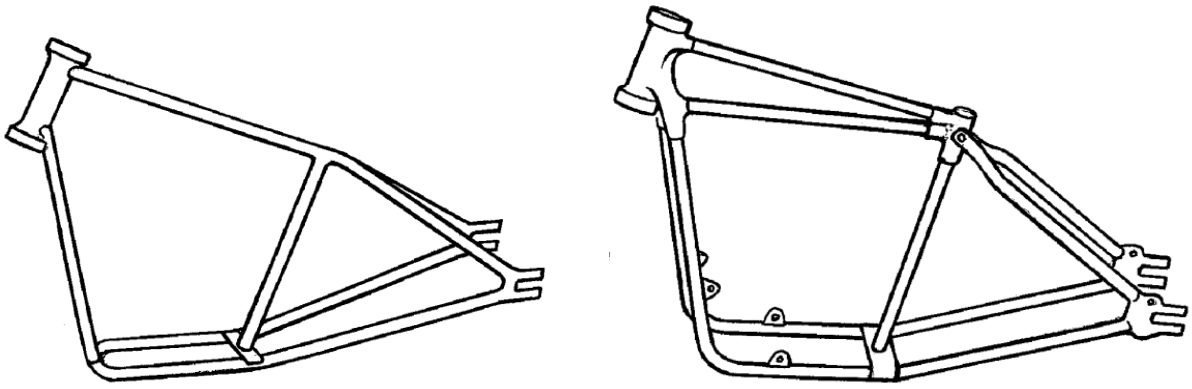
Finally, analysing the steel trellis frame, shown in figure 2.13, is a frame that connects

the steering head to the swing arm axis surrounding the engine. The unique feature of this type of frame is that it is formed by the triangulation of the round sections of steel tubes, thus presenting itself as a solution with good rigidity and structural efficiency accompanied by low weight [32][24].



Figure 2.13: The spine frame of an standard motorcycle [33].

Looking closely at the classic scooter chassis, shown in figure 2.14, we can see an evolution over the years of the connection between the chassis and steering column. This connection, on standard motorcycle frames, is divided into two types: single cradle and double cradle frame. The only difference between them is that on the single cradle, there is only one tube connected to the steering column, as shown in figure 2.14a, while on the double cradle, there are two tubes, like in figure 2.14b. This last solution is an evolution of the first, being used for more powerful and bigger motorcycles [24][27].



(a) Single cradle frame [27].

(b) Double cradle frame [27].

Figure 2.14: Two type of cradle frames.

From figure 2.15 to 2.19, the frames of the models introduced in subchapter 2.2 are presented.

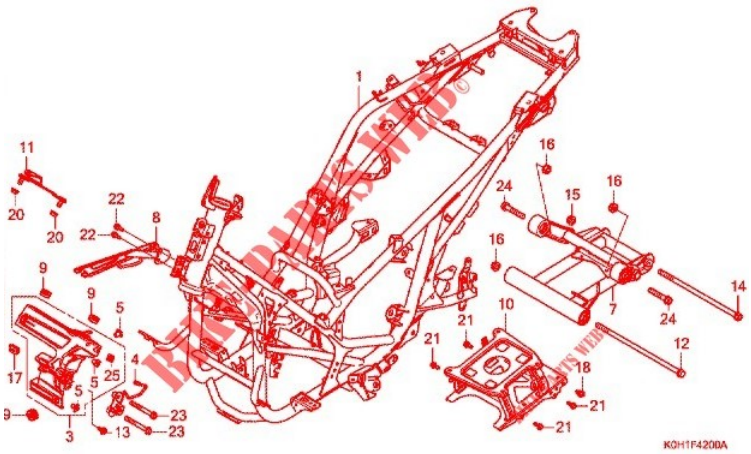
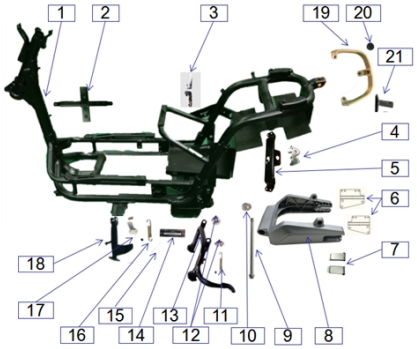
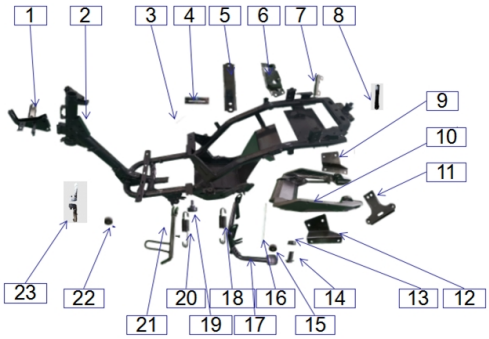


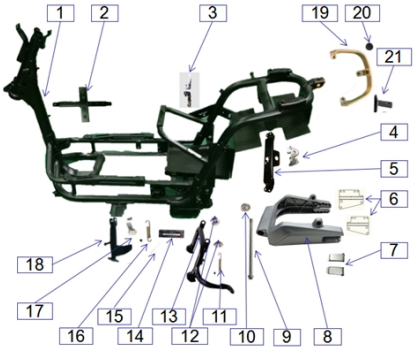
Figure 2.15: Frame of PCx electric of Honda [16].



(a) Frame of LX08 [17].



(b) Frame of LX06 [18].



(c) Frame of Yadea G5S [19].

Figure 2.16: Several frames of the Lexmoto brand.

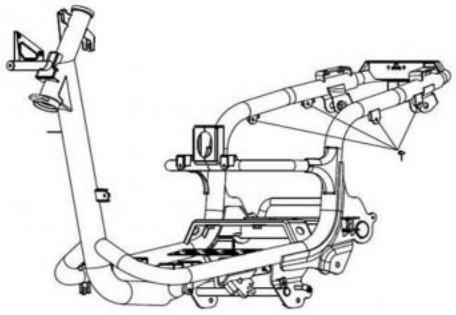
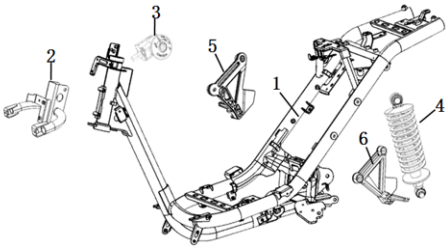


Figure 2.17: Frame of EK3 from Horwin [20].

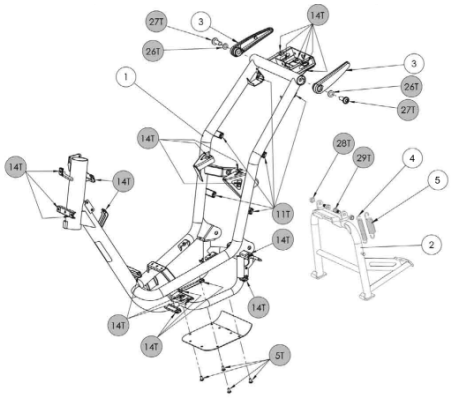


(a) in a sketch.

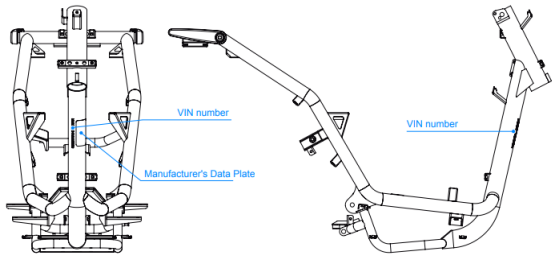


(b) in a realistic view.

Figure 2.18: Frame of CPx from Super Soco [21],



(a) in isometric view.



(b) in a front and side view.

Figure 2.19: Frame of Muvi from Torrot [22],

As can be seen by the various scooter chassis presented, all except the PCx electric model from Honda, are single cradle frames. All have only one connecting tube to the steering

column, except the PCX, which has two connecting tubes. These solutions can be justified since the double cradle frame is typically applied to larger and more powerful motorcycles, and the scooter presents itself as a smaller bike and, as analysed in the subchapter 2.2.1 of the engine analysis, less powerful.

Analysing further the rear side of the frames, it can be noted that they all present a step-like solution, which follows the shape of the rear wheel.

Chapter 3

Frame structure

In this chapter, the solutions developed for this project and the method used will be presented. For these chassis designs, it was used the SolidWorks software, a commercial program that allows the development of 3D solutions.

3.1 Methodology

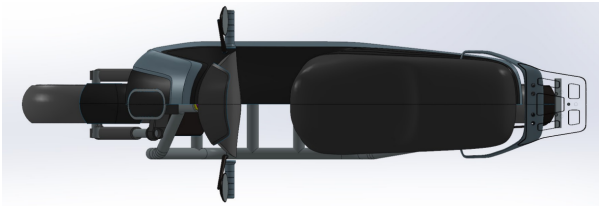
The process of creating and designing a product is an iterative process. This is caused by the different possible ways to obtain the final product and because, throughout the process, the addition of new information allows the improvement and refinery of the product. The following sections present the several iterations, developed to get the final chassis, that were designed with SolidWorks software, using mainly the extrude and sweep features.

3.2 Initial Frame

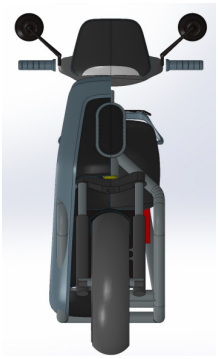
The starting point of this dissertation was the project presented in the following figure, provided by AJP. This assembly is the combined result of each company's projects.



(a) Left view.



(b) Top view.



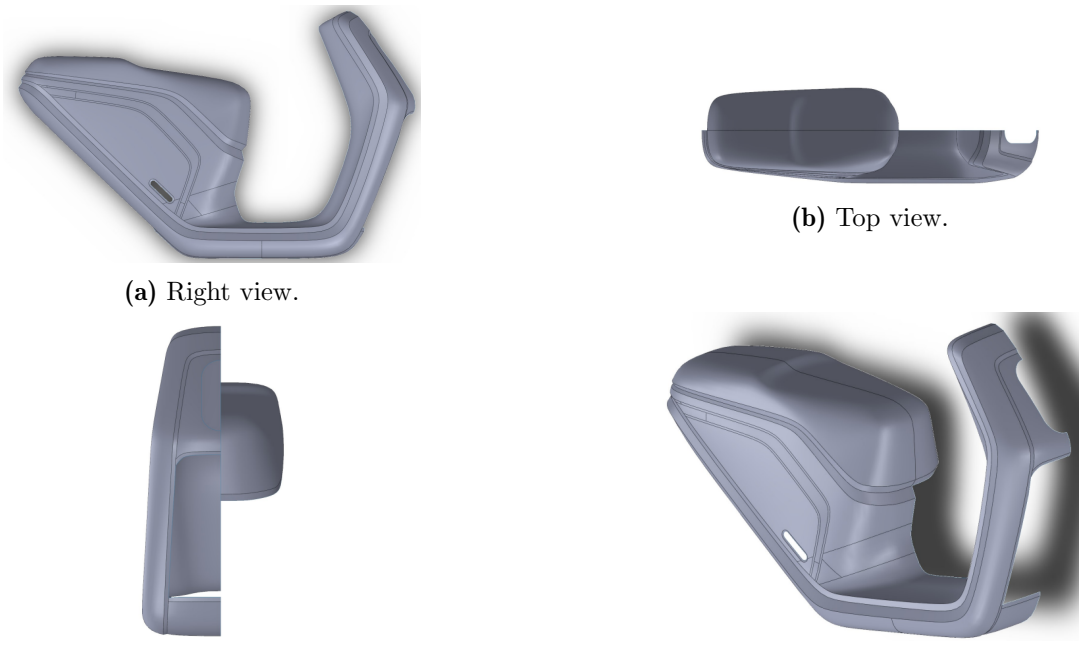
(c) Front view.



(d) Side view.

Figure 3.1: Initial project, provided by AJP, in several views.

In the figure 3.1, it is possible to see the set of several components that constitute the scooter. The exterior design, individually represented in figure 3.2, was developed by one of the consortium's companies, which was responsible for the aesthetic and ergonomic aspects of the motorcycle. This exterior design is a crucial point of this dissertation, as it serves as the basis for creating the chassis. In addition, it is also presented two batteries shown in red, the two wheels with their respective braking discs, the front fork, a shock absorber, a swingarm, and a base frame, also presented individually in figure 3.3.



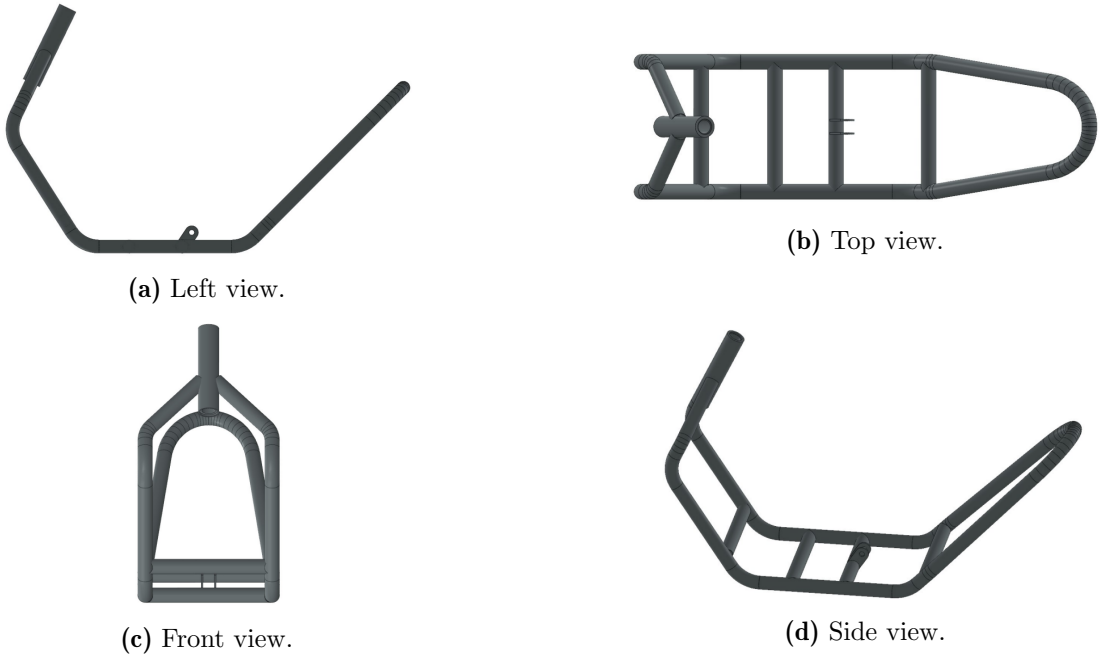
(a) Right view.

(b) Top view.

(c) Front view.

(d) Side view.

Figure 3.2: External design of the scooter, provided by AJP, in several views.



(a) Left view.

(b) Top view.

(c) Front view.

(d) Side view.

Figure 3.3: Initial frame, provided by AJP, in several views.

By analysing the chassis supplied by MobiNext, it can be highlighted that it is divided

into two main components: the main tubes and the intermediate tubes, all with a diameter of forty mm. The intermediate tubes increase the rigidity of the structure, and it is where the connections with the rest of the scooter components are placed.

Upon further analysis of the supplied assembly, it is possible to find several assembly errors. Firstly, it can be observed that some connections of intermediate tubes with the main pipes are not designed correctly, as the tubes intersect and penetrate each other. This type of error can be seen in the figure 3.4, which shows where the errors are located, as well as a zoomed-in view of the area.

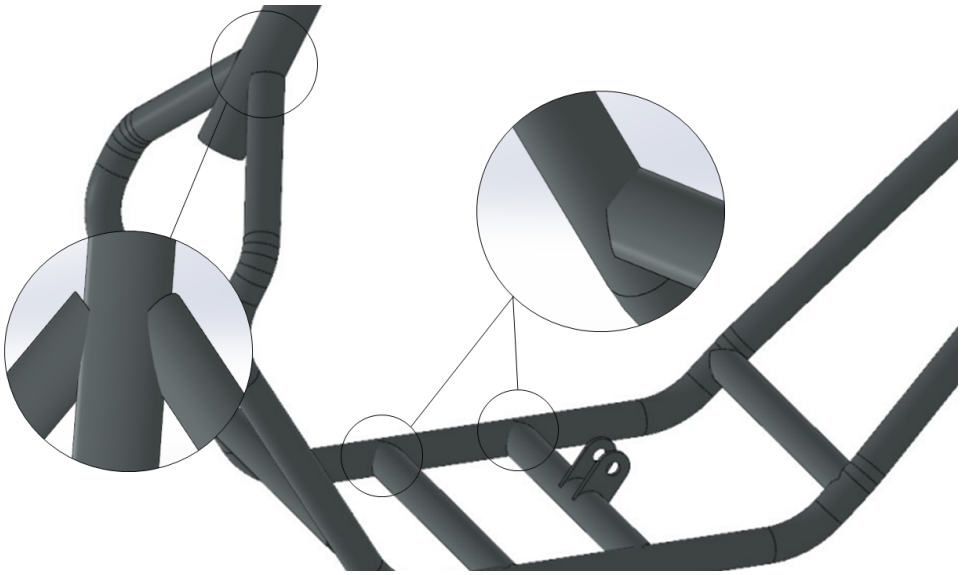
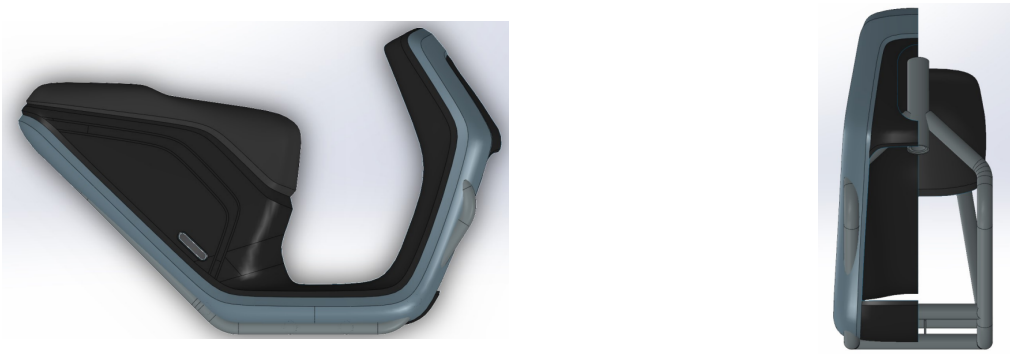


Figure 3.4: Design errors between the chassis tubes, with zoom in views.

In addition to the errors presented, the chassis also does not fit into the external design, sticking out of it, and some components intersect the frame, such as the front fork. These errors are shown in the figures 3.5 and 3.6:



(a) Left view.

(b) Front view.

Figure 3.5: Design error between the chassis and the exterior design.

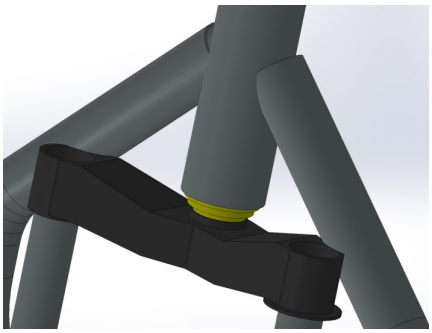


Figure 3.6: Design error between the chassis tubes and front fork.

Besides this, it is also possible to observe in the picture 3.1 that there is no support for the batteries, being placed only in a temporary location. Finally, looking at figure 3.7, which presents a zoom in view of the assembly, it is possible to note that the shock absorber is not fully designed, leaving space between this component and the respective connecting eye. Finally, in the same figure, another error present is that there is no connection between the chassis and the swingarm.

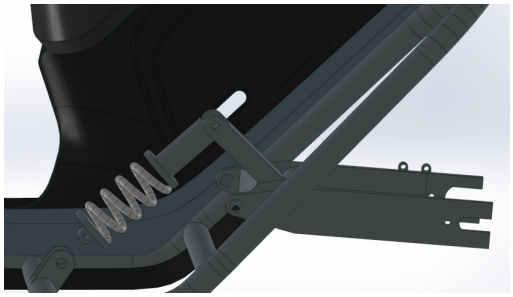
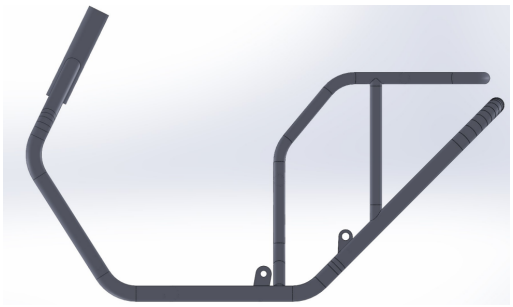


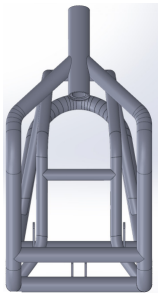
Figure 3.7: More design errors of initial project.

3.3 First Draft

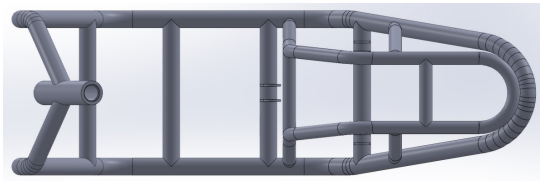
In order to start the design creation process, a first draft was drawn, taking into account that the batteries and the helmet, which will be in the compartment under the seat, need support. For that, using the base provided by AJP, the draft focus only on the rear support, in a way that it would allow supporting the equipment in separate ways, that is, with support for the two batteries and another specifically for the helmet. The designed chassis can be seen in the picture below, in several views.



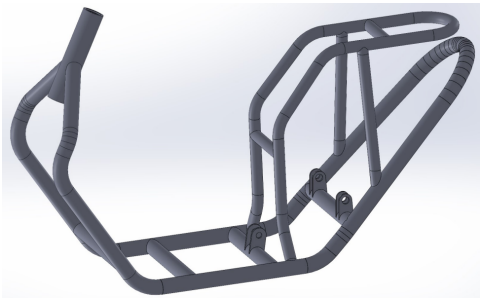
(a) Left view.



(b) Front view.



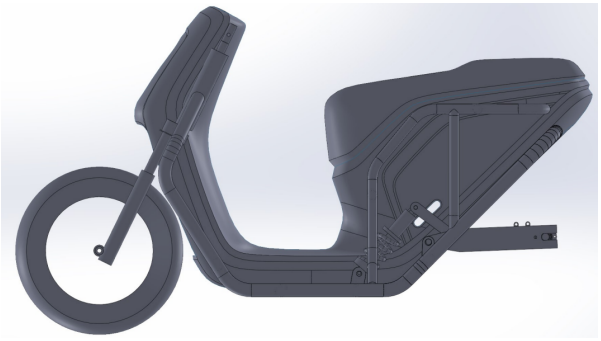
(c) Top view.



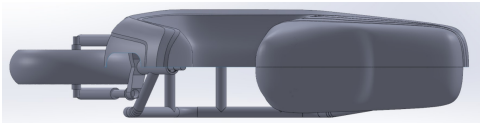
(d) Side view.

Figure 3.8: First draft of the chassis, in several views.

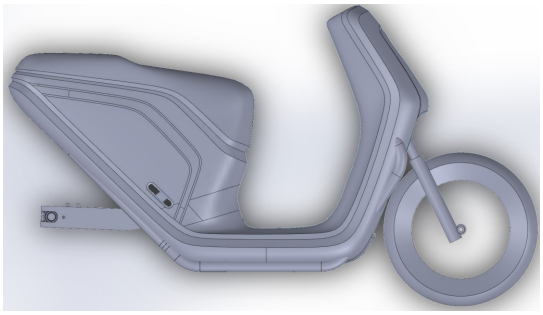
The added rear support is based on the step-type models, discussed in subchapter 2.2.7, and is made of thirty mm diameter tubes. The initial thought was to create two separate compartments to store the two batteries and the helmet and fit under the driver's seat. The following figure shows the chassis together with some major components of the design. These components are the outer design, the front fork with the front wheel, the shock absorber and the swingarm. These components were selected because each one, in its own way, interacts and influences the shape of the chassis.



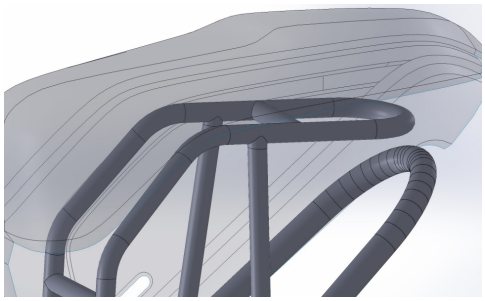
(a) Left view.



(b) Top view.



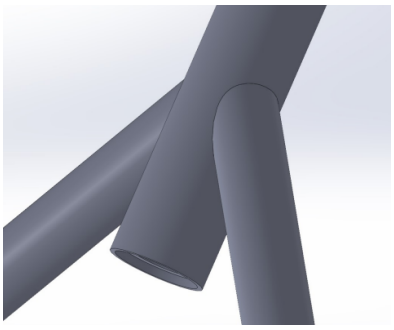
(c) Right view.



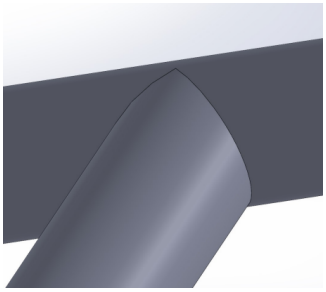
(d) zoom in view.

Figure 3.9: Assembly between the main components of the scooter and the first draft.

Besides the first idea for the back support, some errors found in the base chassis were also corrected. Namely, the connection between the tubes, both with the steering column and the main tubes, as can be seen in the pictures below.



(a) Between the chassis and the steering column.



(b) Example of the final result of the design between main and intermediate chassis tubes.

Figure 3.10: Final result of the corrections done.

The shock absorber was also corrected, considering the total length of 260 mm. Also, in the picture below, it can be seen that eyebolts were created to serve as a connection between the swingarm and the chassis. One of the fundamental points in creating the chassis

is the connections it has to make with the other components. The primary connections to consider are between the steering column and the front suspension, the connection to the shock absorber and the connection to the swing arm.

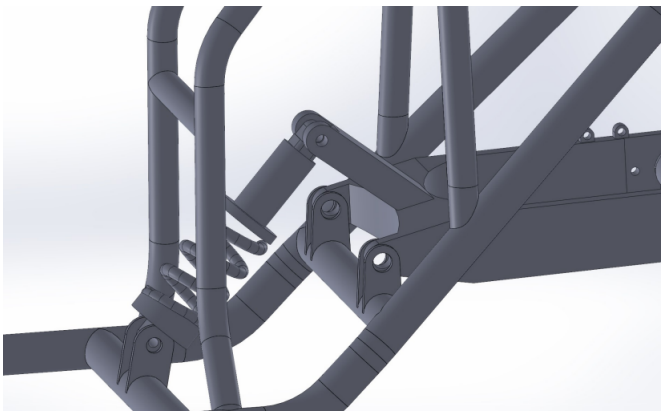
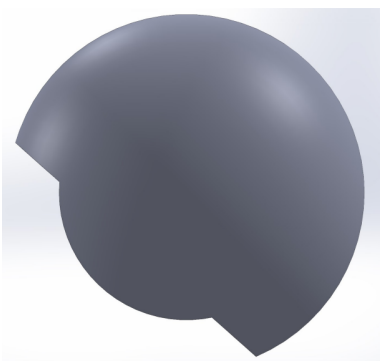


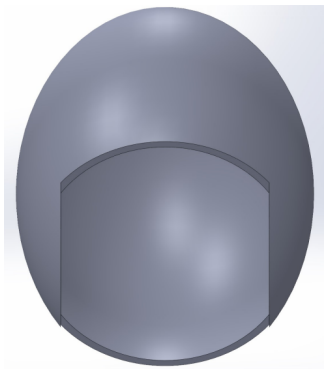
Figure 3.11: Swing arm and eyebolt corrections on the frame.

3.4 First Solution

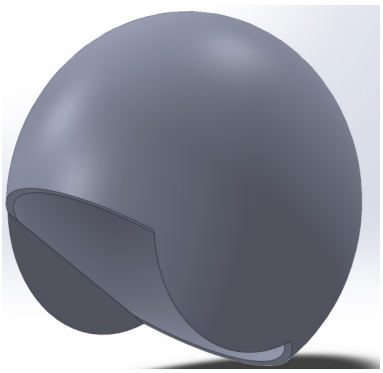
After the draft design, presented in the previous section, the support was improved in order to take into account the real dimensions of the batteries and a normal helmet. The base of the chassis has not been worked on yet, with the main focus still being on storing and supporting the batteries and the helmet. A simple helmet was designed considering that the average perimeter size of a head is about 58 mm and considering a front and back foam of 30 mm and the side foams of 8 mm. In the following figure it is possible to see the helmet designed in different perspectives [34].



(a) Left view.



(b) Front view.



(c) Side view.

Figure 3.12: Simplified drawing of a helmet, in several views.

In addition to the upgrade given to the chassis, two boxes were also designed to serve as storage for the two batteries and the helmet. These boxes, shown in the pictures below, have the dimensions required to fit the new support and are made of one mm welded sheet metal.

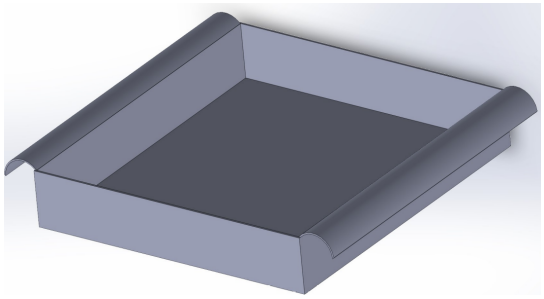


Figure 3.13: Battery support box.

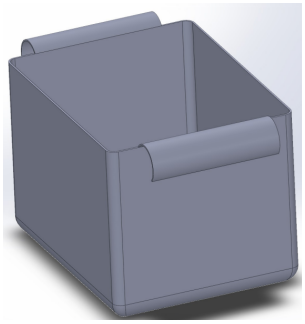
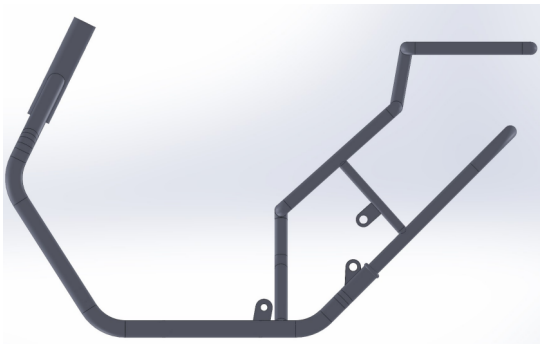
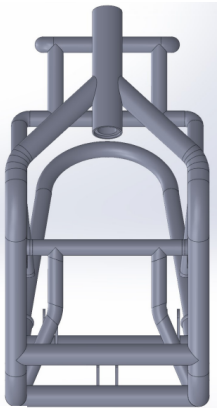


Figure 3.14: Helmet support box.

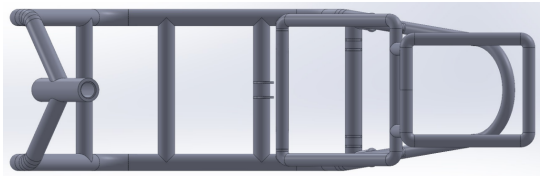
Finally, the chassis obtained, with the new support, is shown in the figure 3.15 in several views:



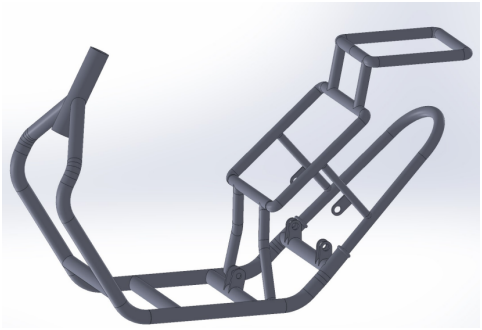
(a) Left view.



(b) Front view.



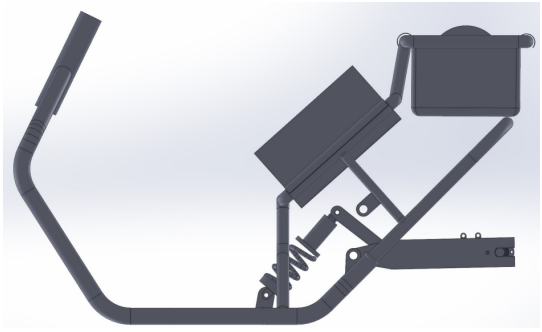
(c) Top view.



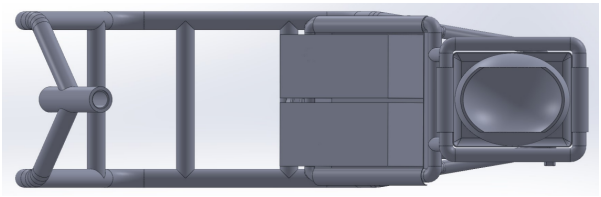
(d) Side view.

Figure 3.15: First solution for the scooter's frame.

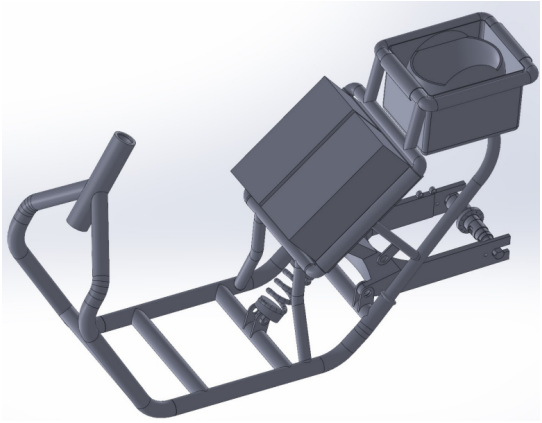
As can be observed, the step effect, initially thought of in the draft, is still used. However, the storage space, under the seat, has been enlarged and standardised in order to be able to fit the designed boxes. The picture 3.16 shows the frame assembly with the batteries and the simple helmet inside their respective boxes and other scooter components.



(a) Left view.



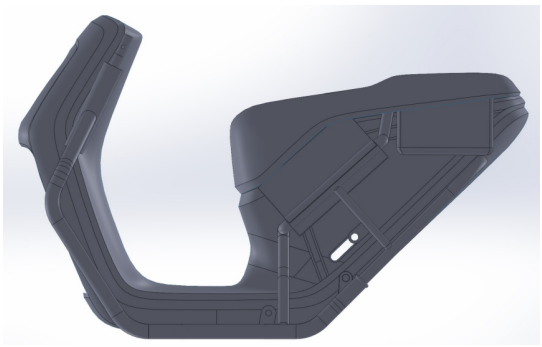
(b) Top view.



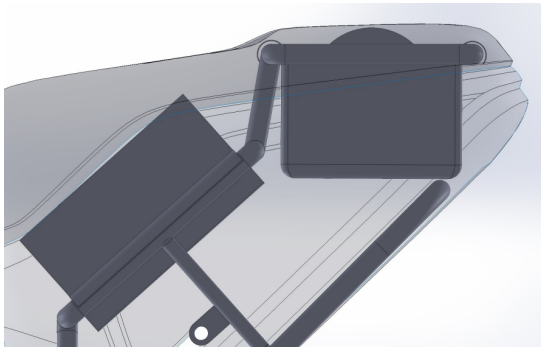
(c) Side view.

Figure 3.16: Assembly between the first solution, the storage boxes, the batteries and the helmet.

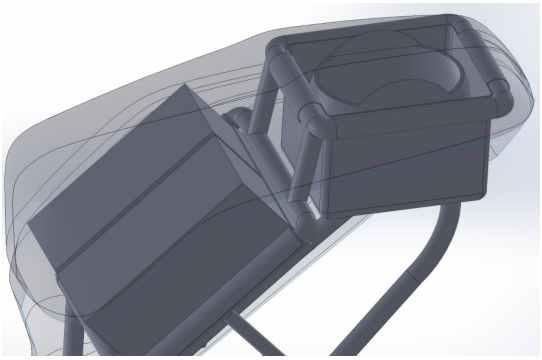
In order to confirm that this solution fitted the exterior design, it was added to the project and attached to the frame. As shown in figure 3.17, the lower part of the chassis still does not fit with the exterior, but the added support do, as do the boxes, the batteries and the helmet. One principle used for developing this support, which will be used afterwards, was considering that there is a gap of five mm, between the support and the exterior sheeting of the scooter body. That means, besides the design not being allowed to penetrate the outer layer, it was also necessary to leave a space of at least five mm with the interior components of the scooter. Regarding the helmet storage, it was necessary to adjust the helmet box so that it would not penetrate the bottom of the chassis but also so that the helmet would fit in the box without intercepting the 5mm thick space of the outer plate.



(a) Left view.



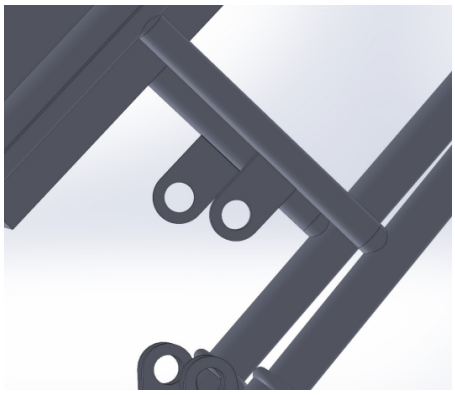
(b) Left view, with more detail.



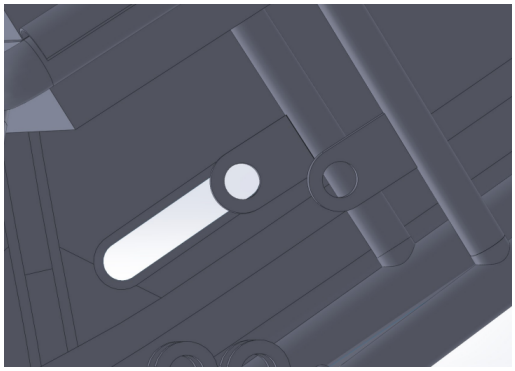
(c) Side view.

Figure 3.17: Assembly between the first solution and the exterior design.

Finally, in the following picture, it is shown another detail added to this solution: the design of the eyebolts that serve as a connection to the passenger's footrest. The location of these took into account the exterior design, which already had a specific place for this function.



(a) View with only the chassis.



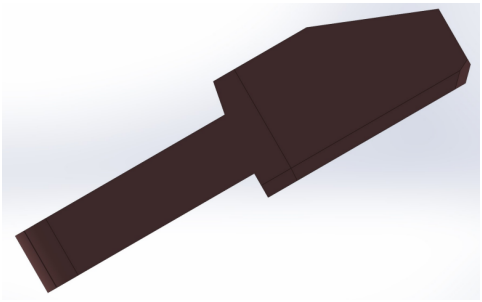
(b) View with the exterior design.

Figure 3.18: Footrest connection eyebolts.

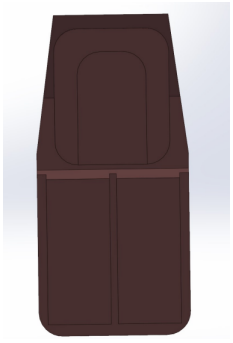
3.5 Second Solution

3.5.1 Storage Box and static prototype

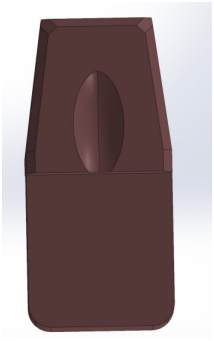
The second solution was created due to the addition of new information provided by AJP. The company suggested that the storage of the batteries and the helmet should be sustained with only one support and provided the draft shown in the following figure. This box serves as a support for the batteries, in the front, and the helmet, in the back. Despite being a draft idea, it was an important element for the design of following solutions.



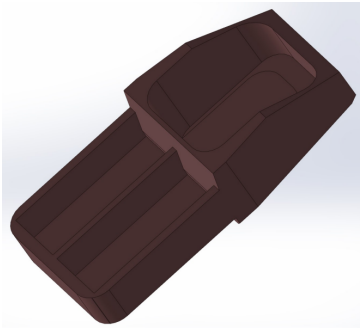
(a) Left view.



(b) Top view.



(c) Bottom view.



(d) Side view.

Figure 3.19: Storage box, provided by AJP, in different views.

In the MobiNext project plan, AJP committed to develop two models of the scooter, these being: a static prototype and a prototype capable of driving and holding a driver. The static prototype was built while this dissertation was being developed, and the author had the opportunity to help in the prototype development. As can be observed in the following figure, the prototype did not include a functional chassis, and everything was just connected with machined and bent aluminium plates, all connected by screws. This structure is shown in detail in figure 3.21. Furthermore, it is possible to see that the exterior design was developed by 3D printing, in smaller separate parts, and that a prototype of the storage box was built, as shown in the figure 3.22.



Figure 3.20: Construction of the static prototype.



(a) Left view.



(b) Front view.

Figure 3.21: Prototype's structure.

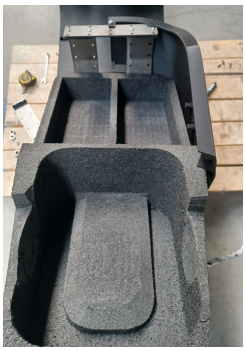


Figure 3.22: Prototype of the storage box.

Finally, the prototype was presented at the Expomoto exhibition in May 2022, where AJP presented to the public the first prototype of the MobiNext. In the following pictures is presented the final look of the scooter.



(a) General view.

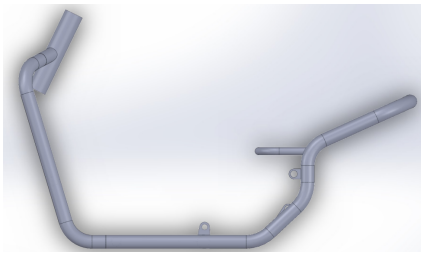


(b) Prototype box with the batteries and the helmet.

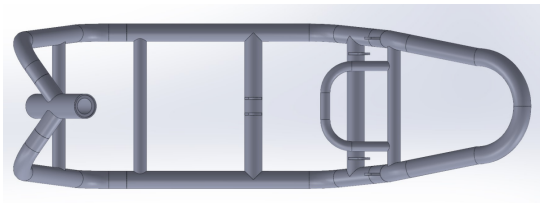
Figure 3.23: First prototype of the scooter, in Expomoto.

3.5.2 Second Solution Frame

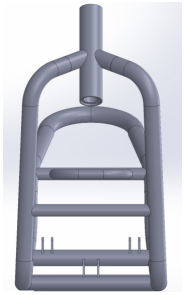
Figure 3.24 presents the newly developed chassis that considers the presented storage box. Besides the different back support, the main frame was also modified to fit the exterior design, as it is possible to observe in figure 3.25, correcting another mistake previously mentioned. For this change, and as already mentioned, it was taken into consideration that the exterior design has a thickness of five mm. With the storage box added and after reviewing the chassis designs on the market, presented in subchapter 2.2.7, a shorter, single-step-type rear solution was chosen. This solution makes the rear area more balanced and less overhanging.



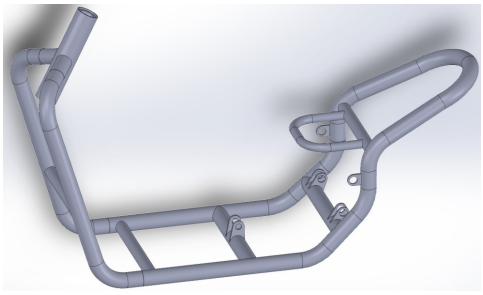
(a) Left view.



(b) Top view.

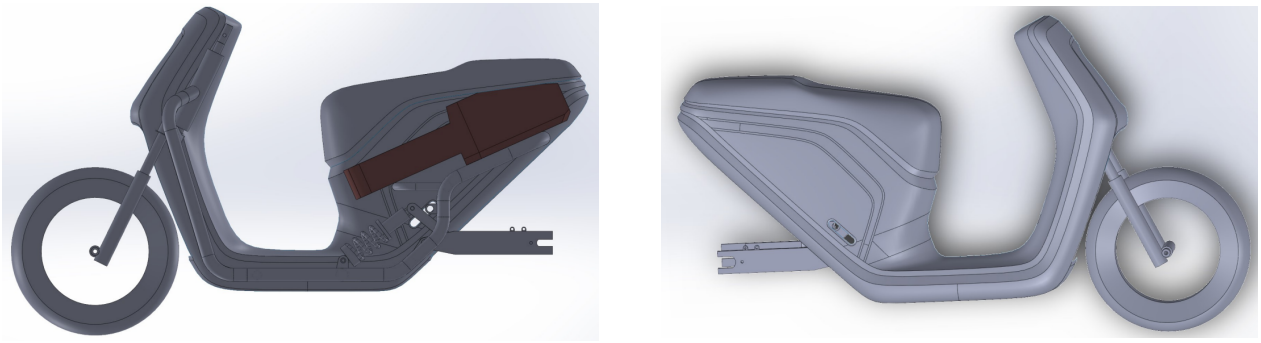


(c) Front view.



(d) Side view.

Figure 3.24: Second solution for the scooter's frame.



(a) Left view. **(b)** Left view.

Figure 3.25: Assembly of the second solution.

In order to show in more detail the support developed, a zoom in view of the support is shown in the following figure. In addition, figure 3.27 shows the support together with the storage box and the exterior design.

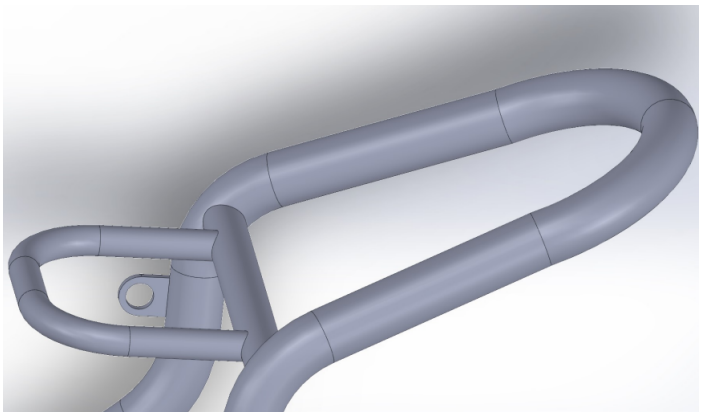
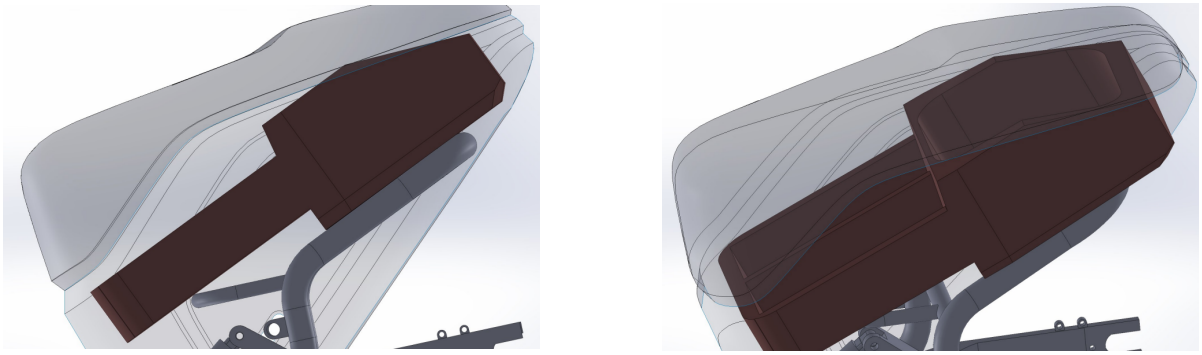


Figure 3.26: Zoom in view of the new support.

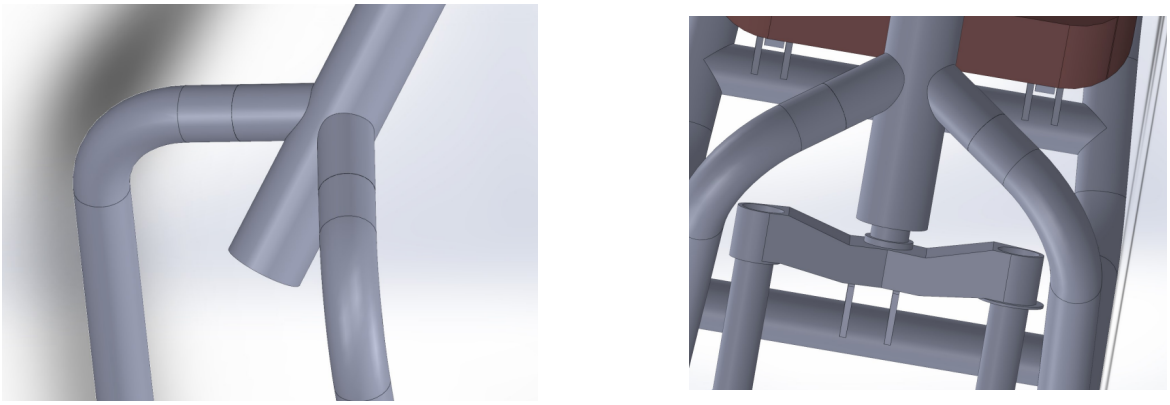


(a) Left view. **(b)** Side view.

Figure 3.27: Support, of the second solution, with the storage box.

As can be observed, the support is designed to support the storage box from below and is composed of three tubes of different diameters: the forty mm tube that continues the frame, the intermediate thirty mm tube, and the extra support, which supports the front part of the box, that is formed by a twenty mm tube.

In addition to the corrected error, shown in figure 3.25, the chassis was also changed so that the front fork does not intersect the main tubes. The main solution of using two tubes connecting to the steering column was preserved, as was the diameter of the tubes. However, the bending radius of the pipes was increased to make space for the fork. This correction is shown in detail in the following figure.



(a) View with frame only.

(b) View with the front fork.

Figure 3.28: Error between the steering column and the main frame tubes corrected.

3.6 Third Solution

After several solutions focusing only on the rear support, a third solution was developed with the aim of creating an alternative steering column connection. In the models presented in the subchapter 2.2.7, it is possible to see that many of them use a single cradle frame solution, thus presenting only one connection tube to the steering column. Therefore, one of the points of differentiation of this third solution would be using only one tube as a connector. Moreover, after observing the scooter presented in figure 3.29, which was available in the laboratories of the mechanical engineering department, it was possible to come up with a new solution for connecting the main frame with the rest of the structure. The scooter evaluated was a Piaggio Liberty 50cc.



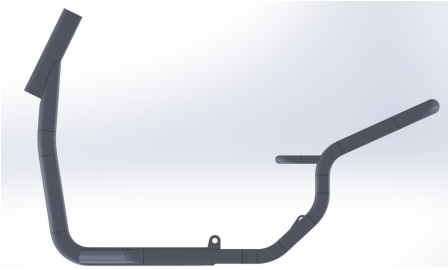
(a) General view [35].



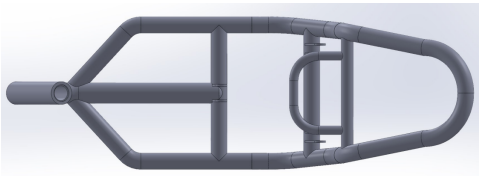
(b) View with more detail on the frame.

Figure 3.29: Scooter available in DEMEC's laboratories.

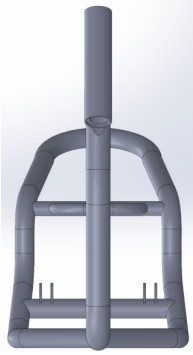
By analysing the figure 3.29, it can be noted that the connection to the steering column is made by a central tube with a larger diameter and which extends to the lower part of the frame. Furthermore, in the flat area of the scooter, two additional pipes are connected to the main tube and constitute the rear part of the frame. The solution shown in figure 3.30 was developed based on this scooter.



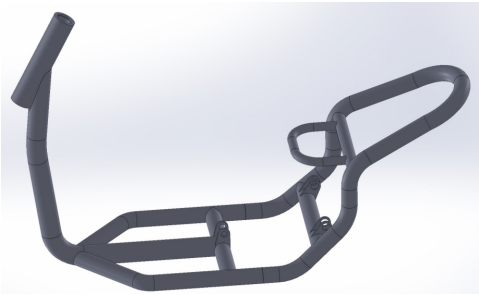
(a) Left view.



(b) Top view.



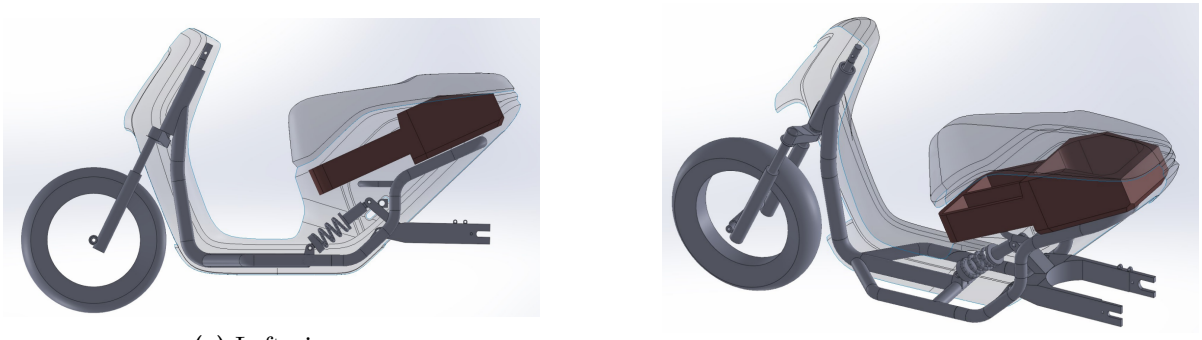
(c) Front view.



(d) Side view.

Figure 3.30: Frame of the third solution.

This chassis combines a new front solution and the back support developed in solution two. As mentioned, the front support consists of the main tube, with fifty mm of diameter, and two side tubes, with forty mm of diameter, which make up the rest of the structure. Therefore, the front area of the structure changes from a two-tube solution to just one, preventing the fork from intersecting the chassis. Figure 3.31 shows the new chassis together with the rest of the scooter components.



(a) Left view.

(b) Side view.

Figure 3.31: Combination of the new solution with the rest of the scooter components.

One of the main problems of this front solution was the connection with the steering column, which, as it is possible to see, cannot have a higher connection as it would clash with the exterior design. Besides that, it was also necessary to find a solution to make the connection between the middle and intermediate pipes, since they have entirely different diameters. The solution, represented in figure 3.32, was to extend the middle pipe to the intermediate tube and add a piece of material to represent the weld that would be made on the area.



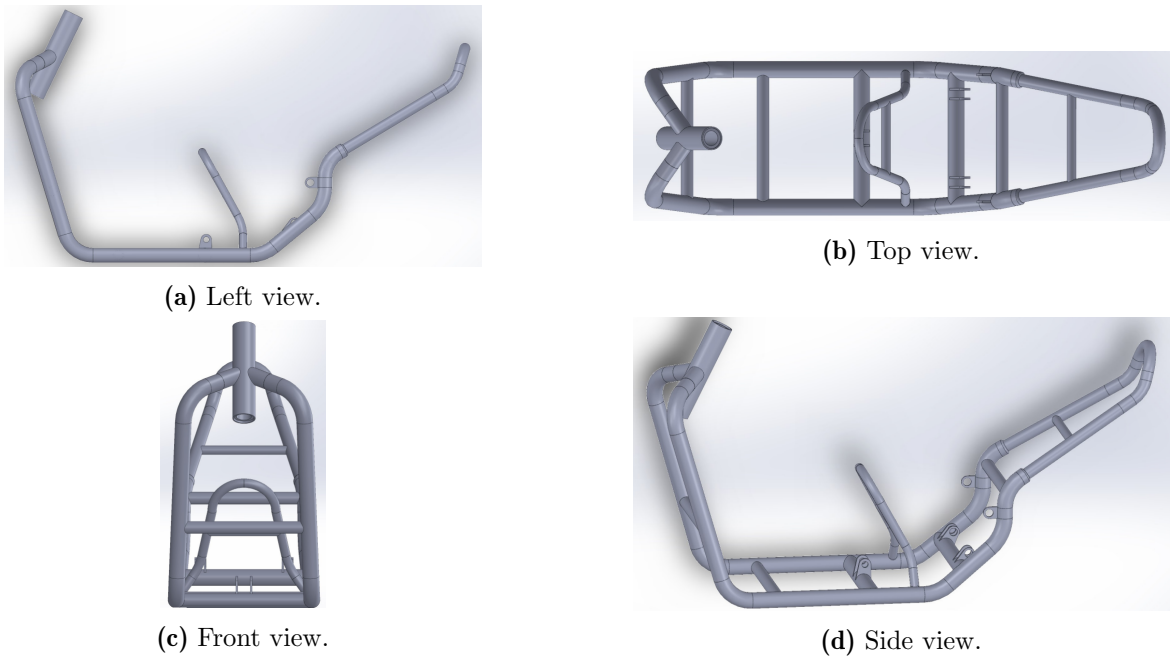
(a) Before correction.

(b) After correction.

Figure 3.32: Connection between the main and intermediate tubes.

3.7 Fourth Solution

The solution presented in this subchapter was developed due to new information from AJP. The company requested that the chassis would be extended to the driver's seat area, in order to provide support for the hinges that allow the seat cover to open. Therefore, returning to the double front tube solution, new rear support was developed, as shown in figure 3.33.



(a) Left view.

(b) Top view.

(c) Front view.

(d) Side view.

Figure 3.33: Frame of the fourth solution.

The new solution for the rear support consists of two main parts: an extended part, which connects to the back of the seat, made up of two types of diameters, and a part that serves as the front support for the storage box, with twenty mm diameter tubes. In order to increase the rigidity of this part, an intermediate tube was added. Regarding the main section of the support, it still follows a step model, but it is extended to the upper area of the scooter. Between the side tubes, there are intermediate tubes, with thirty and twenty mm of diameter, to reinforce and give rigidity to the structure. However, in order to prevent the weight of the chassis from increasing too much, and considering that the rear part of the frame does not have to be as rigid, the support was designed by joining tubes of different diameters. A smaller diameter tube of thirty mm was used at the back, and some material was added between the tubes to represent the welding. This detail is shown in the following figure:

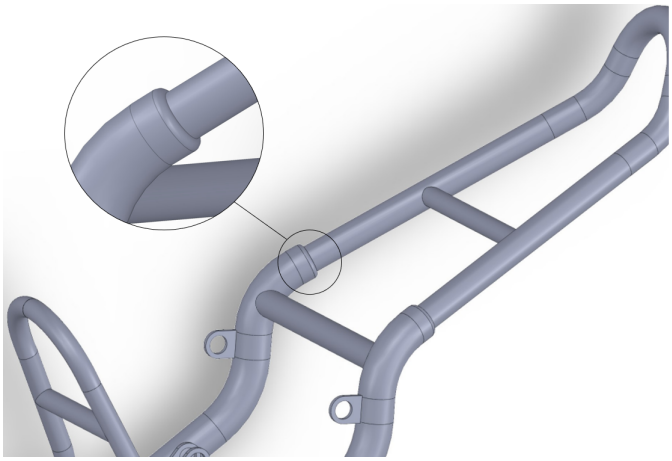
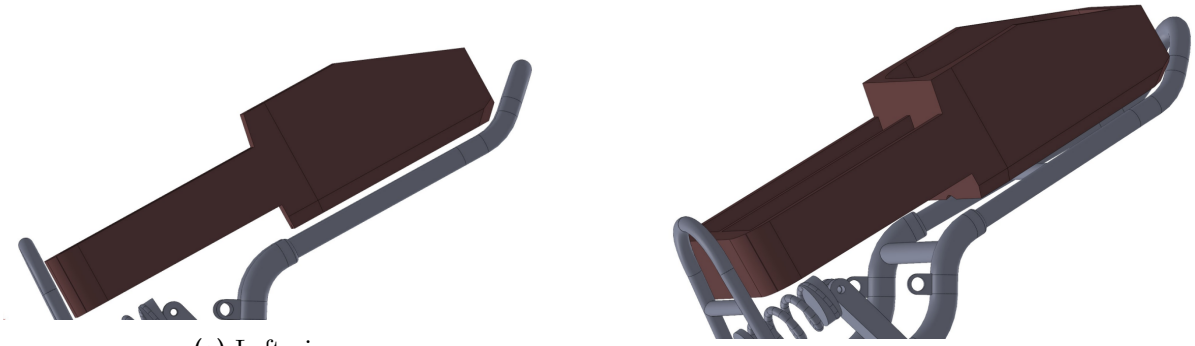


Figure 3.34: Connection between two tubes of different diameters.

The picture 3.35 shows the new holder together with the storage box. As can be seen, the box fits perfectly in the support, thus having a bottom and front support. An alternative, so that the back area would not have the extreme curve at the end of the box, was to draw the tubes through the side of the box and not underneath. However, there is not enough space between the box and the exterior design to fit the frame.

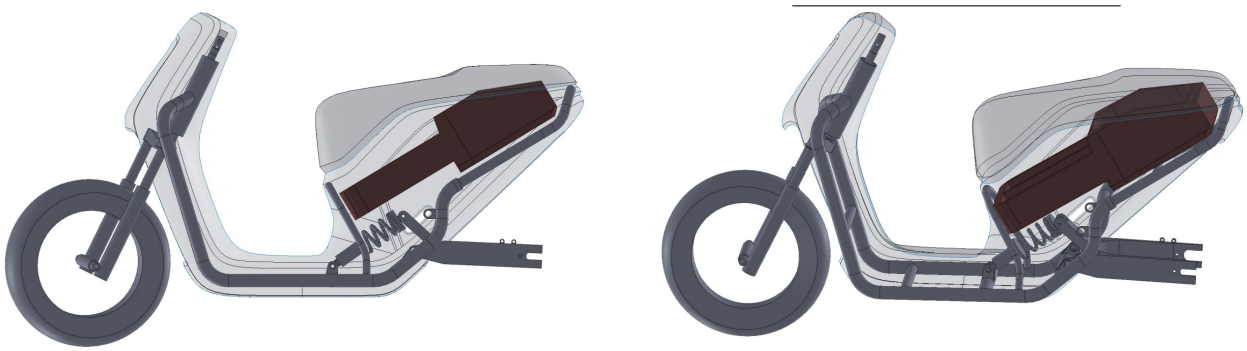


(a) Left view.

(b) Side view.

Figure 3.35: Rear frame assembly with the storage box.

Figure 3.36 shows the set of all the main components of the scooter. The figure shows that the new support's objective has been achieved since it extends to the rear area of the seat where hinges can be placed. In addition, it is also possible to place hinges on the front of the seat since the chassis was also designed to reach that area.

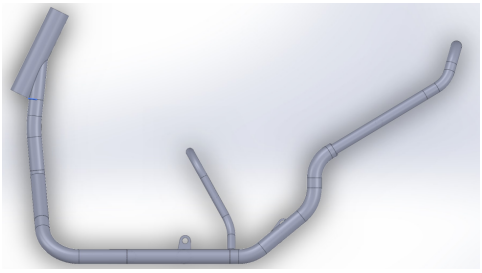


(a) Left view. **(b)** Side view.

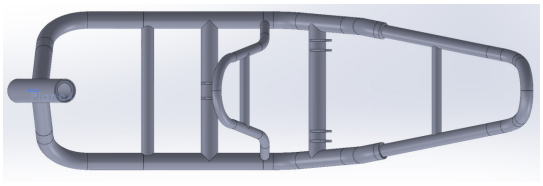
Figure 3.36: Assembly between the fourth solution and main components.

3.8 Fifth Solution

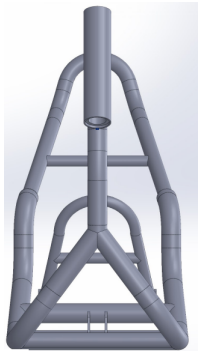
By examining the single cradle frame types in more detail, it was possible to develop a new rearrangement for the front part of the chassis. Similarly to the third solution presented in subchapter 3.6, this solution also features only one connecting tube between the frame and the steering column. However, this solution is inspired by the frames of the Horwin, Super Soco, and Torrot models, shown in figures 2.17, 2.18 and 2.19, where the junction of the side tubes with the main tube is still located in the front area of the frame and not in the lower area. Based on these models, a frame was designed in which the main tube, of forty mm, bifurcates into two main tubes, as can be seen in the figure below.



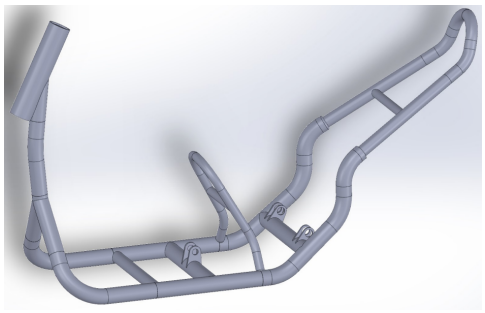
(a) Left view.



(b) Top view.



(c) Front view.



(d) Side view.

Figure 3.37: Frame of the fifth solution.

Figure 3.38 shows the assembly between the new solution with the remaining scooter components.

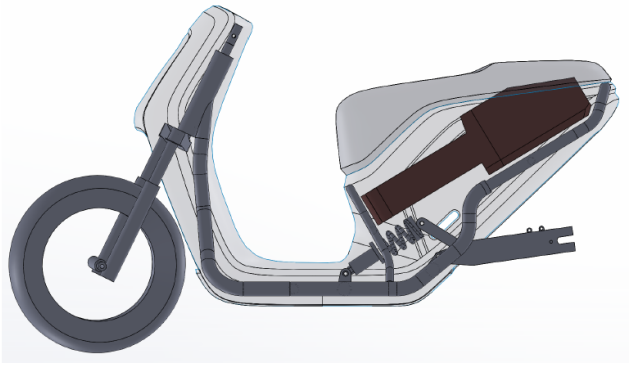
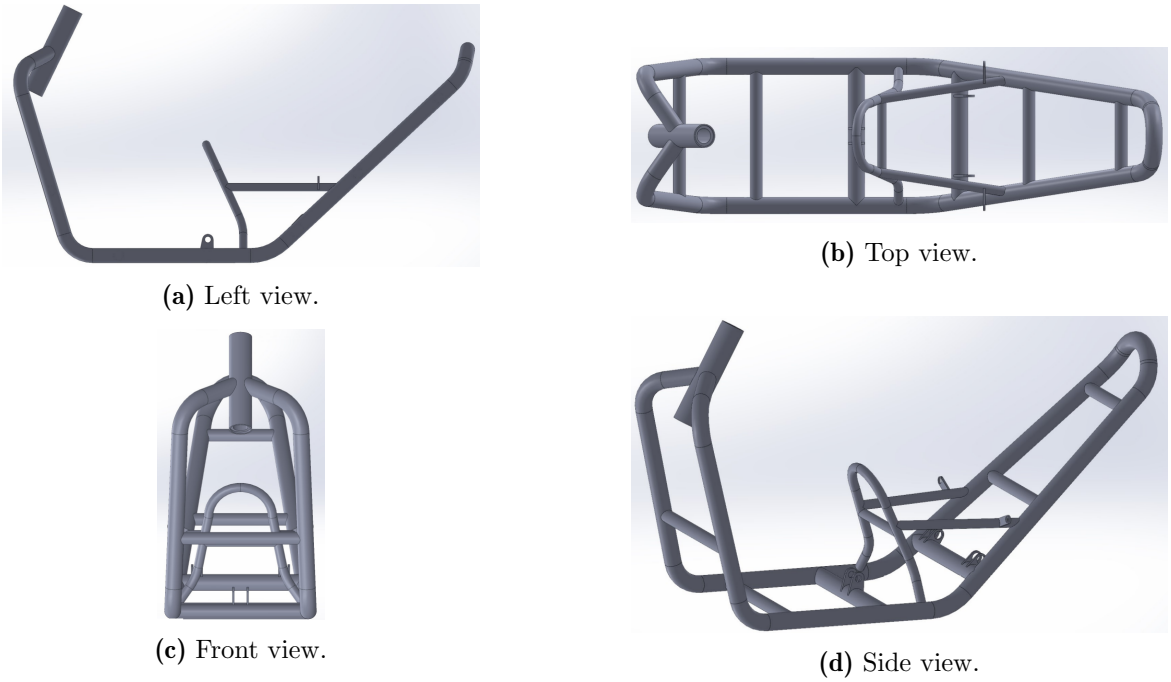


Figure 3.38: Right view of the assembly between the fifth solution and the main components of the scooter.

3.9 Sixth, seventh and eighth Solutions

After developing several frame solutions for the MobiNext scooter, the best front and rear supports were chosen. Regarding the front area of the frame, the three main ideas

presented in solution two(based on the original frame provided by AJP), solution three, and solution five were considered. These were incorporated in the next three frames presented in figures 3.39, 3.41 and 3.40. To integrate the back area of the three frames, a simplified solution of the one presented in the fourth frame was selected. As displayed in the figures below, the rear support was simplified without the need to follow a step model, and two intermediate tubes were added to the frame in order to increase the stiffness and strength to bending of the rear part. In addition, on these two tubes were also added the necessary eyebolts for the connection with the passenger footrest.



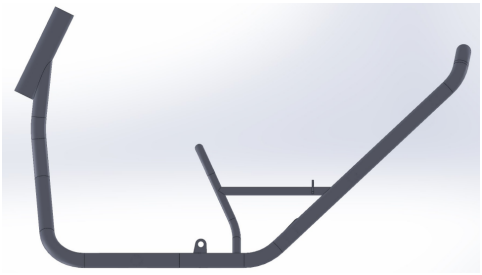
(a) Left view.

(b) Top view.

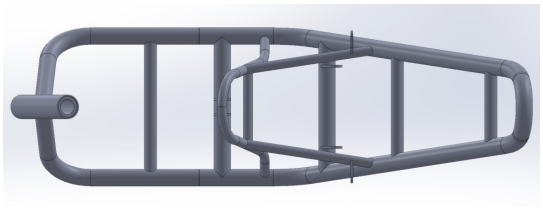
(c) Front view.

(d) Side view.

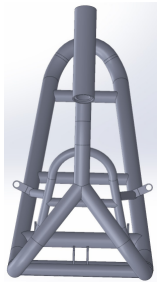
Figure 3.39: Frame of the sixth solution.



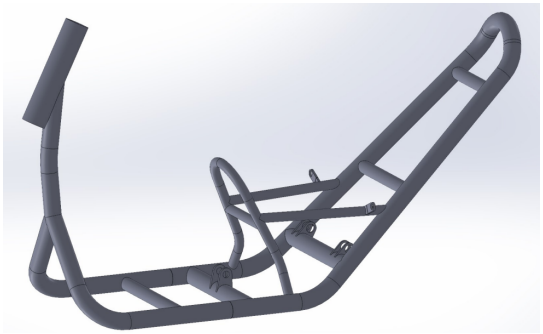
(a) Left view.



(b) Top view.

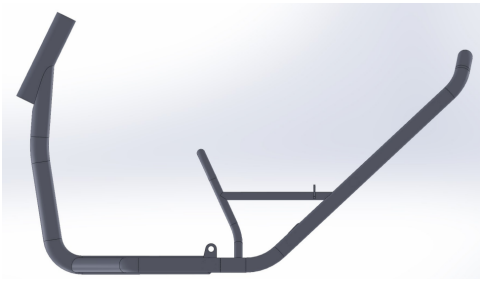


(c) Front view.

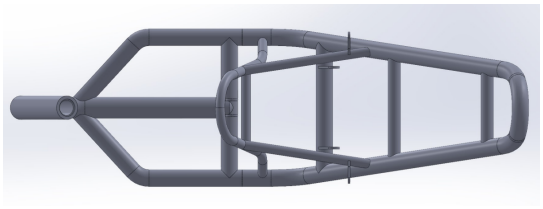


(d) Side view.

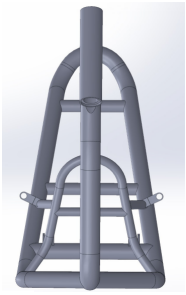
Figure 3.40: Frame of the seventh solution.



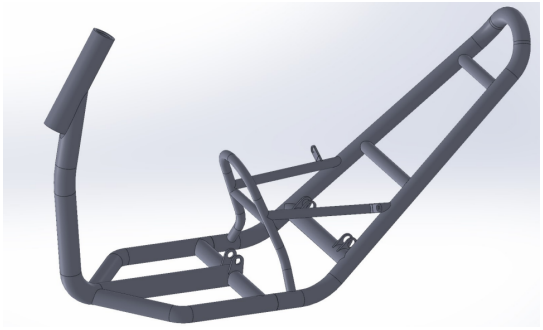
(a) Left view.



(b) Top view.



(c) Front view.



(d) Side view.

Figure 3.41: Frame of the eighth solution.

3.10 Extra Solution

In order to lower the center of gravity of the scooter, to increase the stability, an alternative location for the batteries was thought out. One of the most suitable spaces would be under the driver's feet, in the flat area of the scooter. However, after several attempts it was not possible to proceed with this solution for several reasons.

Firstly, taking into account the dimensions of the batteries, no configuration fits in place without intersecting the scooter body design or the frame. The only possible solution would be the one represented in the figure 3.42, since it allows enough spacing for the chassis to go sideways to the batteries without intersecting the exterior design. However, the height of the batteries would lead to the necessary design change, raising the flat part of the scooter.

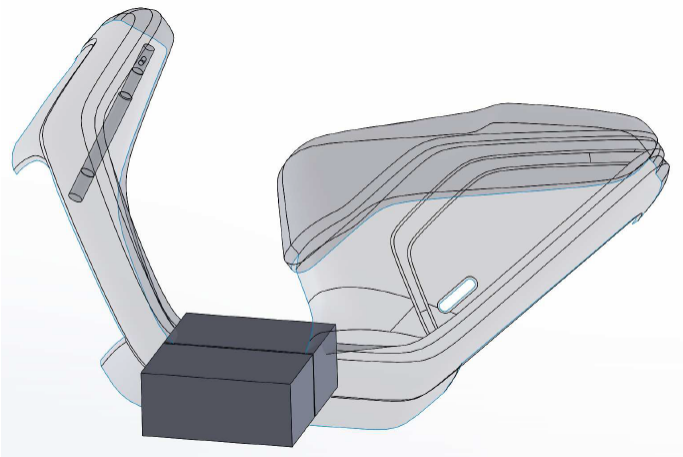


Figure 3.42: Possible configuration for the batteries.

However, another reason that makes this kind of change impossible is that the battery handles have a grip direction that does not allow the configuration shown above. As shown in the picture 3.43, the handles of the batteries, highlighter in red, must face upwards in order to fulfil their function.

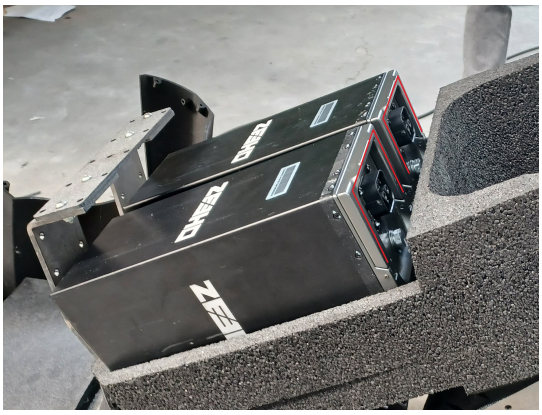


Figure 3.43: Direction of the battery grips.

However, with the suggested configuration, they would be facing sideways, either towards the motorcycle's outside or the inside. So there would be two not very practical alternatives. The first would be for the batteries to be accessed through the side of the bike, which would not be functional. The other solution would be to use a cover on the scooter's flat area, which opens upwards. However, there would have to be a functional box that allows the batteries to be lifted and taken out of place, and only afterwards use the handles to take them out of the extra box. Therefore, a solution using the batteries in a lower location was not pursued.

Chapter 4

FEM Analysis

In order to analyse the structural stiffness of the solutions presented and find possible critical points, the finite element method was applied, using the Abaqus software. In this chapter, it is presented the method followed, the material used and the forces and boundary conditions considered.

4.1 Methodology

Three solutions presented in the previous chapter were chosen to perform the structural analysis, via the Abaqus software. These had to be converted and imported into the software. Since the conversion from SolidWorks to Abaqus does not produce the product strictly as required, it was necessary to rearrange some surfaces, taking the opportunity to perform the necessary partitions to create a good mesh. In order to simplify and decrease the computational power of each simulation and considering that the solutions and the applied forces are symmetrical, the solutions were worked using only half of the structure, as will be demonstrated in the next subchapters.

After creating the mesh and applying all the forces and boundary conditions, properly explained in the subchapters 4.5 and 4.6, it was possible to obtain simulation results. All simulations were created with static, full analysis, jobs that do not consider the plastic deformation of the solution. After evaluating these results, an iterative process of changing some characteristics of the solutions or adding structural reinforcements, in the locations of higher stresses, was initiated.

These structural reinforcements were first tested on only one solution, and after finding the best results, they were imposed on the other two solutions. In order to simplify the process of reaching the best solution, it was assumed that the reinforcements used for one solution would also be the most suitable for the other solutions.

To evaluate the viability of the solutions and also to have a term of comparison between the results obtained, the von Mises stresses are used.

4.2 Material

Initially, the two main constructive solutions, thought by AJP, for this project were using welded tubular steel structures or aluminium, through sand casting. For this dissertation, AJP requested the development of a chassis with a tubular steel structure.

Steel is one of the most widely used materials for the construction of motorcycle components, whether in sheet or tube form. In addition to the relatively low price of this material, as the young's modulus is relatively high, the required stiffness can be obtained with small tube sizes. Therefore, the material initially used for this project would be the structural steel S235. This steel is also designed by EN 10025, according to the European standard, and the properties of this material can be found in annex 7.9, however the main mechanical properties can be found in the following table: [27]

Table 4.1: Main properties of S235 steel [36]

Density $[kg\,m^{-3}]$	Young's Modulus $[GPa]$	Poisson's Ratio	Yield Strength $[MPa]$	Tensile Strength $[MPa]$
7810 - 7890	205 - 215	0,3	235 - 274	360 - 510

This steel is a structural steel that presents a low percentage of carbon which favours welding and malleability, making it easy to form into shape. In addiction, it also presents good impact resistance, good ductility and machinability [25].

After some simulations, it was necessary to change the material to the structural steel S355, since it does not present great differences in price, but has better mechanical properties, like a relatively higher Yield Strength than the S235 steel. The properties of this material can be found in Annex 7.10, of which the main ones have been highlighted in the following table:

Table 4.2: Main properties of S355 steel [36]

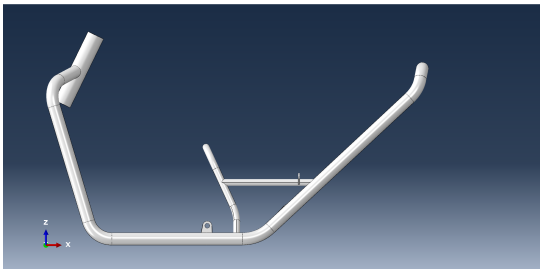
Density $[kg\,m^{-3}]$	Young's Modulus $[GPa]$	Poisson's Ratio	Yield Strength $[MPa]$	Tensile Strength $[MPa]$
7830 - 7840	205 - 215	0,3	355 - 414	470 - 680

Analysing the material presented in the previous table, it is possible to verify that the Yield and tensile strength are slightly higher in relation to the properties of the S235 steel. Therefore, it is possible to maintain the good qualities of the S235 steel, such as weldability, and increase in mechanical strength.

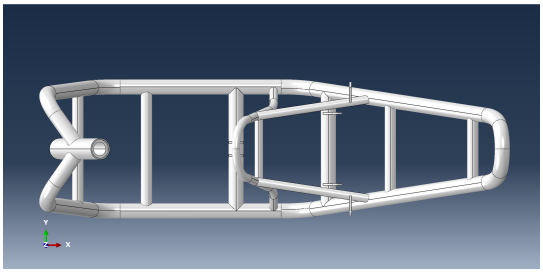
As the tables present ranges of possible values, which for example can vary with temperature, the lowest values of each parameter have been chosen so that the process runs safely. For example, the density chosen for S355 steel was 7830 kg m^{-3}.

4.3 Selected solutions

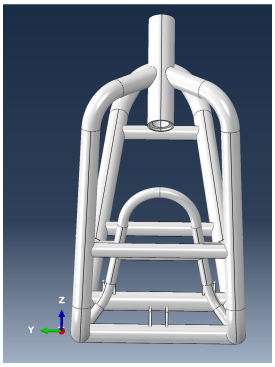
From the solutions developed in chapter 3, the sixth, seventh and eighth solutions were chosen to perform the structural evaluation using the finite element method. The following figures 4.1, 4.2 and 4.3, present the solutions chosen in Abaqus software, in different views.



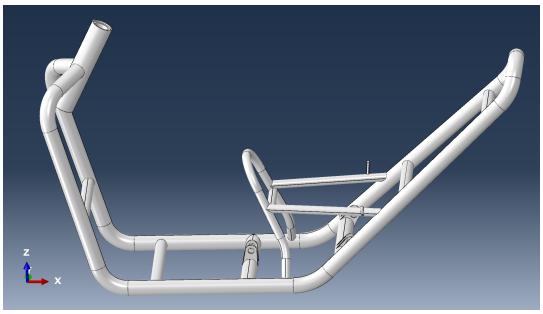
(a) Left view.



(b) Top view.

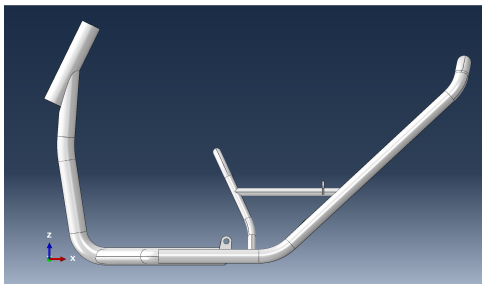


(c) Front view.

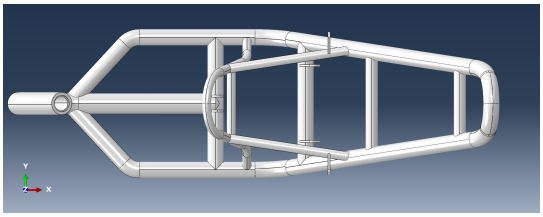


(d) Side view.

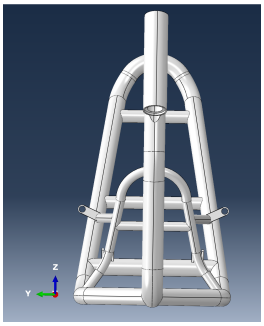
Figure 4.1: Solution six in multiple views.



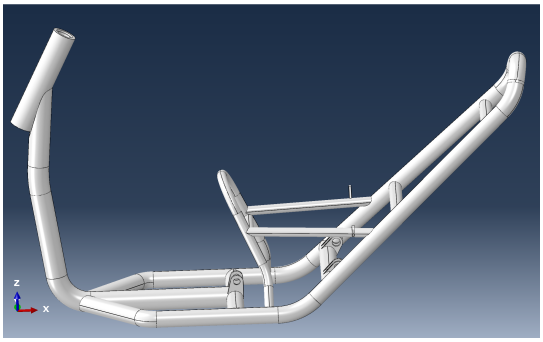
(a) Left view.



(b) Top view.

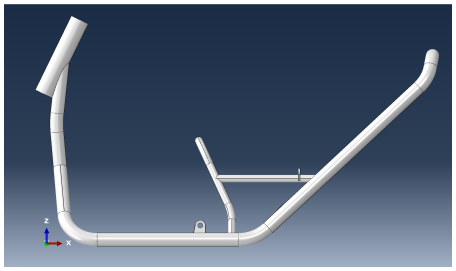


(c) Front view.

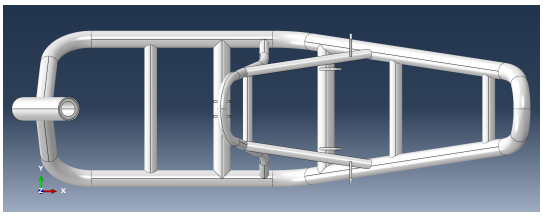


(d) Side view.

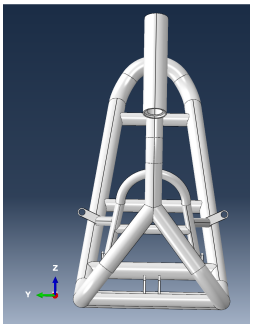
Figure 4.2: Solution seven in several views.



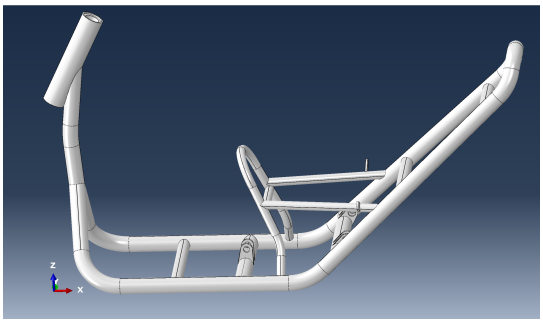
(a) Left view.



(b) Top view.



(c) Front view.



(d) Side view.

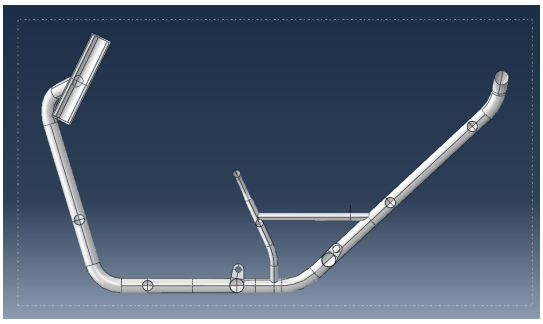
Figure 4.3: Solution eight in multiple views.

4.4 Partitions and mesh

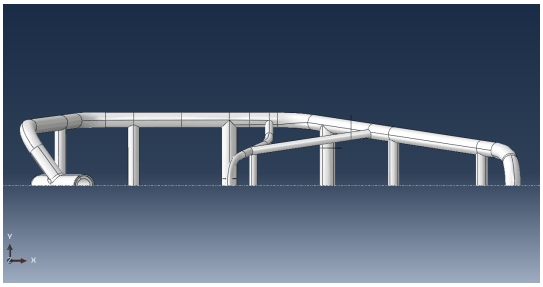
The mesh is one of the most important aspects when creating a model with a software like Abaqus, and it can be a time-consuming process to get a good mesh. However, this step can simplify the commands and calculations the software has to perform to get the pretended results. A model with a flawed mesh leads to less accurate results, with more errors, and also increases the system's analysis and calculation time.

The partitioning is an essential step that can also be slow, but should not be skipped because, when wrongly done may be responsible for the creation of a heterogeneous and unstructured mesh. This step is especially required when the model has a complex geometry, such as round shapes and sharp corners. A model with good partitioning allows Abaqus to create a smooth mesh because the model is divided into smaller and simpler parts.

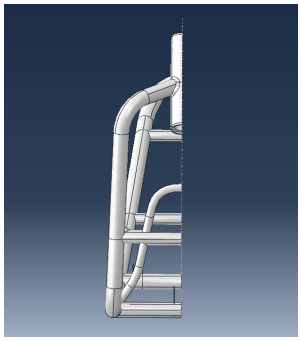
In this thesis, one of the main points of the partitions performed was using only half of the solutions since the structures and the applied forces are symmetrical. Therefore, it is possible to observe as an example, in the following figure 4.4, the solution six with only half of the structure:



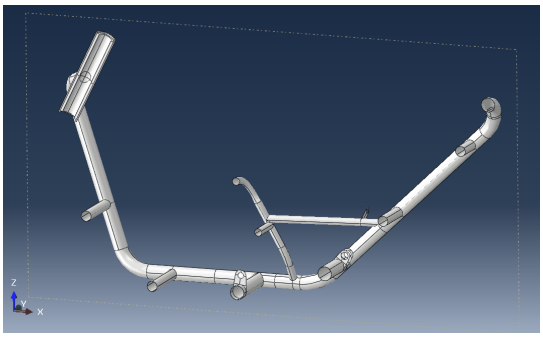
(a) Left view.



(b) Top view.



(c) Front view.



(d) Side view.

Figure 4.4: Solution sixth with only half of the structure, to simplify the analysis.

Regarding the method used for the partitions and the choice of which type of elements to use, initially, it was thought to use a single solid element with everything connected since,

with the automatic conversion, several separate solids were created. Therefore, the steps to this method would be, firstly, to convert all the surfaces of the solids to shell elements, paying attention to the orientation of the surfaces' normals. This parameter is changed using the "Repair face normals" feature, and it is essential to explain to the software what is considered the outside and inside of the surfaces, when forming the solid. After this, the conversion from shell elements to a solid element would be done by the "Create solid: from shell" feature .

However, after attempting to apply this method, it was changed to use only shell elements, due to small details in the structure created in the conversion to Abaqus. Shell elements are mainly used when two of the model dimensions are significantly large compared to the third one and the analysis of this third dimension can be neglected. Moreover, using this type of element decreases the required number of elements, the computational power and the simulation time. Furthermore, the structuring of a mesh is relatively simpler using shell elements. Thus, since all the pipes of the chassis have a constant and small thickness, shell elements were used in the simulations.

Regarding the change from all elements to shell elements, the method used was the design of all intermediate surfaces of the tubes and the association of thickness by section designation. The main resources used to create the intermediate surfaces are shown in the following diagram.

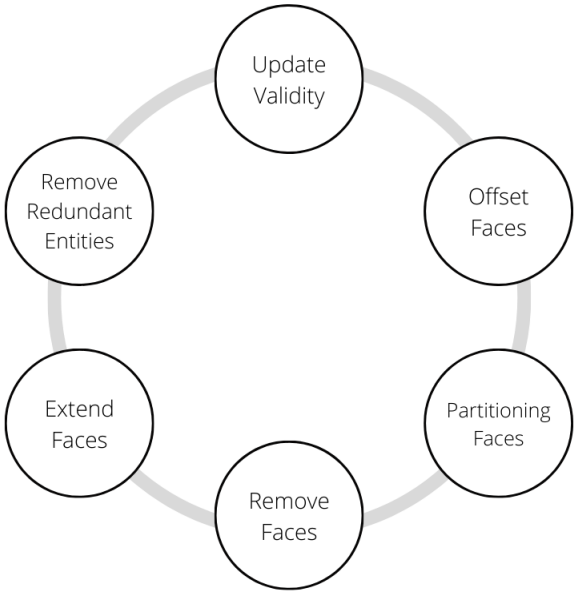


Figure 4.5: Scheme of the main features used in Abaqus software.

The diagram intends to explain that the process of rearranging the structures is a process with continuity and with several steps. From the offset of the faces, to the partition and removal of the unnecessary faces. The partitioning was made through sketches, datum

planes, extension of faces and even the use of projection of points to use the feature "Partition face: Use shortest path between two points". Later, using the resource "Extend Faces", it was possible to extend and make the connection between the tubes correctly. Finally, it followed a step of removing all the unnecessary edges and points and revalidation of the structure.

Regarding the mesh parameters, every meshes created used the parameters shown in the figure 4.6.

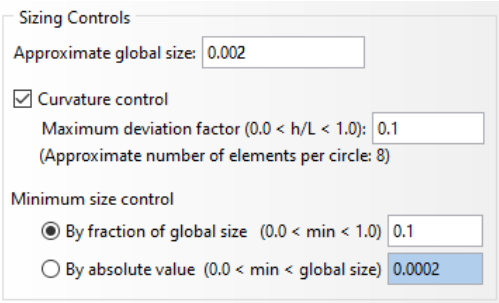


Figure 4.6: Mesh parameters used.

In all the meshes created, it was used quadratic triangular elements in order to simplify the process and obtain a more automatic and homogeneous mesh, despite the partitions created. The use of this type of elements shape increases exponentially the number of nodes, since the use of linear triangular elements always presents a mathematical error, having therefore to be quadratic elements. In the last simulations, a more structured mesh was used and built with linear quadrilateral elements.

4.5 Boundary conditions

In order to impose the necessary conditions in the structure, like boundary conditions and forces, a reference point and constraint method was used. In the figure below are presented the reference points and constraints used.

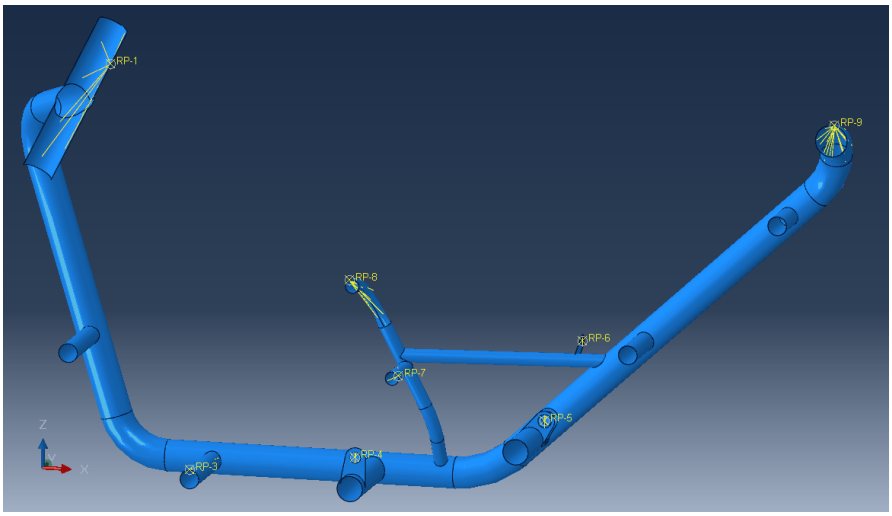


Figure 4.7: Regions with constraints.

Regarding the boundary conditions, we can observe in figure 4.8 the boundary conditions applied to the structure.

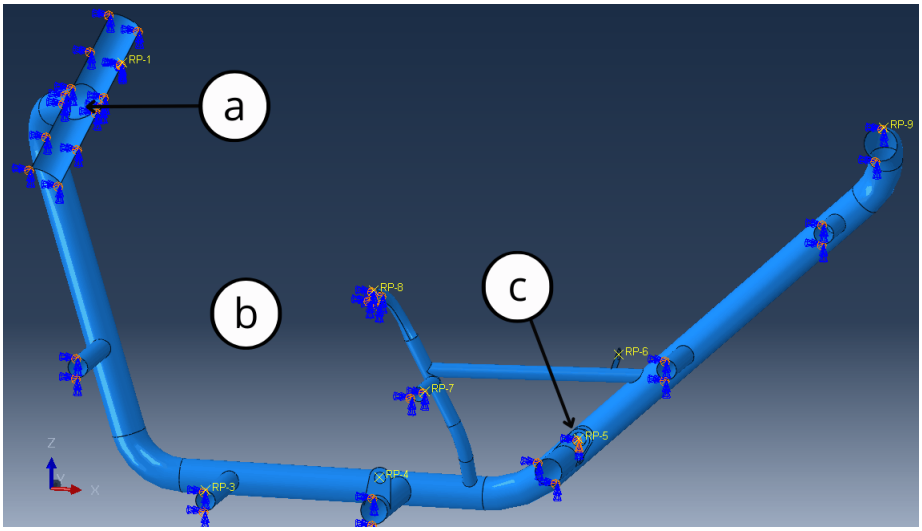


Figure 4.8: Solution seven with boundary conditions imposed.

Region a, which represents the connection between the steering column and the front fork, has been embedded, blocking displacement and rotation in all directions.

The zone c represents the lines in the inner area of the eyebolt, which will be in contact with the oscillating arm. For this connection, a boundary condition has been applied which prevents displacement in y and z axis, as well as rotation in x and z axis.The y-displacement has been locked since the swingarm is connected to the eyebolts and it is assumed that the

swingarm will not deform in the y-direction. The displacement at z axis was also locked since it is assumed that the shock absorber is at its maximum travel, thereby the suspension is fixed. The only rotation allowed was on the y-axis since the swingarm has its rotation point in the eyebolts.

Finally, it was essential to define the symmetry boundary condition (area b) that was applied on all symmetry edges, locking the displacement in y axis and the rotations in x and z axis.

4.6 Loads

In order to calculate the static forces applied to the chassis structure, for an extreme case, it was considered the existence of two people seated on the motorbike: a 75 kg driver and a 50 kg passenger. In addition, it was also considered a total mass of the motorcycle components of 80 kg, including the battery pack of 25 kg, as referred to in the subchapter 2.1.

Six application points were considered for the forces, shown in the figure below by the letters a to f. The points a and e represent the foot support areas of the driver and the passenger, respectively. The b zone represents the eyebolt where the shock absorber will discharge the loads applied to it. Finally, zones c, d and f correspond to simplified supports of the structure. For simplification, the batteries will only be supported by the area d and the supports c and f will be the supports by which the weight of the occupants will be distributed.

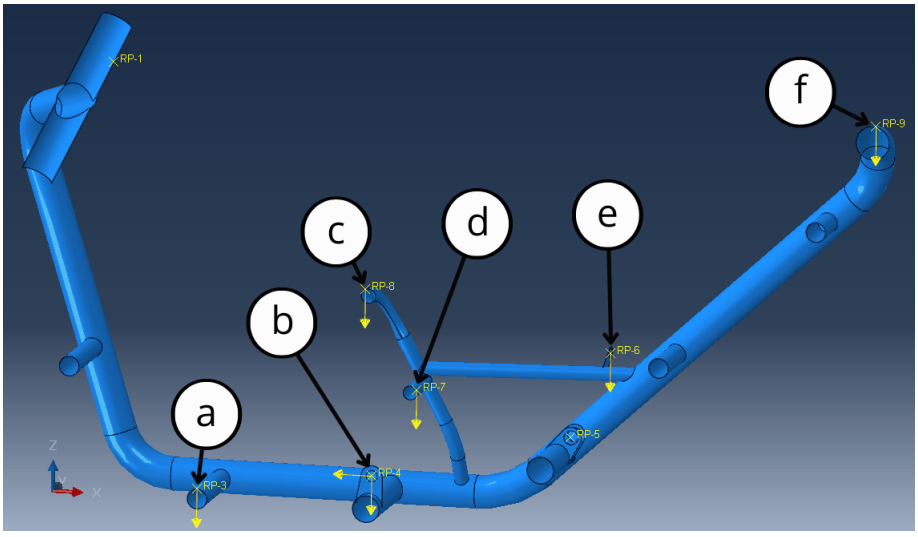


Figure 4.9: Areas of the structure for application of forces.

To perform the analysis in the most extreme static situation, a safety coefficient of 1,5 and a dynamic coefficient of 2 were considered. These values were chosen since they are

widely used in the dimensioning of structures. Therefore, a total safety coefficient of 3 was considered. This way, all the weights were multiplied by this coefficient.

4.6.1 Weight Distribution

When analysing the weight distribution of the occupants, it was considered that when the driver and the passenger have their feet supported, they distribute about one-third of their weight to the feet support and two-thirds are supported by the place where they are seated. Thus, calculations of the forces they impose are presented below:

$$F_{driver} = (\underbrace{75}_{Weight} \times \underbrace{3}_{Safety\ coefficient}) \times \underbrace{9,81}_{Gravity\ acceleration} \tag{4.1}$$

$$F_{driver} = 2207,25\,N \tag{4.2}$$

$$F_{driver\,foot} = \frac{1}{3} \times 2207,25 = 735,75\,N \tag{4.3}$$

$$F_{driver\,seat} = \frac{2}{3} \times 2207,25 = 1471,5\,N \tag{4.4}$$

$$F_{passenger} = (\underbrace{50}_{Weight} \times \underbrace{3}_{Safety\ coefficient}) \times \underbrace{9,81}_{Gravity\ acceleration} \tag{4.5}$$

$$F_{passenger} = 1471,5\,N \tag{4.6}$$

$$F_{passenger\,foot} = \frac{1}{3} \times 1471,5 = 490,5\,N \tag{4.7}$$

$$F_{passenger\,seat} = \frac{2}{3} \times 1471,5 = 981\,N \tag{4.8}$$

Since no other forces are applied to the footrests, the forces shown in equations 4.3 and 4.7 correspond to the forces applied in areas a and e, respectively.

Regarding the distribution of forces present in the scooter seat, and considering that the driver and the passenger are seated at different distances from the supports c and f, the distribution of the weights will be different. For analysis of this system, a simpler model of a beam doubly supported at the ends, subjected to the calculated forces in 4.4 and 4.8 was assumed. For simplification, it was assumed that the distances from the centre of mass of each occupant were 200 mm and 540 mm from the support represented by c. The following schematic serves as a support for the equations 4.9 and 4.10:

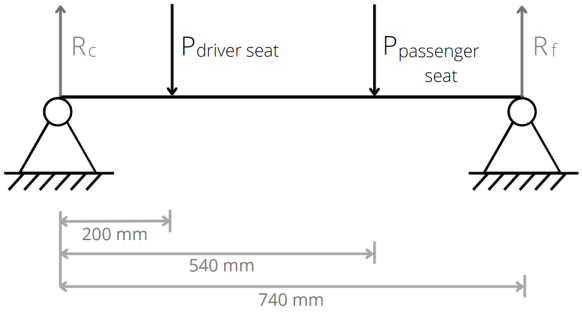


Figure 4.10: Force application diagram.

$$\begin{cases} \sum F_y \ = \ 0 \ = \ R_c + R_f - F_{driversseat} - F_{passengerseat} \\ \sum M_c \ = \ 0 \ = \ F_{driversseat} \times 0,2 + F_{passengerseat} \times 0,540 \end{cases} \tag{4.9}$$

$$\begin{cases} R_c \ = \ 1338,932\,N \\ R_f \ = \ 1113,568\,N \end{cases} \tag{4.10}$$

Thus, the forces present in the equation 4.10 will be the symmetrical forces imposed on the area c and f respectively.

4.6.2 Forces applied by the shock absorber

In order to calculate the effort that the shock absorber transmits to the structure, it was necessary to consider the weights of both the occupants and the bike as a whole. As the situation under study is an extreme static case, it was assumed that the shock absorber was fully compressed, transmitting all the forces applied to it.

Considering the existing connection between the damper and the swingarm and using the base assembly, shown in Figure 3.1, it was possible to construct a simplified scheme, shown in the following figure, of the existing relationship of angles.

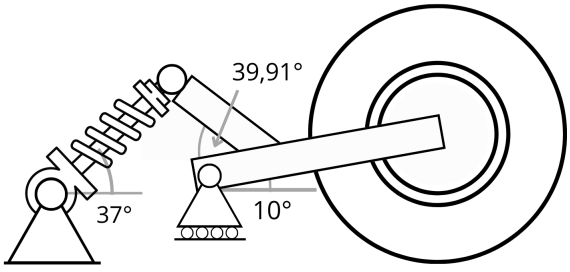


Figure 4.11: Angle ratio between the shock absorber and the swingarm.

It was also assumed that the distribution of the weights to the front and rear wheels did not occur equally. Since the occupants are situated more at the rear of the motorcycle, it was considered that about thirty percent of their weight was unloaded at the front and seventy percent was supported by the rear wheel. Thus, in the following equations are presented the forces applied by the driver and the passenger, at the front and rear of the scooter.

$$F_{driver\,front} = 0,3 \times 2207,25 = 662,175\,N \tag{4.11}$$

$$F_{driver\,back} = 0,7 \times 2207,25 = 1545,075\,N \tag{4.12}$$

$$F_{passenger\,front} = 0,7 \times 1471,5 = 441,45\,N \tag{4.13}$$

$$F_{passenger\,back} = 0,3 \times 1471,5 = 1030,05\,N \tag{4.14}$$

It was also assumed that the weight distribution of the scooter was not symmetrical. Thus, it was assumed that sixty-five percent of the weight was carried by the rear and the front carried thirty-five percent. In the following equations, the distributed forces are calculated:

$$F_{motorcycle} = (\underbrace{80}_{Weight} \times \underbrace{3}_{Safety\ coefficient}) \times \underbrace{9,81}_{Gravity\ acceleration} \tag{4.15}$$

$$F_{motorcycle} = 2354,4\,N \tag{4.16}$$

$$F_{motor\,front} = 0,35 \times 2354,4 = 824,04\,N \tag{4.17}$$

$$F_{motor\,back} = 0,65 \times 2354,4 = 1530,36\,N \tag{4.18}$$

Therefore and with the help of the diagram shown in figure 4.12, it is possible to write the equations 4.19 and 4.21, which allow the calculation of the force that the damper imposes on the chassis.

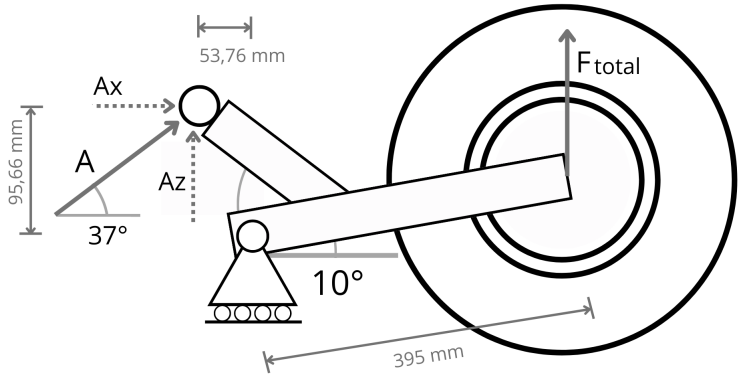


Figure 4.12: Diagram of the forces between shock absorber and swingarm.

$$F_{total} = F_{driver\,back} + F_{passenger\,back} + F_{motor\,back} \tag{4.19}$$

$$\Leftrightarrow F_{total} = 1545,075 + 1030,05 + 1530,36 = 4105,485\,N \tag{4.20}$$

$$\begin{cases} \sum M \;=\; 0 \;=\; F_{total} \times 0,395 \times cos(10°) - A_x \times 0,09566 - A_z \times 0,05376 \\ A_x = A \times cos(37°) \\ A_z = A \times sin(37°) \end{cases} \tag{4.21}$$

$$\begin{cases} A = 14682,752\,N \\ A_x = 11726,168\,N \\ A_z = 8836,301\,N \end{cases} \tag{4.22}$$

Thus, the forces A_x and A_z, presented in the equation above, are the symmetrical components of the forces applied in zone b.

4.6.3 Final forces

The following figure presents the solution six with the forces applied and the table 4.3 gives a brief overview of the forces explained and calculated in the previous subchapters, by area of application and by axis:

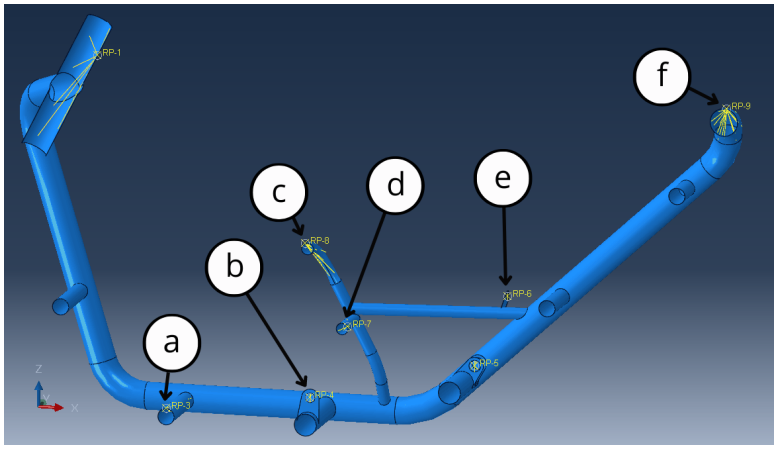


Figure 4.13: Solution six with the applied forces.

Table 4.3: Table of the forces applied to the structure

Letter	**Local**	**Applied Force**	
		Axis x	Axis Z
a	Driver's footrest	-	-735,75
b	Shock absorber eyebolt	-11726,168	-8836,301
c	Front support	-	-1338,932
d	Battery support	-	-735,75
e	Passenger's footrest	-	-490,5
f	Back support	-	-1113,568

It is important to mention that as only half of the structure will be used for the simulations, the forces applied in the simulations will be half of those presented in table 4.3. Finally, in figure 4.14 is presented the sixth solution with the boundary conditions and the forces applied. This case will be imposed similarly to the other two solutions.

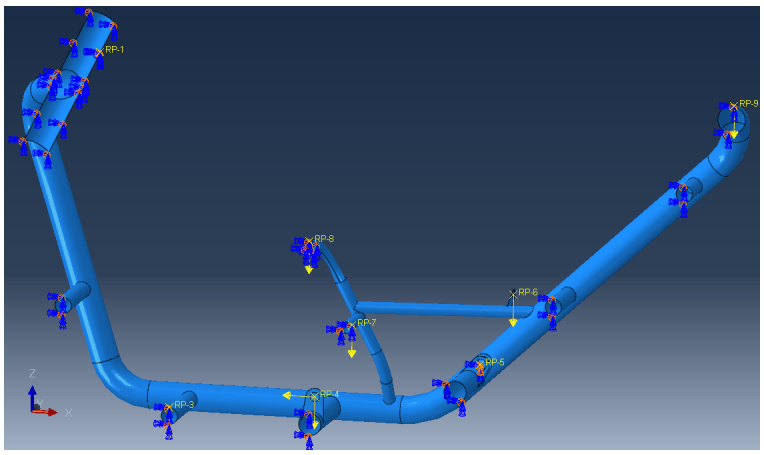


Figure 4.14: Solution six with boundary conditions and forces applied.

Chapter 5

Results and discussion

This chapter presents the results of the simulations described in the previous chapter for the three selected solutions. Besides the results, the structural reinforcements that were added to the structures in order to reinforce the most critical areas are also presented. Finally, a minor revision of the weight requirement initially requested by the AJP is re-evaluated.

5.1 Results with shell elements

When performing the conversion of the SolidWorks models to Abaqus, automatically the structures were divided into small parts, all with solid elements. Thus, the initial idea would be the transformation of the simple parts into a total assembly that connects all the tubes of the frame.

Despite all the work done in order to transform several solids into just one, it was not possible to conclude this step since there were always small details badly created, when converting to Abaqus. Thus, it was decided to transform everything into shell elements, that is, transformation of the tube faces to only one, which would be designated the relative thickness.

In order to start the simulations, the whole solution six was then transformed to shell elements, as can be seen in figure 5.1. For this transformation was created a parallel to the faces of the tubes in order to be in the intermediate zone of the thickness, being this assigned later to each face, with the detail of being selected as middle surface.

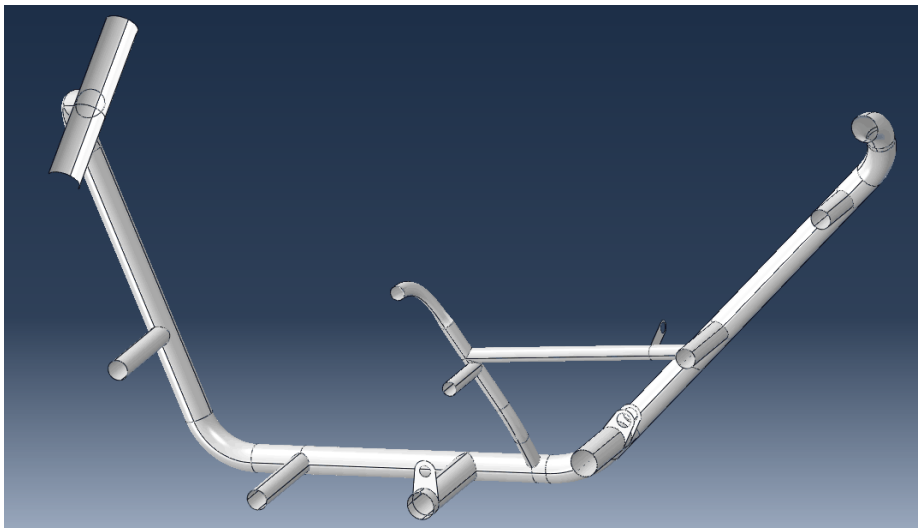
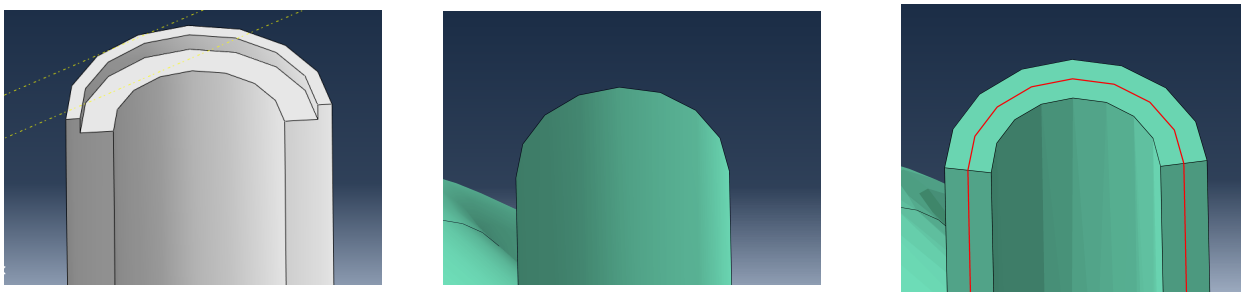


Figure 5.1: Part of the solution six, in Abaqus.

The following figures show the simplification that had to be made to the steering column. This piece is a machined part that presents different thicknesses, so for the shell element transformation, it was assumed that the steering column presented its maximum thickness over its entire length.



(a) initial. **(b)** no visible thickness. **(c)** with visible thickness.

Figure 5.2: Detail of the steering column,

After applying the forces and boundary conditions, explained in the previous chapter, the result presented in figure 5.3 was obtained.

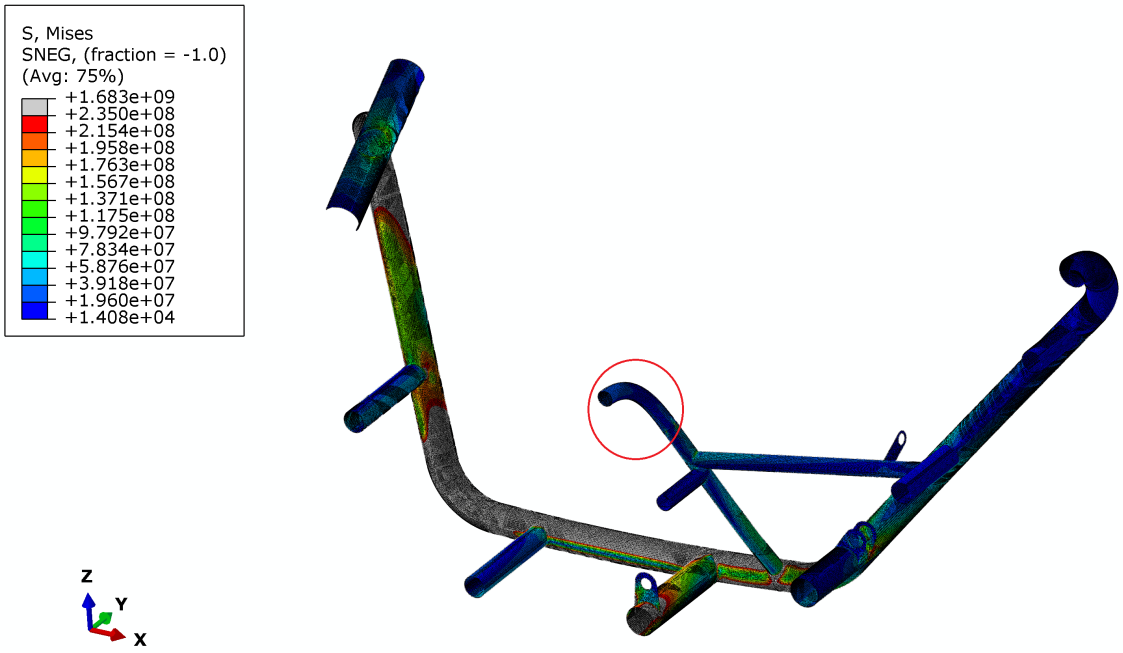


Figure 5.3: von Mises stress of the first simulation of solution six [Pa].

It is clearly noticeable in the figure above that the von Mises stresses resulting from the applied forces are significantly above the yield strength of the S235 material, with the upper value being above 1 GPa. Using the Abaqus function to delimit the visualisation of the results, it is possible to distinguish the areas where the stresses are higher than the yield stress by the grey colour. As can be seen, extensive areas are under enormous stress throughout the structure. In addition to the areas affected, it was noted in the highlighted area the detail presented in the following figure.

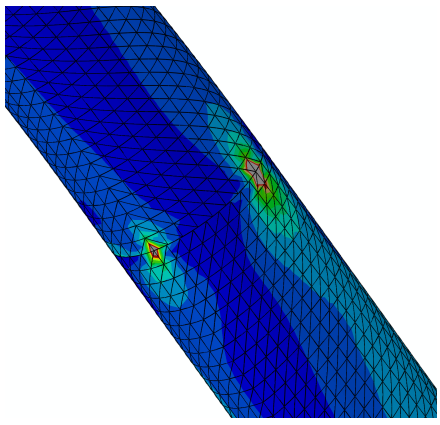


Figure 5.4: Detail between the end of the support and the rest of the structure [Pa].

In figure 5.4, it is possible to observe several distinct points presenting high stresses at

the connection between the front end of the support and the rest of the structure. These results are due to poor conversion and inaccurate design when creating the intermediate faces for the transition to shell elements. The solution to this problem was to separate the front end of the support from the rest of the structure and apply a tie constraint between the edges that connect the two pieces. Figure 5.5 shows the solution six, where it is possible to observe, by the different colours, the two pieces.

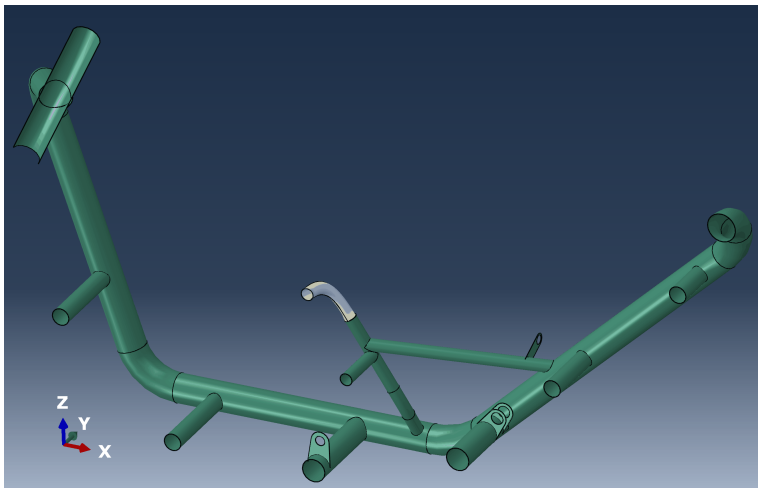


Figure 5.5: Frame of the six solution with a division between the front edge of the support and the rest of the structure.

With the presented solution, it was then possible to obtain the results presented below.

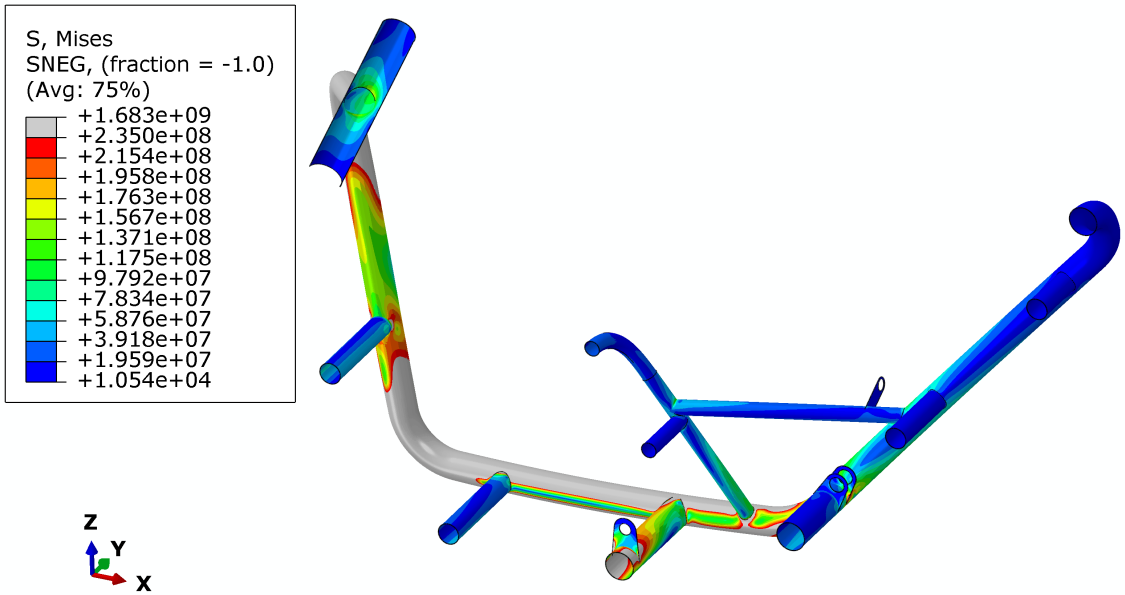
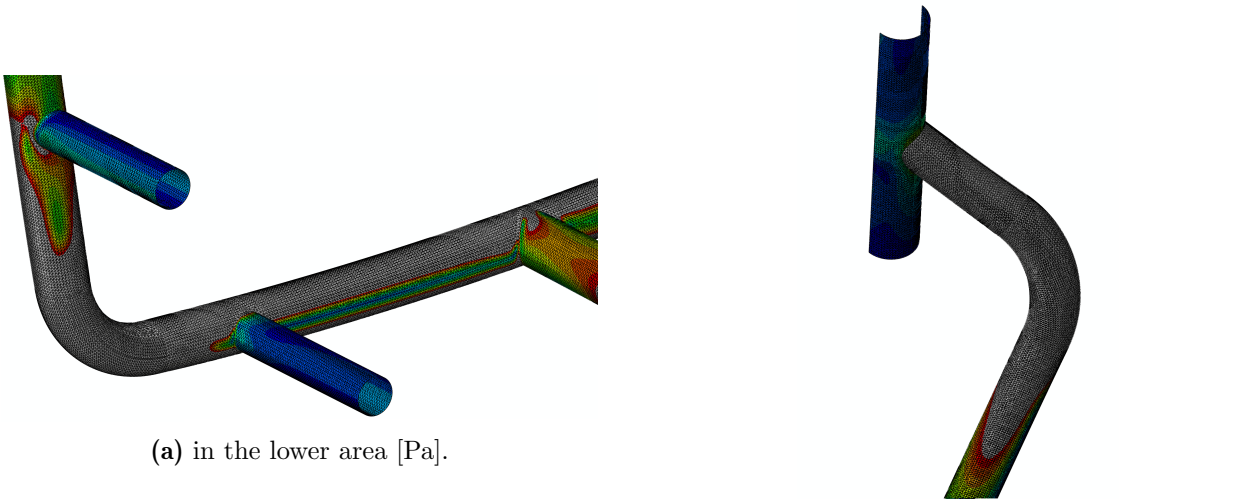


Figure 5.6: von Mises stress of the second simulation of solution six, with the detail fixed [Pa].

By analysing the results, it is possible to observe that the maximum von Mises stress does not decrease, as the large areas that are affected by too high stresses, highlighted in the figures 5.7a and 5.7b. However, in figure 5.8, it can be seen that the connection problem has been corrected, and there is now a correct connection between the two pieces.



(a) in the lower area [Pa].

(b) in connection with the steering column [Pa].

Figure 5.7: Details of the most stressed areas,

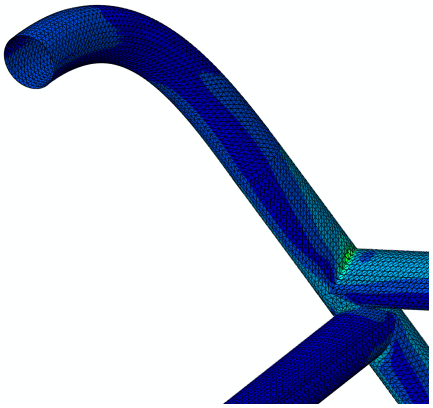


Figure 5.8: von Mises stress of the correction made to the connection between the two parts [Pa].

Regarding the simulations obtained for solution six, it is possible to see that several improvements would have to be made to make the structure viable. However, before making these improvements, the simulations of solutions seven and eight were performed in order to understand if it was a general problem of the structures. Then, solution seven, presented

in figure 5.9, was analysed. As the back part of the solutions is the same in the three selected frames, the conversion made for solution six was used to analyse the seventh and eighth solutions. Thus, as can be seen in the figure below, the structure is divided into three different colours, one representing the front part, another the back part, and finally, the tip of the support separated, as occurred for solution six.

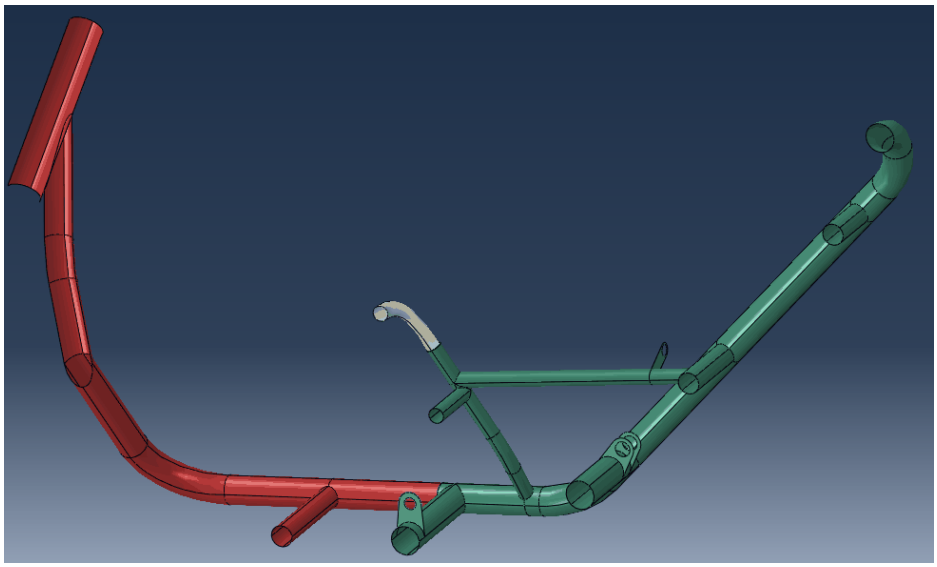


Figure 5.9: Frame of the seventh solution with the several constituent parts.

As it happened for the connection between the tip and the rest of the structure, a tie constraint was used between the edges that join the front and back parts of the solution. In the figure 5.10, it is possible to observe the representation of this connection.

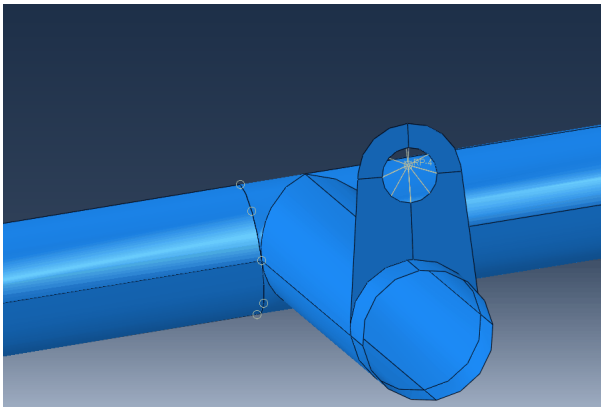


Figure 5.10: Detail of the tie constraint.

An essential detail of the solution, represented in figure 5.11, is that the connecting tube to the steering column is in the symmetry plane. This way, it was necessary to consider

that the delimiting edges of this tube also suffered from the boundary condition of symmetry, as explained in the subchapter 4.5.

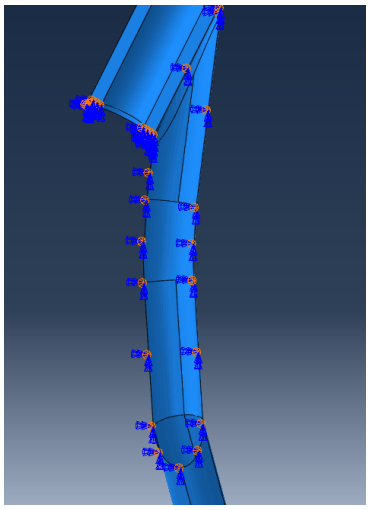


Figure 5.11: Detail of the boundary condition on the tube edges.

After these minor changes, it was possible to obtain the result shown below, with details in figures 5.13a and 5.13b.

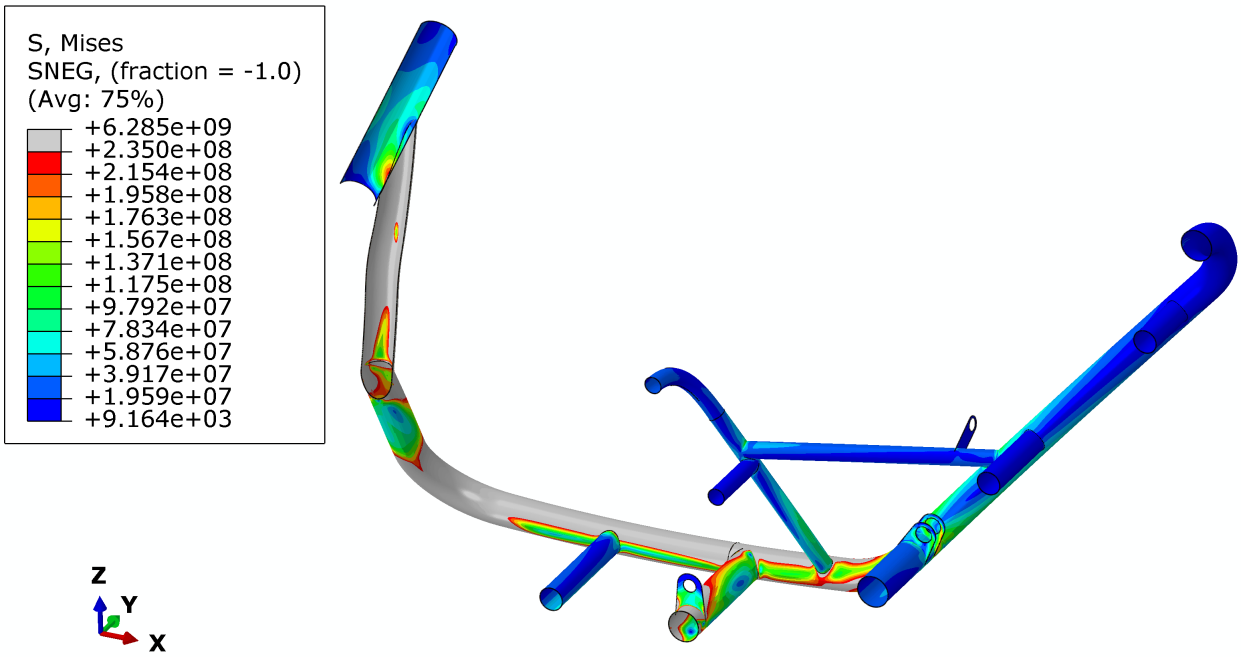
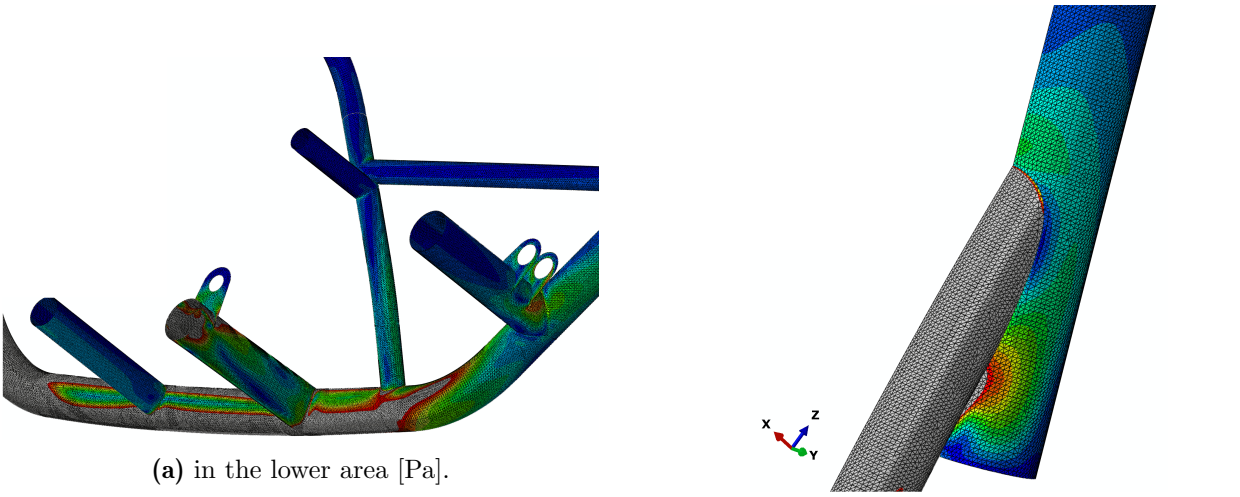


Figure 5.12: von Mises stress of the first simulation of solution seven [Pa].



(a) in the lower area [Pa].

(b) in connection with the steering column [Pa].

Figure 5.13: Details of the most stressed areas in solution seven,

After analysing solution seven, it can be seen that the relatively large areas where high stresses are applied are a general structural problem. In order to prove this, the simulation of solution eight was performed. In figure 5.14 is the solution eight, also presented with different colours, distinguishing the various parts of the structure. It can be seen that the connection made between the front and back of this solution is different from the one shown in solution seven, because the design of the chassis at the bottom is different.

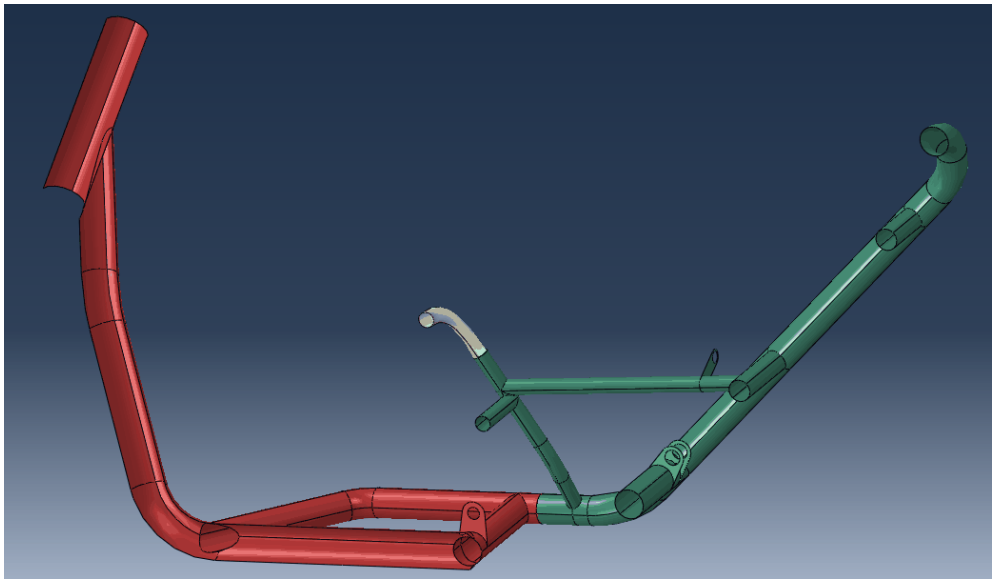


Figure 5.14: Frame of the eight solution with the several constituent parts.

As presented earlier, the following figure shows the tie constraint that links the two

main parts of the structure.

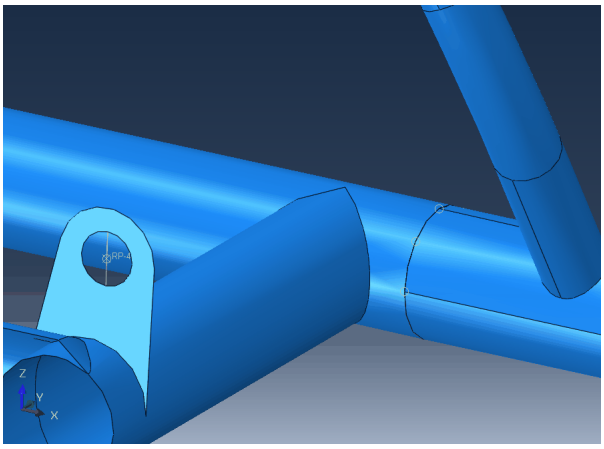


Figure 5.15: Tie constraint between the two parts.

Regarding solution eight, it is important to reinforce that the main tube is in the symmetry plane in the inferior and frontal zones of the structure. Thus, the symmetry boundary condition was applied in the delimiting edges of this tube, as the figure 5.16 intends to show.

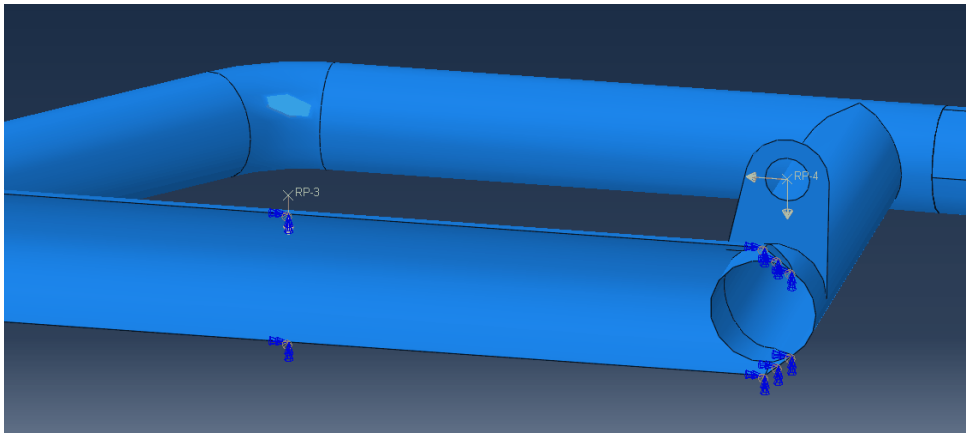


Figure 5.16: Detail of the boundary condition on the tube edges.

In addition, as the design of the lower part of the chassis is different from the two already presented, the application of the force from the passenger's feet was re-evaluated, which has been applied in an intermediate tube since then. As can be seen in the figure 5.17, for this solution it was simplified that the force, caused by the weight of the feet, is distributed over the main tube.

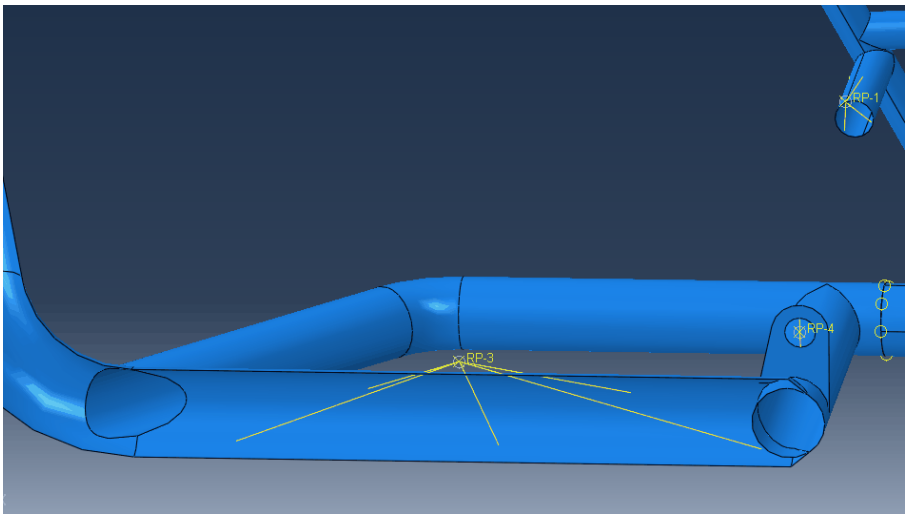


Figure 5.17: Detail of the area associated with the application of the driver's feet force.

With all the details presented, the result obtained in the simulation of solution eight is presented below, with the details of the result in figures 5.19a and 5.19b.

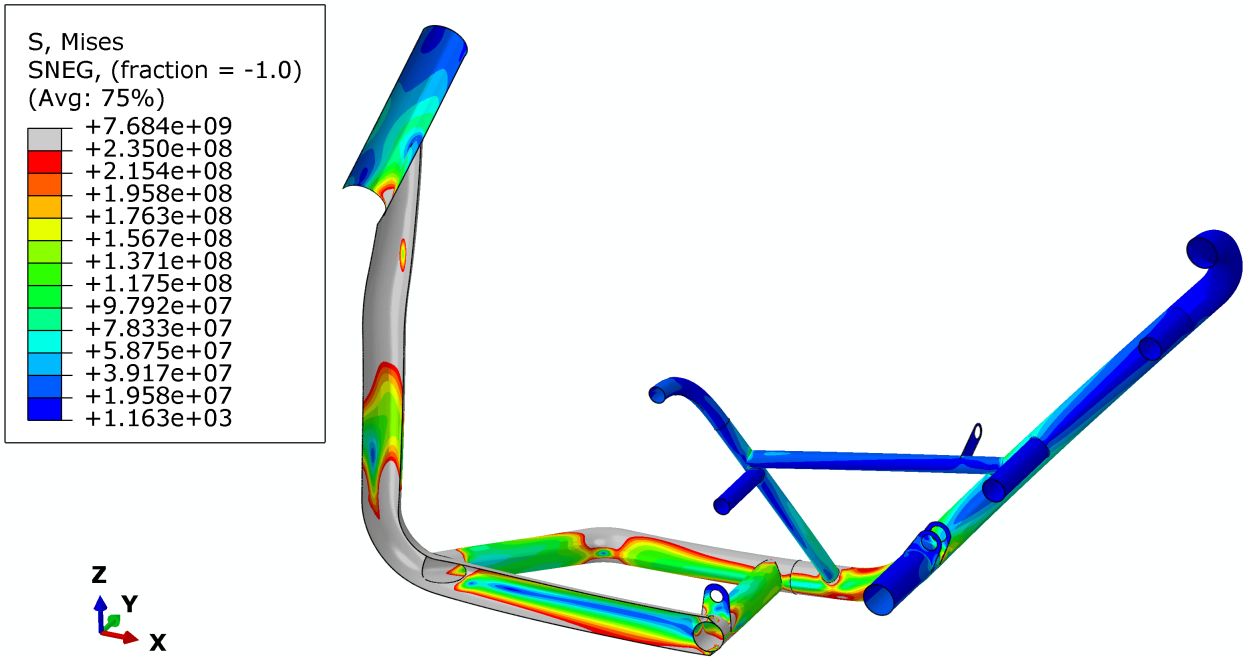
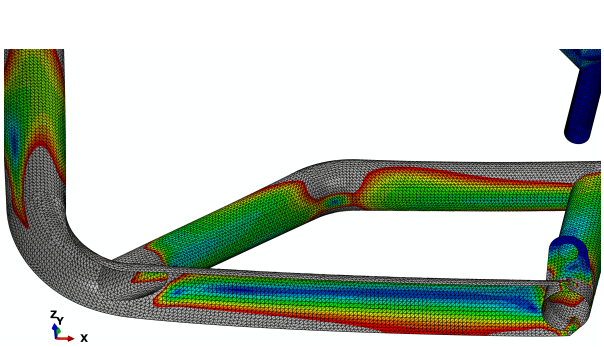
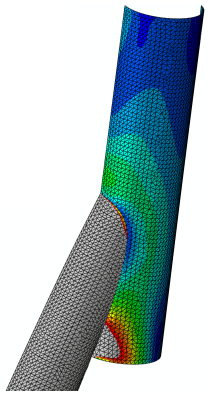


Figure 5.18: von Mises stress of the first simulation of solution eight [Pa].



(a) in the lower area [Pa].

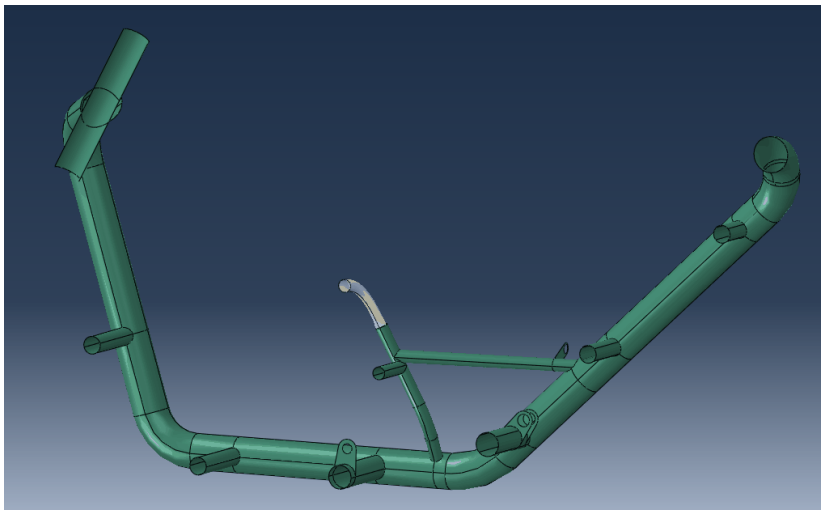


(b) in connection with the steering column [Pa].

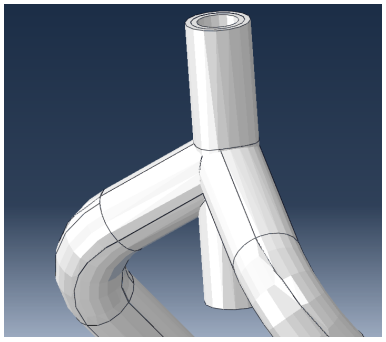
Figure 5.19: Details of the most stressed areas,

As can be seen, the simulation result of the eighth solution was relatively similar to the previously mentioned results. Therefore, since the areas affected in the solutions were considerably large, it was concluded that a major change in the chassis would be necessary. This change was the modification of the steel material from S235 to an S355 steel, whose differences have already been presented.

Besides the material, the increase of the diameter and thickness of the main tubes of the chassis was also considered. Thus, for solution six, which had a tube size of 40 mm with 2 mm thickness, it was then tested a tube diameter of 60 mm and 50 mm, for 3 mm thickness. In figure 5.20a is presented the part of the solution with the alteration to 60 mm diameter and in figure 5.20b is presented the solution with the visible thickness to facilitate the visualisation of the final result.



(a) Frame of the solution.

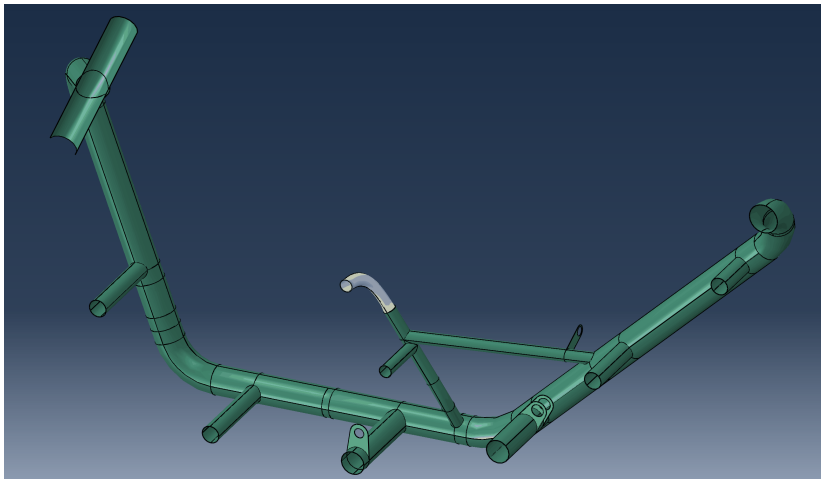


(b) View with the thickness visible.

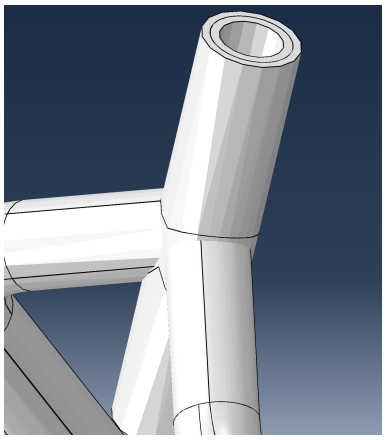
Figure 5.20: Solution six with a 60mm diameter on the main tubes.

As can be seen in figure 5.20b, the larger diameter pipes will intersect at the connection with the steering column and this is a problem to be checked both because of the possible construction of these pipes and because of the stresses caused.

Figure 5.21a and 5.21b show the part of the solution with the pipe alteration for a 50 mm pipe and 3 mm thickness and a detailed view with the visible thickness in order to observe the final result.



(a) Frame with the several constituent parts.



(b) View with the thickness visible.

Figure 5.21: Solution six with a 50 mm diameter on the main tubes.

With a diameter of 50 mm, it is possible to observe that the tubes no longer come into so much contact, although they still interest one another. The following figures show the results obtained for the two simulations described.

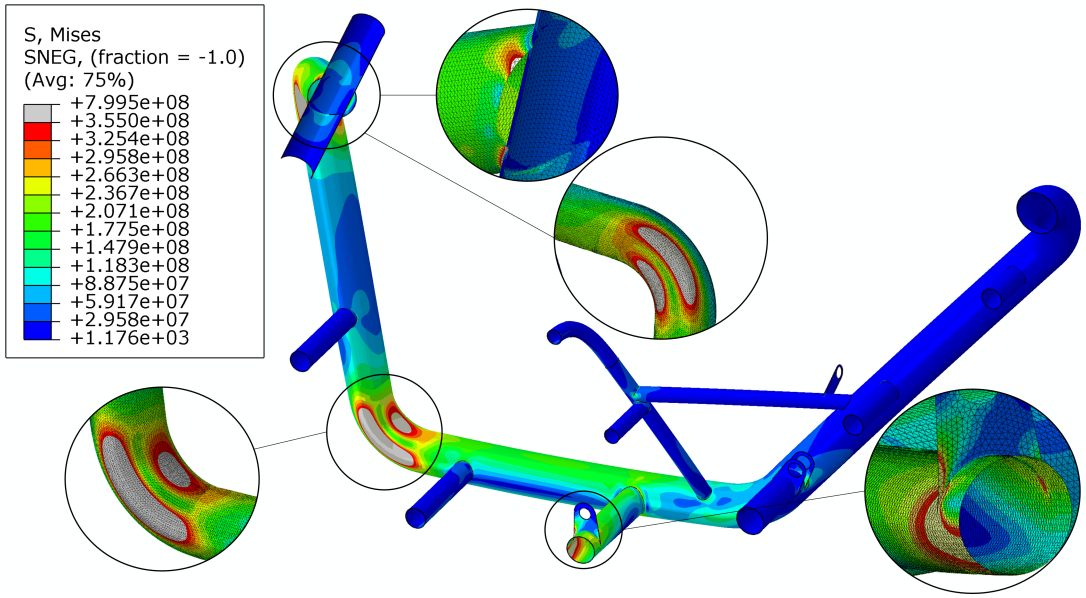


Figure 5.22: von Mises stress of the frame simulation, with the modification of 60 mm for the diameter [Pa].

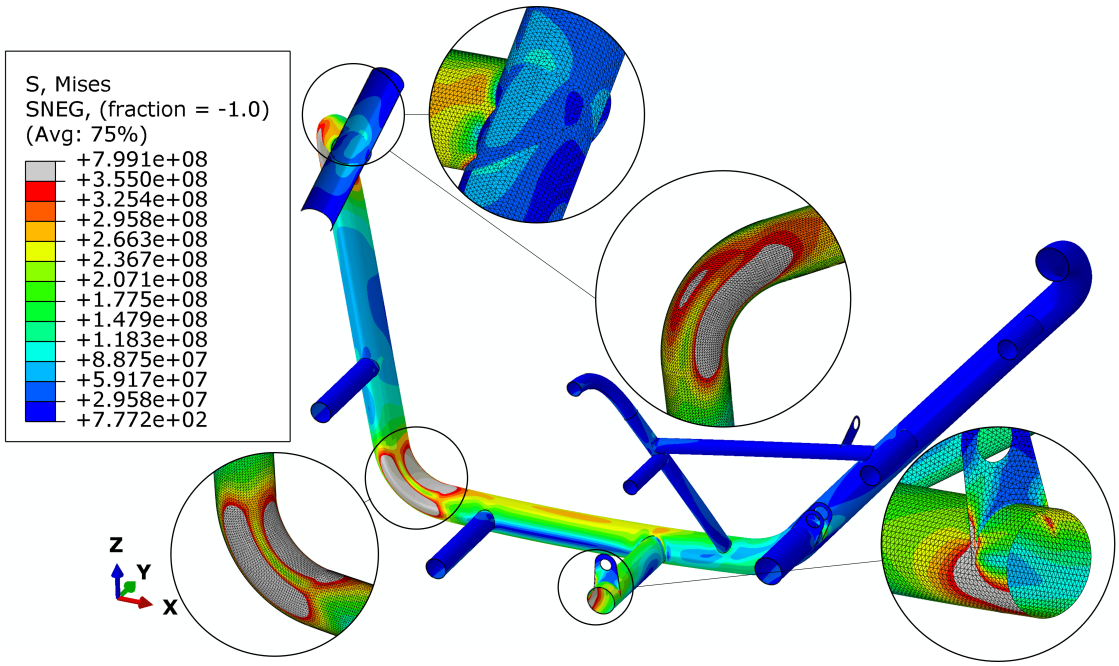


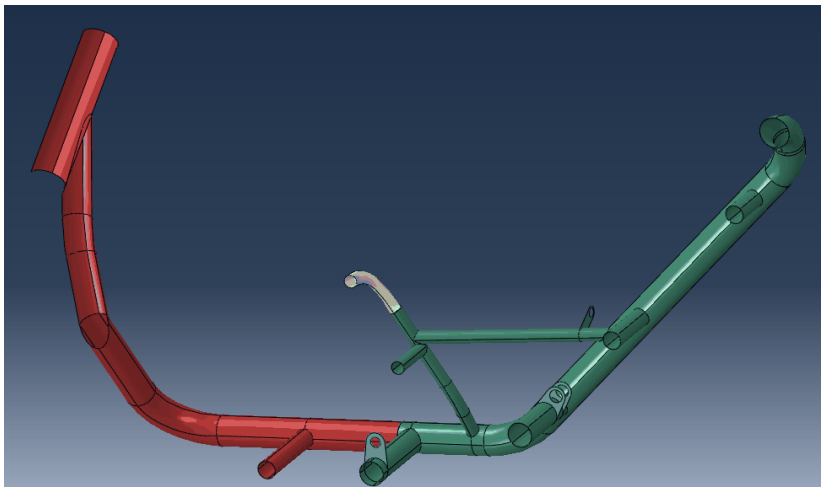
Figure 5.23: von Mises stress for the frame simulation, with the modification of 50 mm for the diameter [Pa].

Analysing the two results obtained, it can be seen that there are certain points of

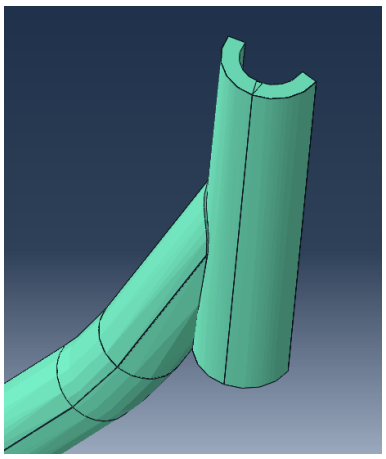
difference between the two solutions. Regarding the stresses in the area of connection of the tubes, in the direction column zone, it can be observed an accumulation of stresses when the tubes have 60 mm, and that in the solution with 50 mm does not happen so severely. Furthermore, it can be noted that although some areas of greater stress are greater in the solution with 50 mm the maximum stress of von Mises decreases.

Although the overall results were worse in the 50 mm solution, the intersection of the tubes in the 60 mm solution was considered to be an important factor, so it was decided to continue with the 50 mm diameter tubes.

Then, the same changes were made in solution seven in order to check if the results had the same evolution as in solution six. In the following figure is presented the part of solution 7 with the change of the material and the diameter and thickness of the main pipes, with the presentation of the detail of the connection to the steering column, with the visible thickness.



(a) Frame with the several constituent parts.



(b) View with the thickness visible.

Figure 5.24: Frame of the seven solution.

After running the simulation, it was possible to obtain the results shown in figure 5.25.

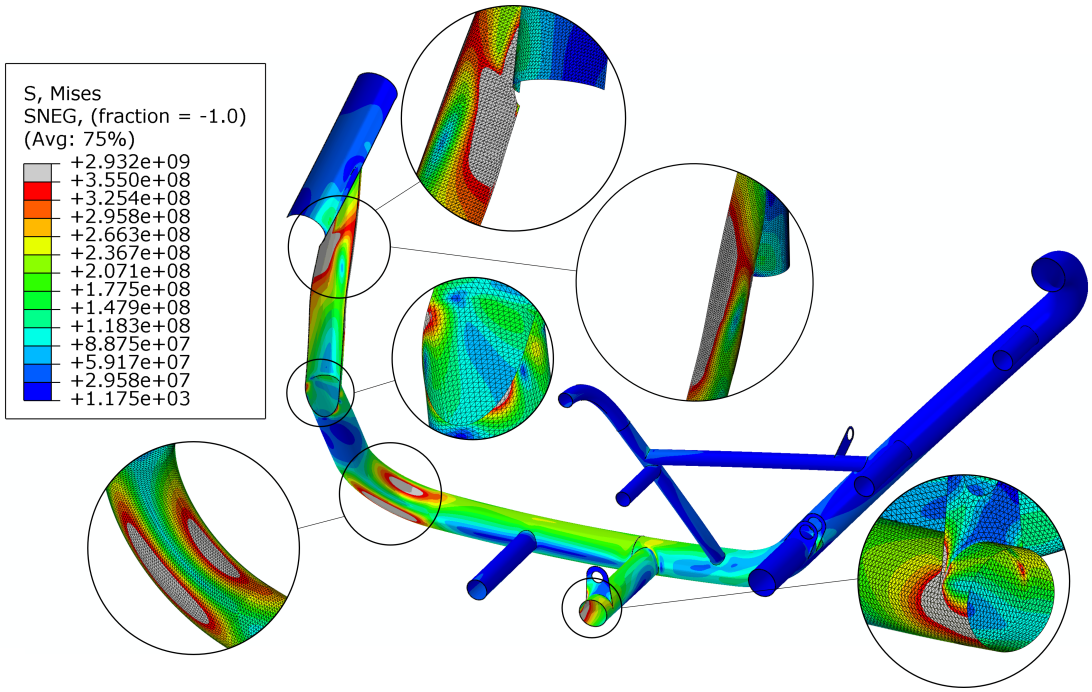


Figure 5.25: von Mises stress of the solution seven, after some modifications [Pa].

As it is possible to observe, comparing the results obtained after the modifications with the results presented in figure 5.12, it is possible to see a big difference both in the maximum value of stresses and in the areas presenting stresses above the yield stress

After observing that the method used to make modifications in a single solution and apply them to the following solution is a method with good results, it was decided to carry out the same procedure for the other solutions. In this way, the following chapter will be dedicated to the application of structural reinforcements in solution six, and then to apply the reinforcements with better results in the other solutions.

The solution eight was not presented with the changes of diameter, thickness and material, since the solution itself already had a diameter of 50 mm in the main pipes, so the only changes were those of thickness and material. It was decided to make these changes after all the analysis of the solution six in order to apply them all at once. The changes made to solution eight are presented in chapter 5.4.

5.2 Structural reinforcements in solution six

As already mentioned, this subchapter focuses on the structural reinforcements that need to be added to the solution in order to avoid stresses above the yield strength. Furthermore, this chapter will be divided by the areas highlighted in figure 5.26, which are the areas of greatest concern in solution six.

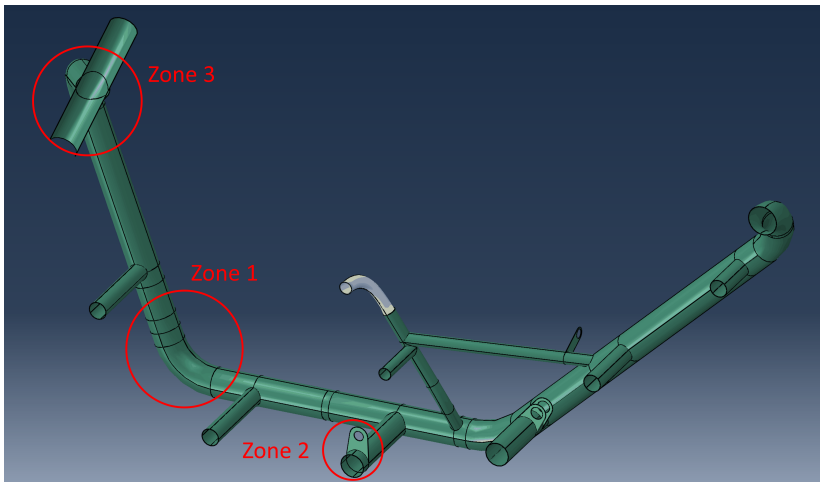


Figure 5.26: Solution six with the main areas highlighted.

5.2.1 Zone 1

The first zone to be analysed is the area of the curve before the chassis rises to connect to the steering column, since a reinforcement at this location can not only improve the stresses at the location itself, but also reduce the stresses in the other zones. Therefore, several iterations of reinforcement were designed and simulated.

The first iterations were to develop a relatively triangular plate, such as the one shown in Figure 5.27, which follows the tubes through the central zone of the tube. This sheet was tested with a thickness of 5 and 3 mm in order to compare which is the best thickness for this type of reinforcement.

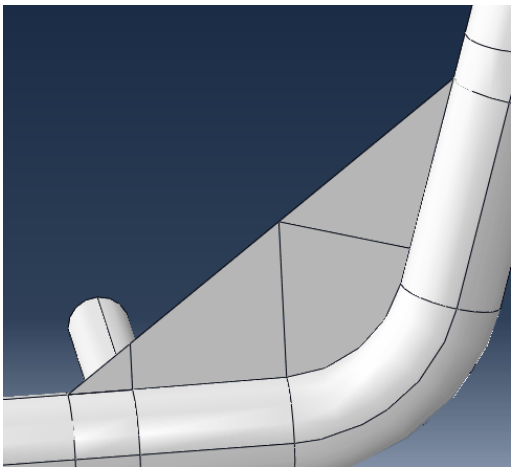


Figure 5.27: View of the middle plate reinforcement.

Figures 5.28 and 5.29 show the simulation results for a thickness of 5 mm and 3 mm,

respectively.

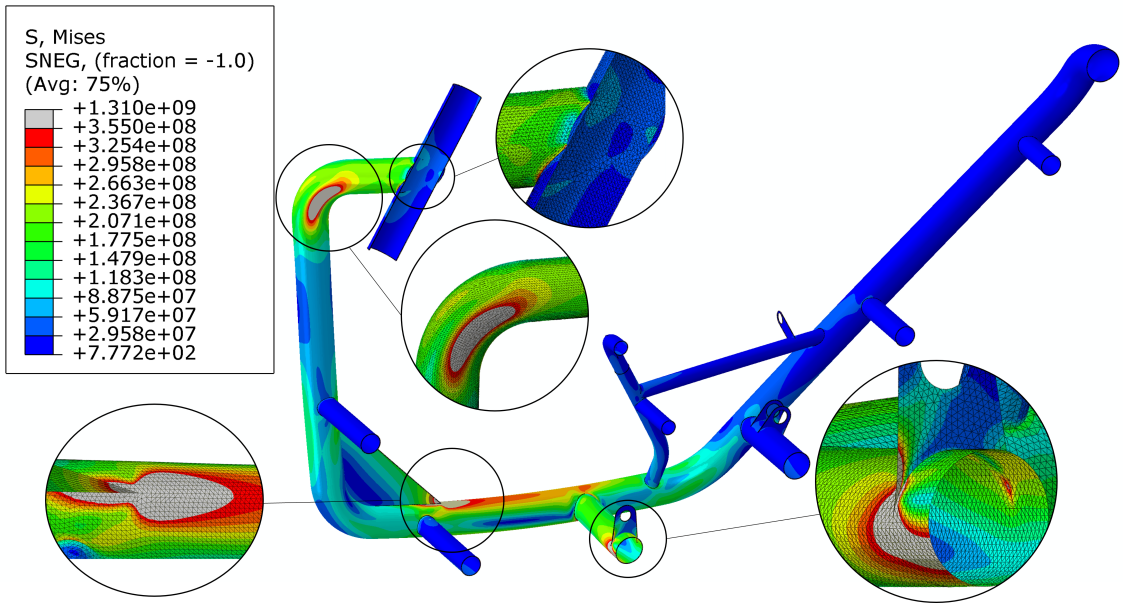


Figure 5.28: von Mises stress of the simulation with a sheet of 5mm [Pa].

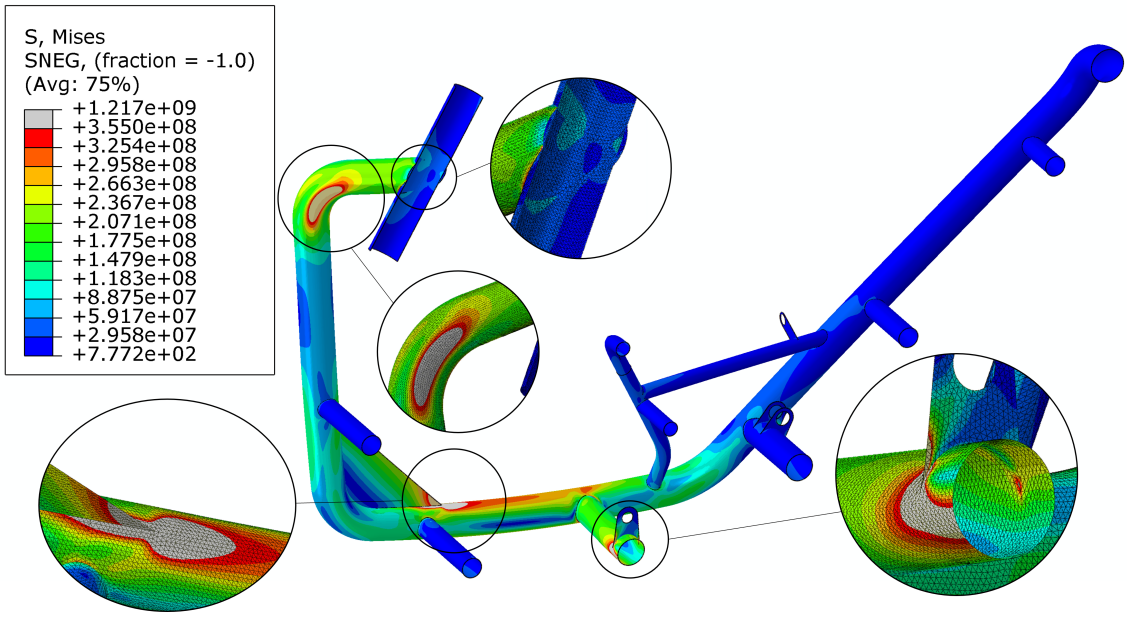
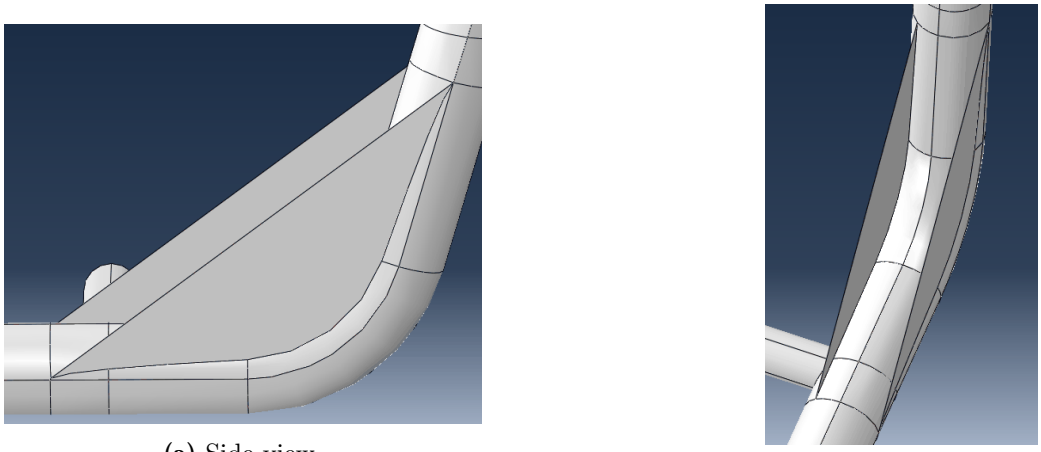


Figure 5.29: von Mises stress of the simulation with a sheet of 3mm [Pa].

Comparing the two results obtained, it can be concluded that the results are extremely similar. Besides improving the stresses of the zone in question, it also dampens the stresses in

zone 3. In zone 2, the results were not altered by the modification. Regarding the thickness, besides the value of the maximum stresses being lower in the 3 mm solution, this one presents similar results to the 5 mm one. In this way, it was chosen to follow with 3 mm reinforcements, also so that the reinforcements don't add too much mass to the structure.

The next step was to test a solution composed of 2 plates similar to the previous one, but instead of following the tubes through the central area, each plate follows the tubes limits in order to give more rigidity. This solution is presented in figure 5.30 with several perspectives.



(a) Side view.

(b) Top view.

Figure 5.30: Several views of the double plate reinforcement.

The simulation results described above are presented in the figure below. As zone 1 is being studied in more detail, the results presented do not show the whole structure, but rather the study area in more detail.

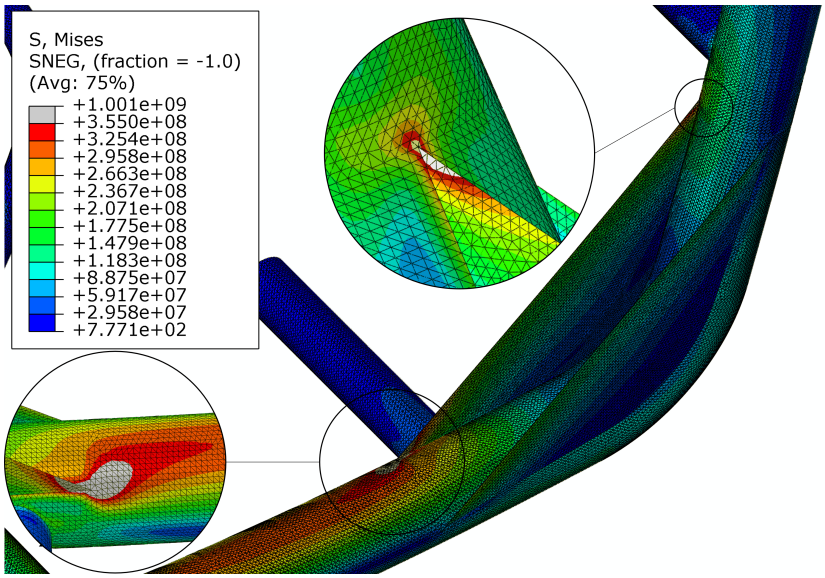
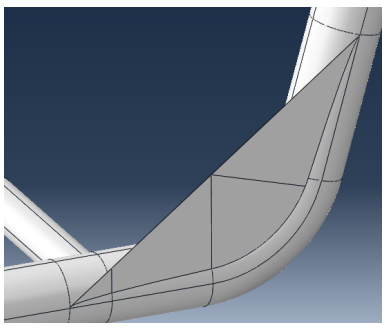


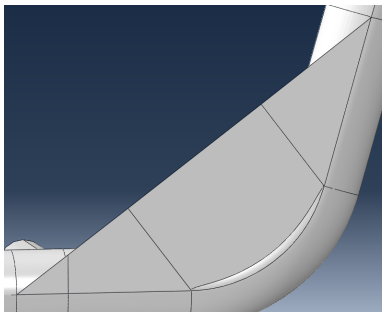
Figure 5.31: von Mises stress of the simulation with the double plate reinforcement [Pa].

As it is possible to observe, the maximum of the stresses decreased and the stresses in the area under study are mainly in the inner sheet of the reinforcement. Thus, the simulation was carried out with only the outer plate in zone 1.

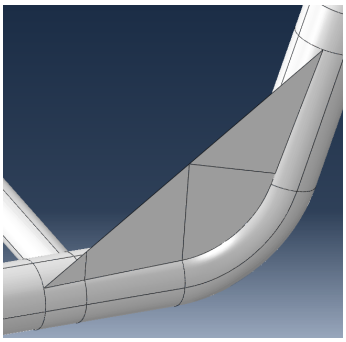
An important point to mention is that the details are very important in the results obtained with the Abaqus software. For example, for the design of the outer sheet, three different design forms were tested. The first, shown in figure 5.32a, was designed by transferring the outer points of the partitions to the extrusion plane and joining these points with a straight line. The second and third solution, presented in figures 5.32b and 5.32c respectively, were designed by directly transferring the straight lines that define the exterior of the tube to the extrusion plane of the sheet. In solution 3, these tangent straight lines were used but with an offset for the interior of 2 mm.



(a) view of first design.



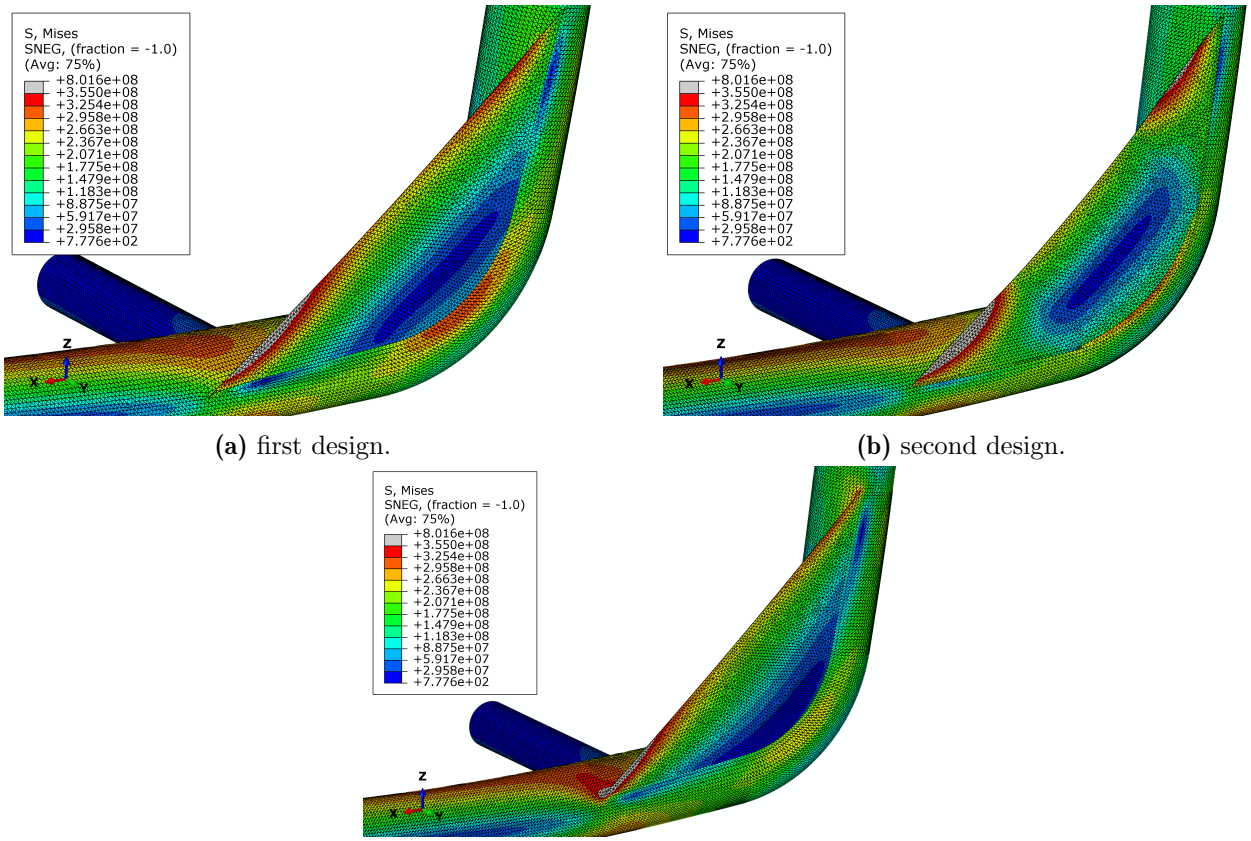
(b) view of second design.



(c) view of third design.

Figure 5.32: Different views for the external reinforcement,

Following, in figures 5.33a to 5.33c are the results of the different iterations, where the stresses in the reinforcement area are presented in detail. The presented results show how important the details are and how the structures are designed in the Abaqus software.



(a) first design.

(b) second design.

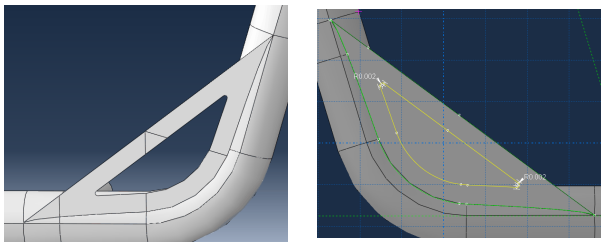
(c) third design.

Figure 5.33: von Mises stress of the simulations with the several designs for the external plate reinforcement [Pa].

As can be seen, although the sheet creation is relatively similar, certain details can totally influence the final results. The results differ mainly in the areas of the sheet that are affected by high stresses. In the first and second solution the stresses accumulate at the top of the sheet, while in the third solution the stresses are concentrated at the tips of the sheet and even at the connection of the sheet with the tube. Although the results of the first and second iteration were very similar, it was considered that the best design would be the first one, because the highlighted area is only at the bottom of the sheet, while in figure 5.33b there are two areas with high stresses. Thus, it was decided to continue with the method used for the first external plate for the remaining iterations for the reinforcement.

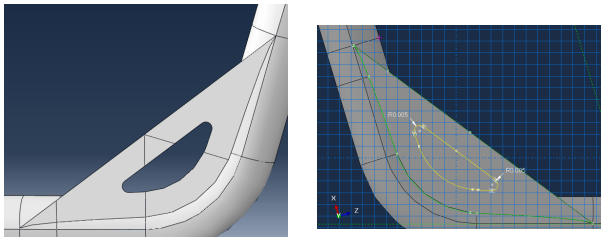
Since the stresses were concentrated in the plate itself, several designs were tested on the plate to evaluate if it was possible to reduce the weight and improve the results by eliminating

the stresses generated in the plate. Therefore, several types of holes were designed in the sheet, as shown in Figures 5.35 to 5.41, which include the presentation of the sketch used to make the hole.



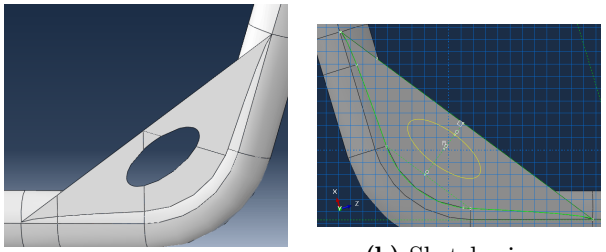
(a) Side view. **(b)** Sketch view.

Figure 5.35: First design of the hole.



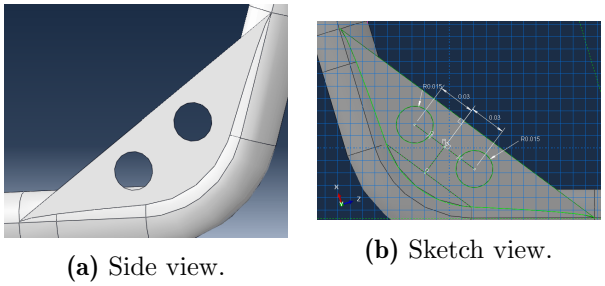
(a) Side view. **(b)** Sketch view.

Figure 5.37: Second design of the hole.



(a) Side view. **(b)** Sketch view.

Figure 5.39: Third design of the hole.



(a) Side view. **(b)** Sketch view.

Figure 5.41: Different design with two holes.

In the following figures 5.42 to 5.45, the results obtained from the different sheet solutions are presented.

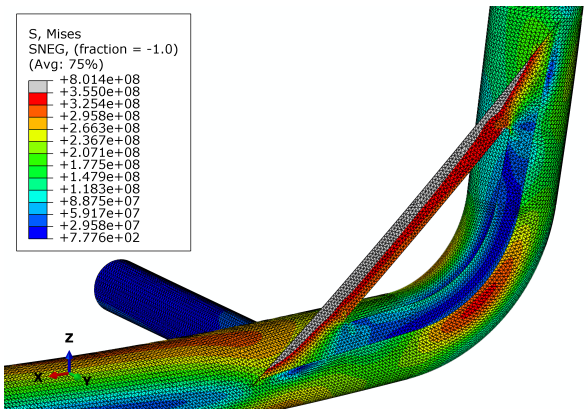


Figure 5.42: von Mises stress of the simulation with the first design [Pa].

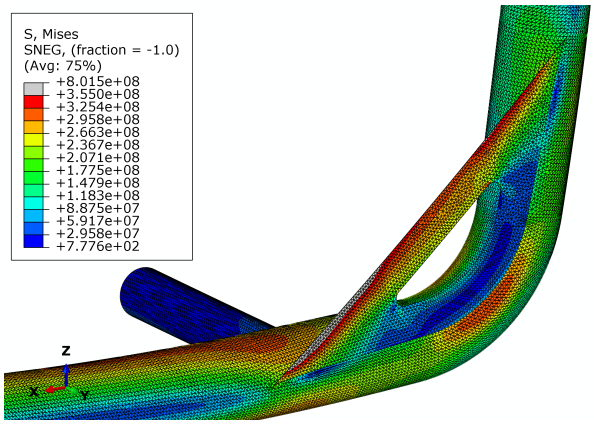


Figure 5.43: von Mises stress of the simulation with the second design [Pa].

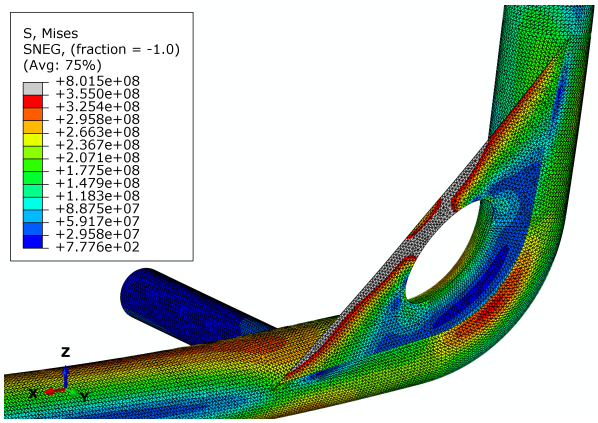


Figure 5.44: von Mises stress of the simulation with the third design [Pa].

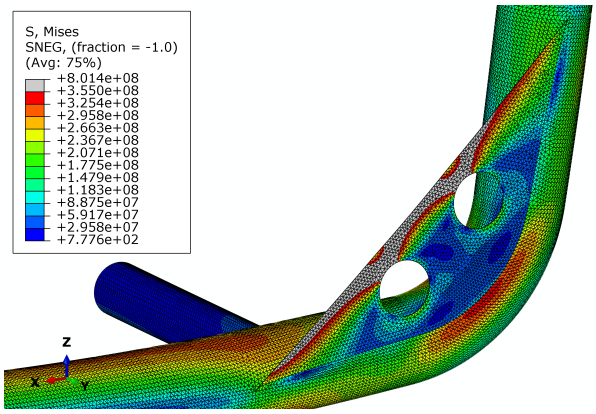
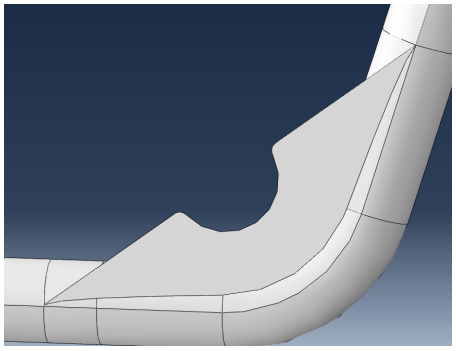
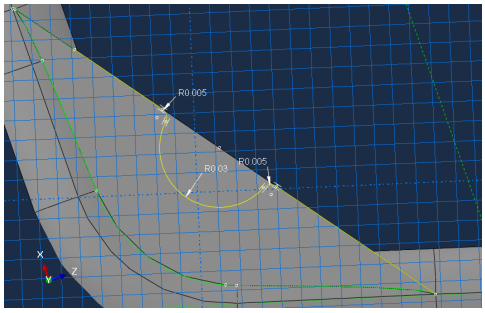


Figure 5.45: von Mises stress of the simulation with the two holes design [Pa].

In figure 5.42, relative to the first design, it can be seen that the hole removes the rigidity of the sheet, leading to an increase of concentrations in the sheet. Figure 5.43 shows the same hole format but smaller, which led to better results but did not solve the stresses that initially appeared. Moreover, in figures 5.44 and 5.45, the results of a different hole format, formed by an ellipse, and the results of a design with two holes in the plate are presented. As it is possible to observe neither design presents better results than when the plate was without holes. Thus, an iteration was advanced where the hole is not in the middle of the sheet but on top of it, as shown in figure 5.46. It was a small iteration only to observe if it would be a strategy to decrease the stresses of the sheet.



(a) Side view.



(b) Sketch view.

Figure 5.46: Reinforcement with the hole at the top.

The results of this iteration are shown in the following figure.

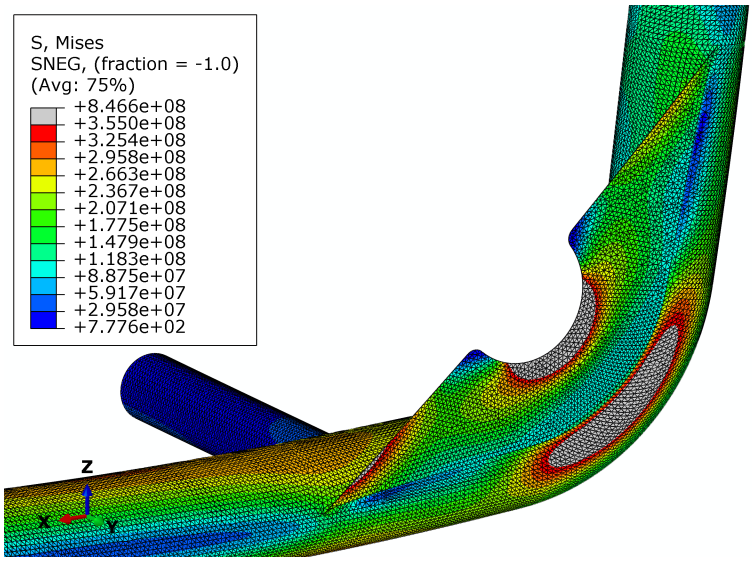
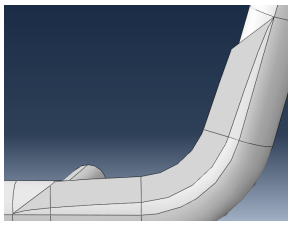


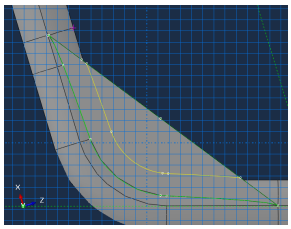
Figure 5.47: von Mises stress of the simulation with the hole at the top design [Pa].

As can be seen, the results obtained were not satisfactory, not only because it creates a concentration of stresses in the inner zone of the hole, but also because it decreased the stiffness of the sheet to such an extent that the stresses in the tube increased.

Following, a different reinforcement was tested, also concentrated in a sheet, but not a triangular one, a strip that follows the curvature of the tubes, like the ones presented in the following figures. These figures also show the sketch used to create the plates, varying the distance between the plate and the tubes' external line and the way it follows the tube.

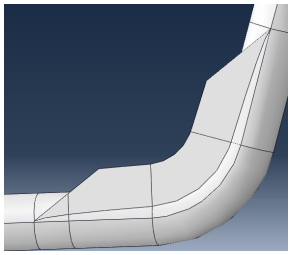


(a) Side view.

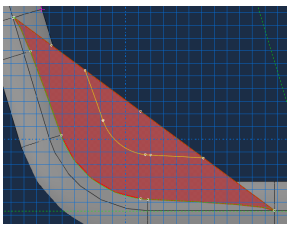


(b) Sketch view.

Figure 5.49: First design of the strip reinforcement.

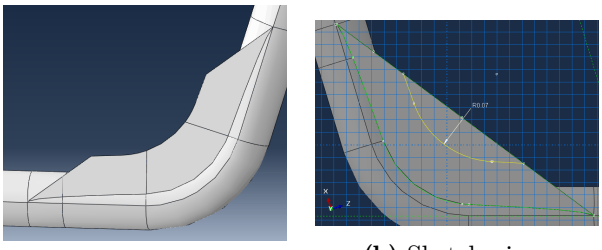


(a) Side view.



(b) Sketch view.

Figure 5.51: Second design of the strip reinforcement.



(a) Side view. **(b)** Sketch view.

Figure 5.53: Third design of the strip reinforcement.

The results obtained for the three configurations are shown in figures 5.54 to 5.56.

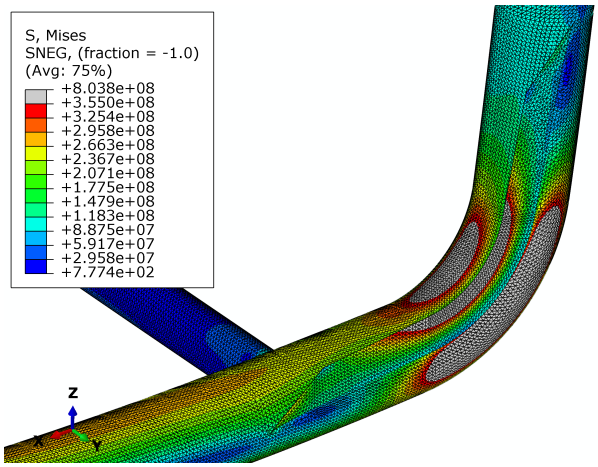


Figure 5.54: von Mises stress obtained from the first design of the reinforcement [Pa].

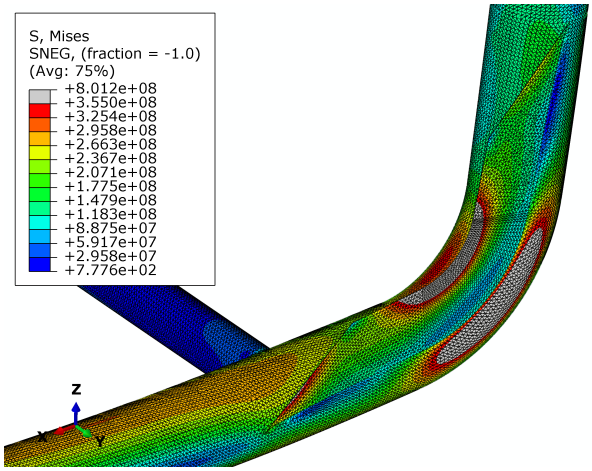


Figure 5.55: von Mises stress obtained from the second design of the reinforcement [Pa].

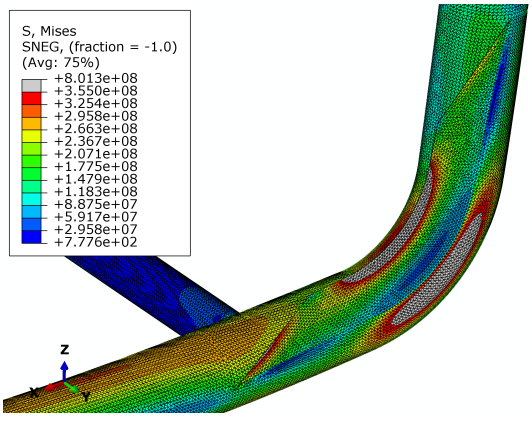


Figure 5.56: von Mises stress obtained from the third design of the reinforcement [Pa].

By analysing the results obtained, it can be seen that the results are extremely similar and that no solution is good enough to be used as reinforcement, since not only does the plate itself present tensions, but these also pass through and affect the tube.

Therefore, after returning to the initial thought of the triangular outer plate, two small changes were developed: one, shown in figure 5.57, would be to extend the upper part of the plate giving more material for the stresses to spread. The second would be to remove the connection that the plate has with the tube, since in the result obtained in the plate as a whole, shown in figure 5.58, it can be observed that the removed area was in low stresses.

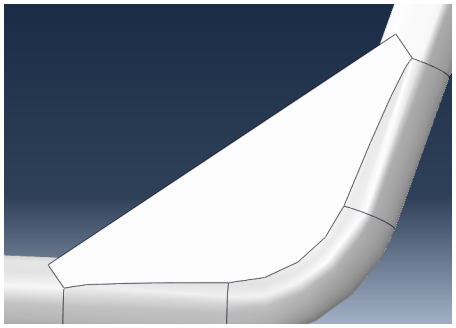


Figure 5.57: Extension of the sheet reinforcement.

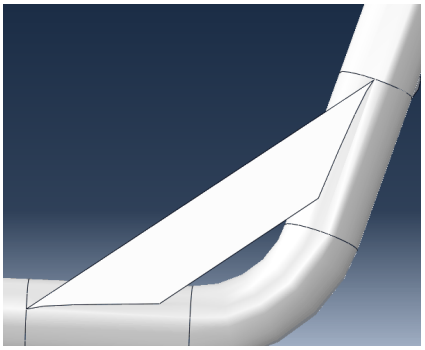


Figure 5.58: Reinforcement with no connection to the curve.

The results of the changes made are shown in the two figures below.

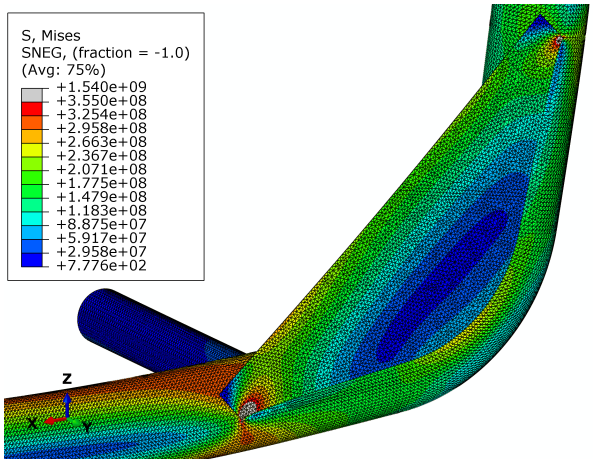


Figure 5.59: von Mises stress obtained with the extension of the plate [Pa].

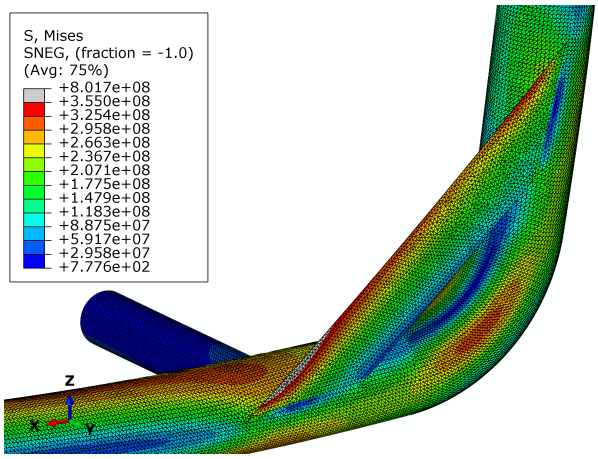
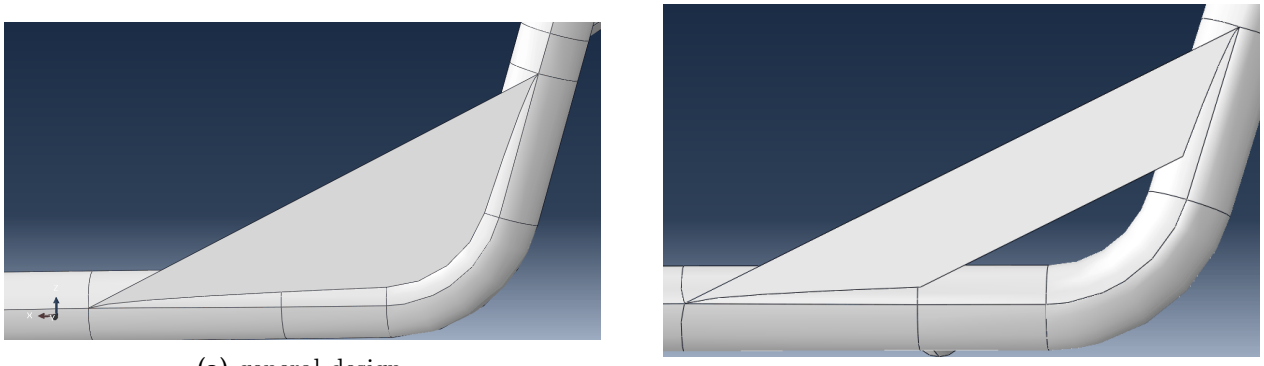


Figure 5.60: von Mises stress obtained with the design with no connection to the curve [Pa].

Analysing the results, it can be seen firstly that the extension of the plate manages to remove the high stresses in it, but accumulates these stresses in the connection with the

chassis tube. Secondly, looking at result 5.60 it can be seen that the design was not very successful because the stresses in the sheeting remain high in the upper area.

After verifying the amount of iterations created for the plate shown in figure 5.33a, it was necessary to change the perspective and decided to extend the plate in order to provide more rigidity in the curve. Thus, the plate was extended as shown in figure 5.61a and also, in a similar way to the last configuration presented, it was also analysed a solution with a longer plate but without following completely the tube, presented in figure 5.61b.

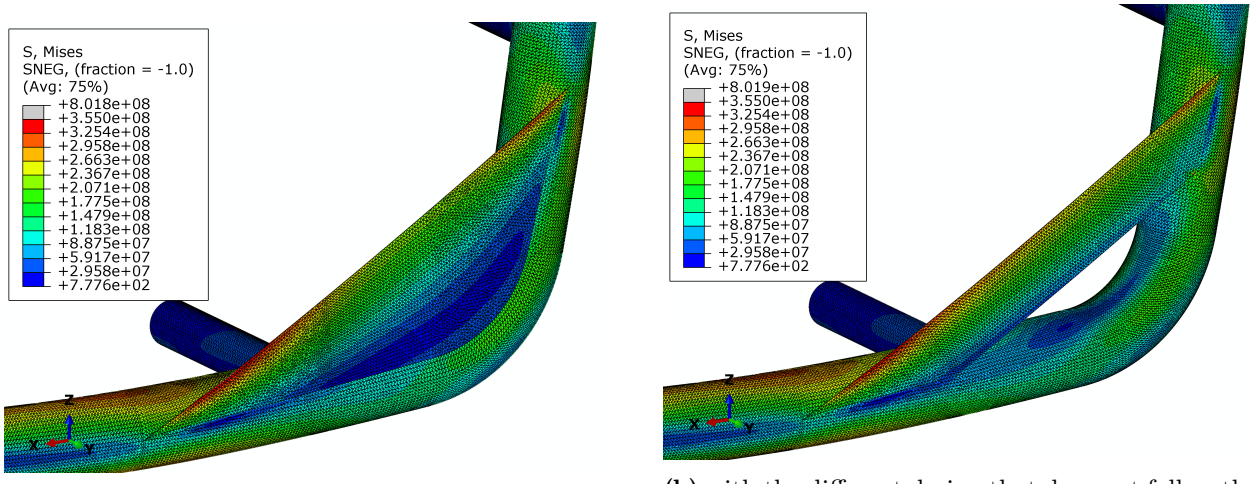


(a) general design.

(b) different design without following the tube.

Figure 5.61: Longer reinforcement in zone 1,

The following figures show the results for the two iterations described.



(a) with the general design.

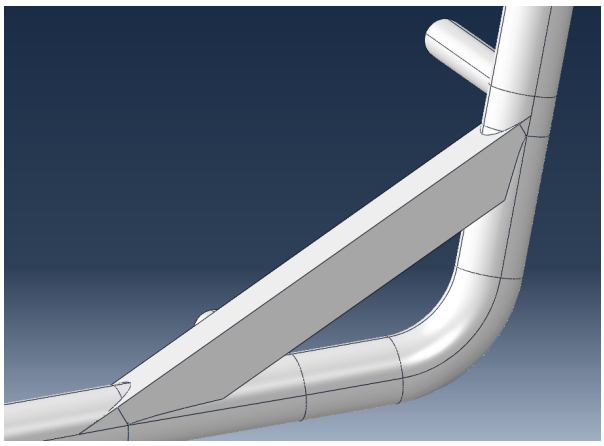
(b) with the different design that does not follow the tube.

Figure 5.62: von Mises stress obtained with the longer reinforcement [Pa],

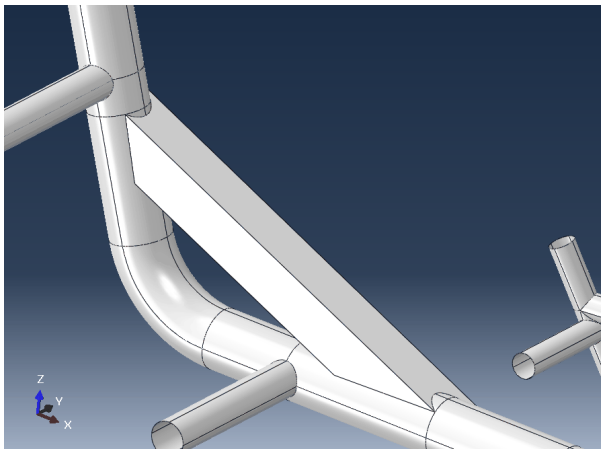
As it is possible to observe the results obtained with a plate extension are better because they present smaller areas where the stresses are high, and the maximums were lowered. Of

the two solutions, the iteration of figure 5.62b was considered the best, although figure 5.62a presents a lower maximum. This is because it presents less material, less welding zone with the tube, and similar results.

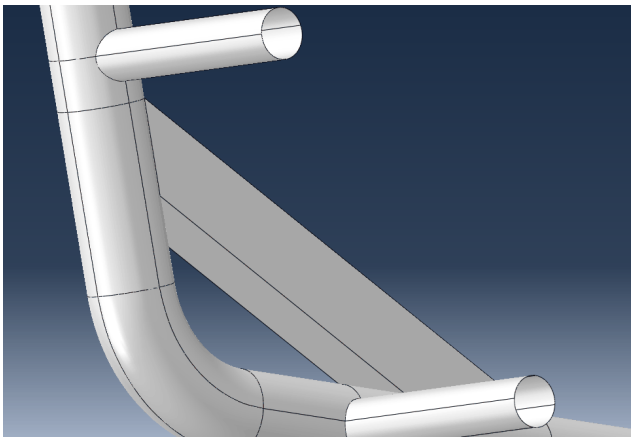
Simultaneously with the iterations developed, the chassis presented in chapter 2.2.7 were analysed in more detail in order to find some answer to how the market developed the reinforcements. Then the solution of figure 5.63 was designed based on the reinforcements found. The reinforcement consists of a set of three welded plates, or even a U-shaped profile bent to follow the curve of the chassis.



(a) Right view.



(b) Left view.



(c) Bottom view.

Figure 5.63: Several views of the reinforcement created,

Figure 5.64 shows the results of the profile solution developed.

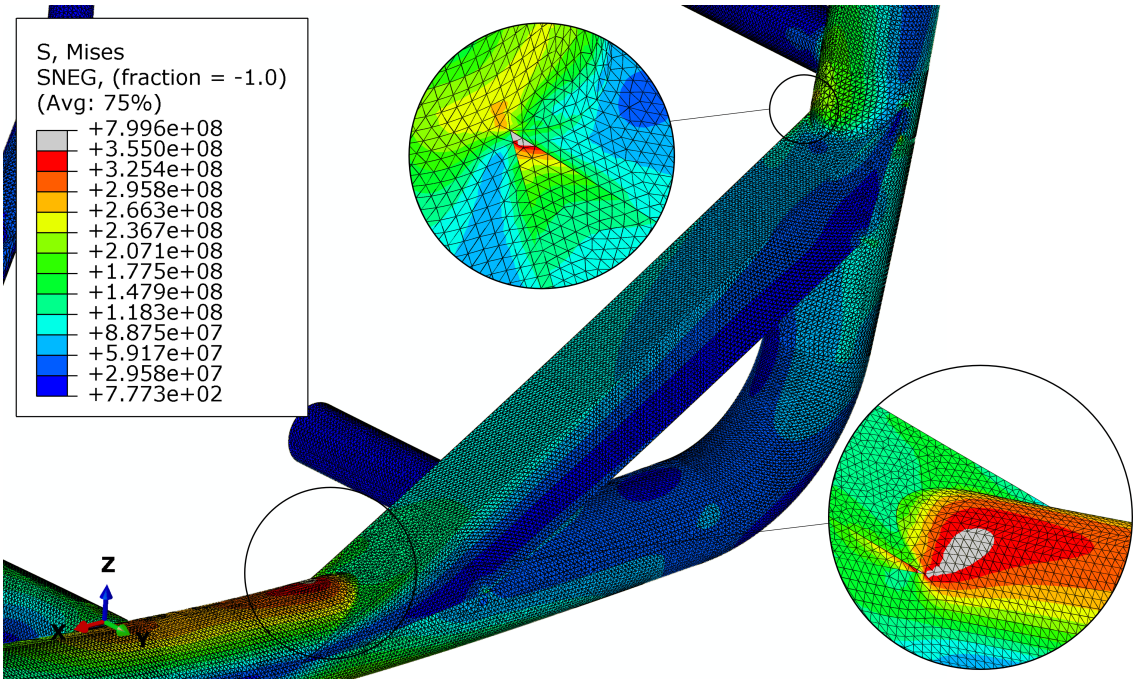


Figure 5.64: von Mises stress obtained with the new reinforcement [Pa].

By analysing the results obtained, it can be verified that this solution can be a good reinforcement for zone 1, as it presents minimum areas where stresses are high. Nevertheless, another iteration of this solution was developed, presented in figure 5.65. The iteration consists in the removal of the lateral plates of the reinforcement, presenting only the upper plate.

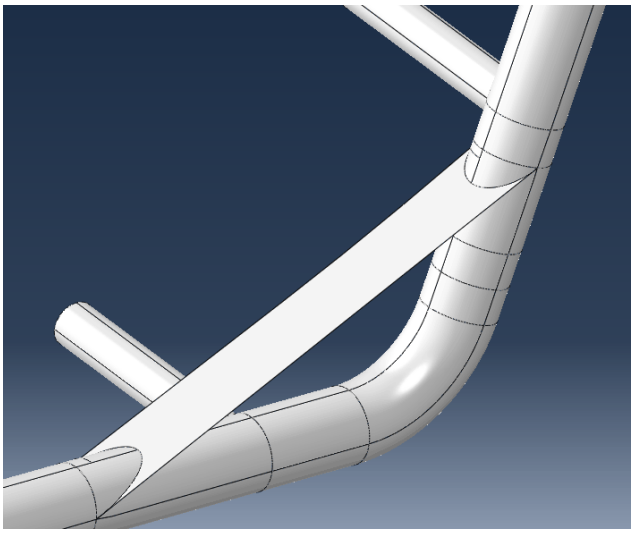


Figure 5.65: Reinforcement without the lateral plates, in zone 1.

The results for the solution described are shown in figure below.

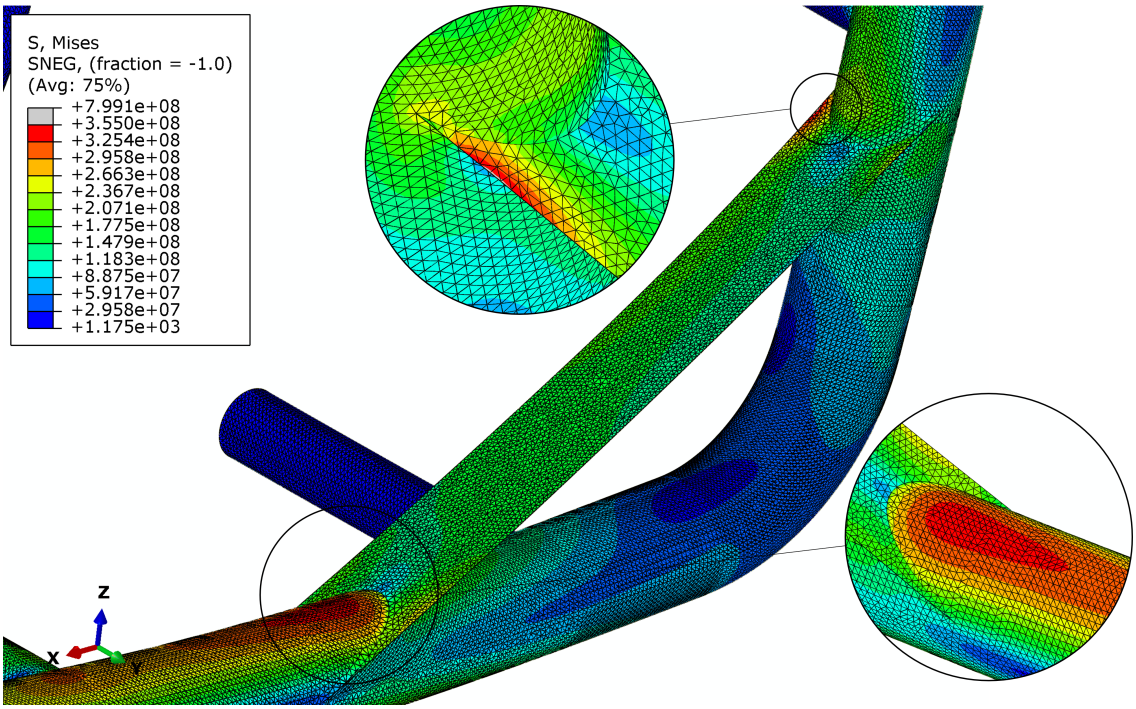


Figure 5.66: von Mises stress obtained by the simulation with the reinforcement without the lateral plates [Pa].

By analysing figure 5.66 and comparing it with the results presented in 5.64, it can be seen that although the maximum has not changed significantly, the areas of greatest stress have disappeared, presenting stresses below the yield stress.

After this intense analysis of reinforcements and iterations for zone 1 of solution six, it was possible to distinguish three main solutions for the reinforcement, these being the ones presented in figures 5.61b, 5.63 and 5.65. After a comparison of the results, it was decided to continue with the solution of figure .

In figure 5.67 the results of this solution are presented, as in figure 5.62b, but not only focused on the plate but on the whole structure to give a better perception of how the reinforcement influenced the stresses applied in the other two zones.

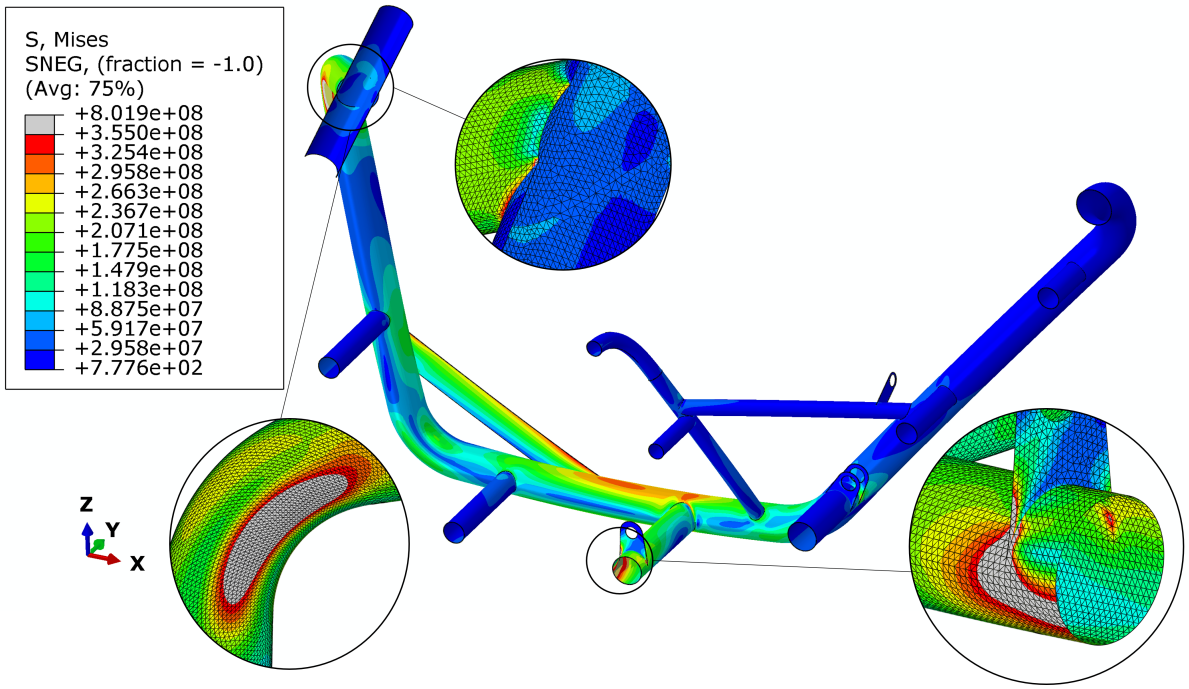


Figure 5.67: General von Mises stress obtained by the simulation with the reinforcement in zone 1 [Pa].

5.2.2 Zone 2

This subchapter focuses on the evaluation of the best solution for zone 2, presented in figure 5.26. One of the first changes that were made to this zone was the increase of the pipe diameter from 40 mm to 50 mm, like the main pipes of the solution. Thus, it was possible to obtain the following result presented in figure 5.68.

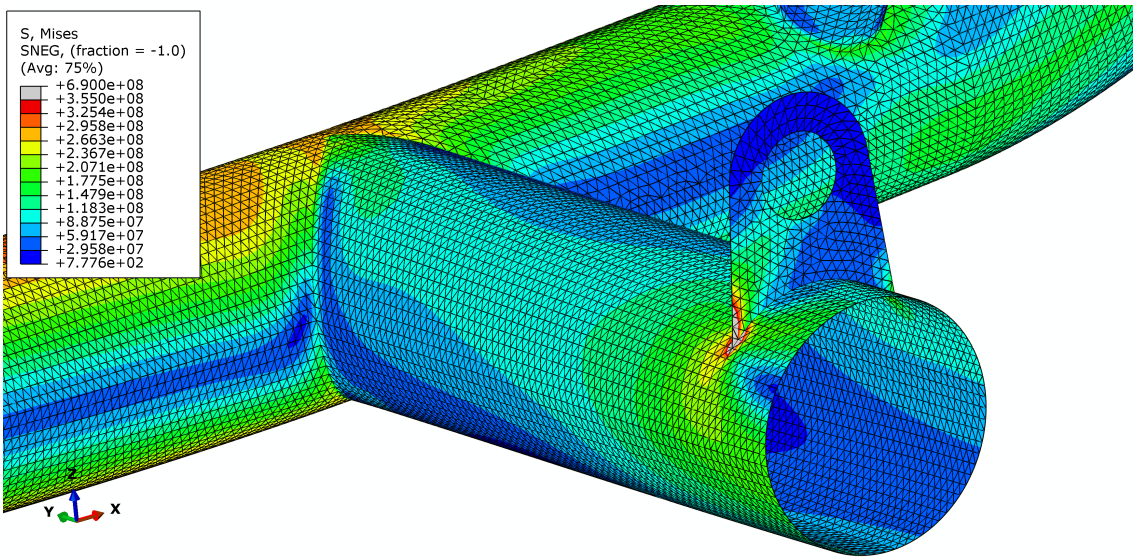


Figure 5.68: von Mises stress of the simulation with the increase of the tube diameter [Pa].

As can be seen, the stresses were reduced spontaneously, leaving only a simple area of high stresses. As the forces applied at the eyebolt, present in the tube, are extremely high, a solution to reinforce this area was considered. A reinforcement plate of 3 mm thickness and 50 mm length was added between the eye and the tube, following the circular shape of the tube. The aim would be that after the application of the intermediate pipe, this plate would be welded to the pipe and then the eyebolts would be welded to this plate. To simulate the plate, it was then necessary to create a partition in the tube with the size of the plate and the thickness of this section was changed for 6 mm, being 3 mm of thickness of the tube plus 3 mm of thickness of the new plate. It is important to mention that for the definition of this thickness it was necessary to change the parameter of shell offset for "Specific Value" in order to guarantee that from the face of the tube to the inside there was 1.5mm of thickness and to the outside 4.5mm, as demonstrated in the figure 5.69.

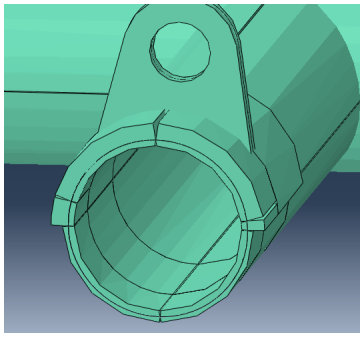


Figure 5.69: Detail section with thickness visible.

The following figure shows the results obtained with the new change.

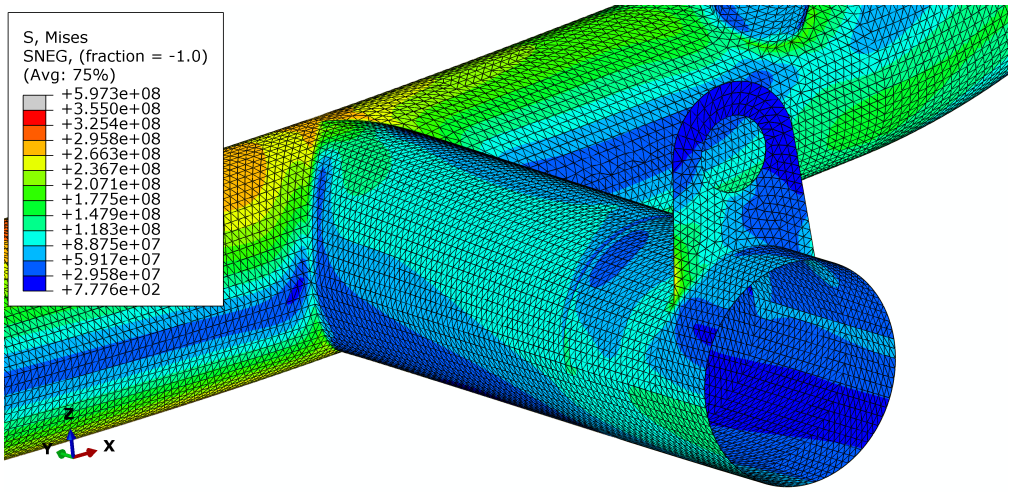


Figure 5.70: von Mises stress obtained with the addition of the reinforcement plate, in zone 2 [Pa].

As can be seen, the addition of the reinforcement plate removed all the high stresses in zone 2, thus concluding the analysis of this zone.

5.2.3 New design SolidWorks

Before proceeding to the reinforcements required in zone 3, marked in figure 5.26, of solution six, the zone was reassessed and it was decided to make some changes to the structure. These changes were made in SolidWorks software and aimed to change some directions of the tubes and also to ensure that the reinforcements chosen up to this point did not intersect the outside of the scooter.

Regarding the pipes, the main changes were: change the diameter of the main pipes to 50mm, as changed in Abaqus, increase the radius of curvature that the pipe makes in zone 1 in order to reduce the stresses applied there and also change the direction of the connecting pipes to the steering column. The structure with the new changes was then converted to SolidWorks and adjusted again as required for the first conversions. The updated solution six is shown in figure 5.71.

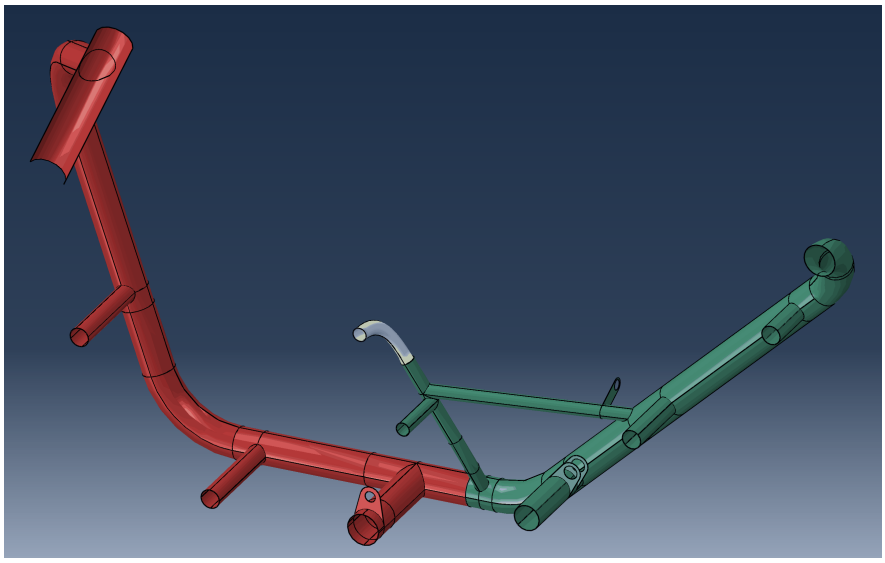


Figure 5.71: Frame part of solution six with the new modifications.

As it is possible to note, one of the major changes was the modification of the area where the tubes intersected the steering column. It was chosen to change the direction, so that the right pipe does not intersect with the left pipe and also to open space to be able to fit a reinforcement in zone 3 if needed. The result of the simulation of the updated structure, without any type of reinforcement, is shown in the following figure.

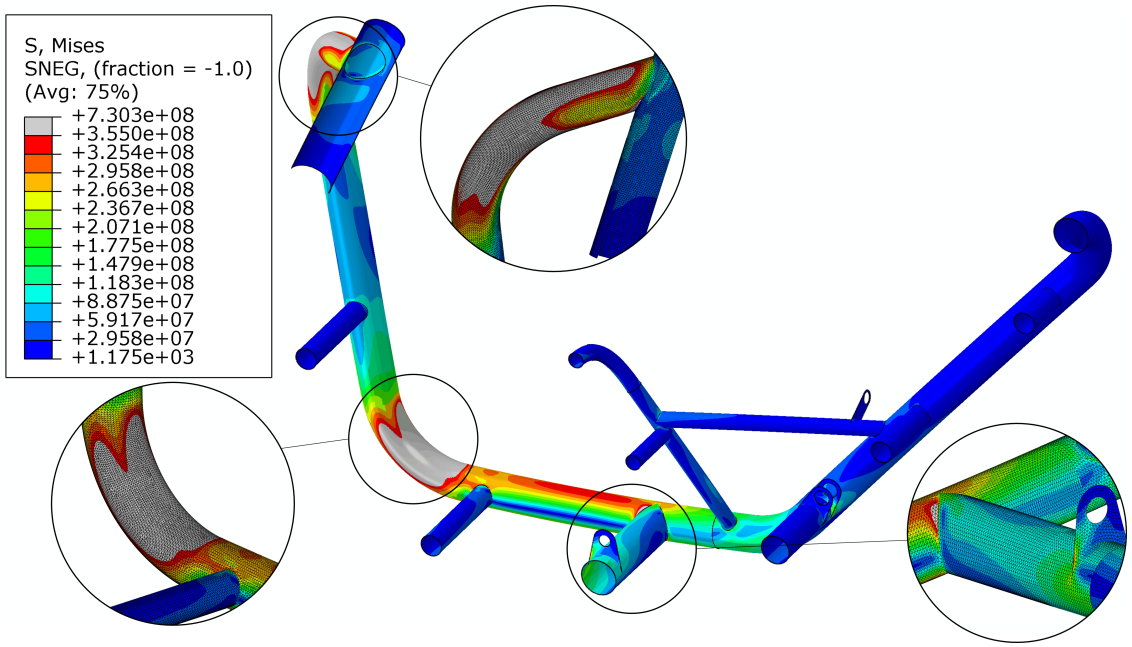


Figure 5.72: von Mises stress of the solution six without any reinforcements [Pa].

Comparing the result of the modified solution with the result of the initial solution, presented in figure 5.23, it can be seen that the maximum stresses have decreased but the areas where the highest stresses are found are greater in zones 1 and 3. Following this, the aim would be to analyse the new structure with the reinforcements selected so far. However, when the reinforcements were crossed with the scooter body it was noticeable that the reinforcement in zone 2 did not present any problems, but that the reinforcement in zone 1 did not fit into the structure. Therefore, the reinforcement of this zone was adapted in order to follow the external structure, resulting in the shape shown in figure 5.73. For zone 2, it was decided to continue with the same selected reinforcement.

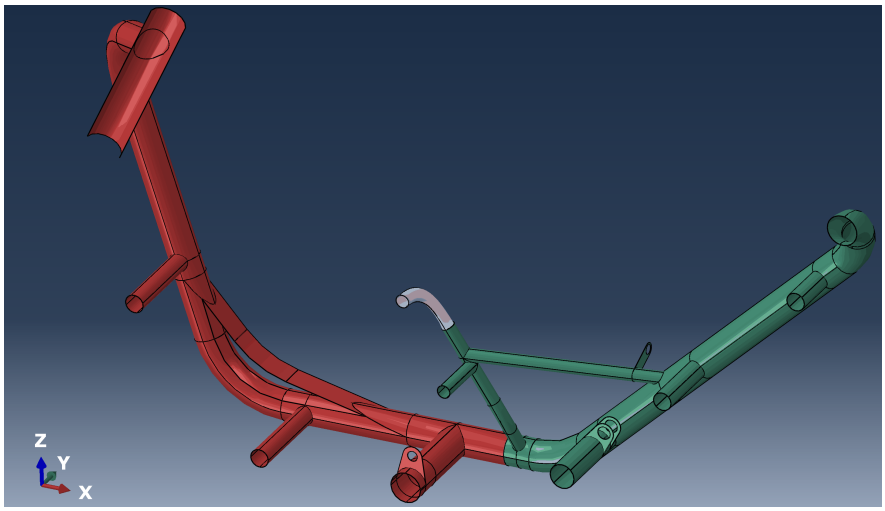


Figure 5.73: Frame part of the sixth solution with the main reinforcements.

The result of the simulation of the structure with modifications and reinforcements is shown in the following figure

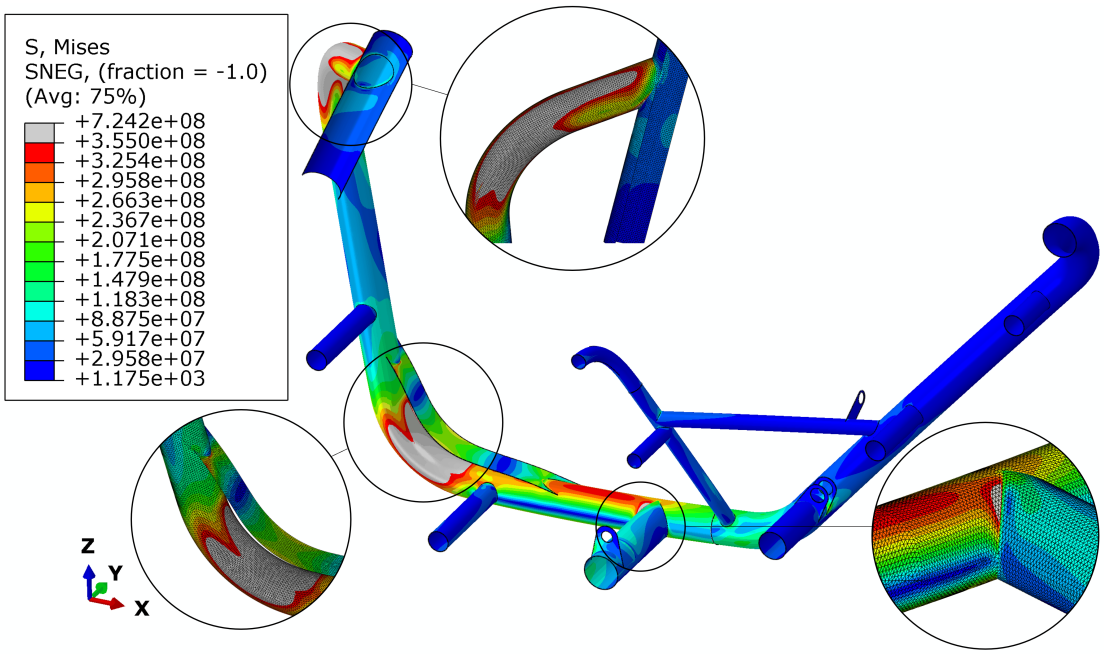


Figure 5.74: von Mises stress obtained with the simulation with the main reinforcements applied [Pa].

With the change of the reinforcement in zone 1, it is possible to observe that it did not have the same effect that it had before the modification, intensifying the resulting stresses in the zone. The next step was to analyse of the 3 reinforcement options that had better results, presented in subchapter 5.2.1, which one could be a better solution than the one presented. Thus, it was chosen to try a combination of the current solution with the u-shaped profile configuration. Lateral plates were then designed to the current one as shown in figure 5.75.

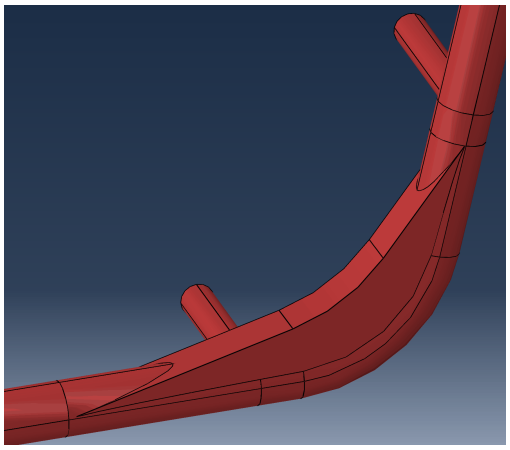


Figure 5.75: Reinforcement with the lateral plates.

The simulation result with the new reinforcement is shown in figure 5.76.

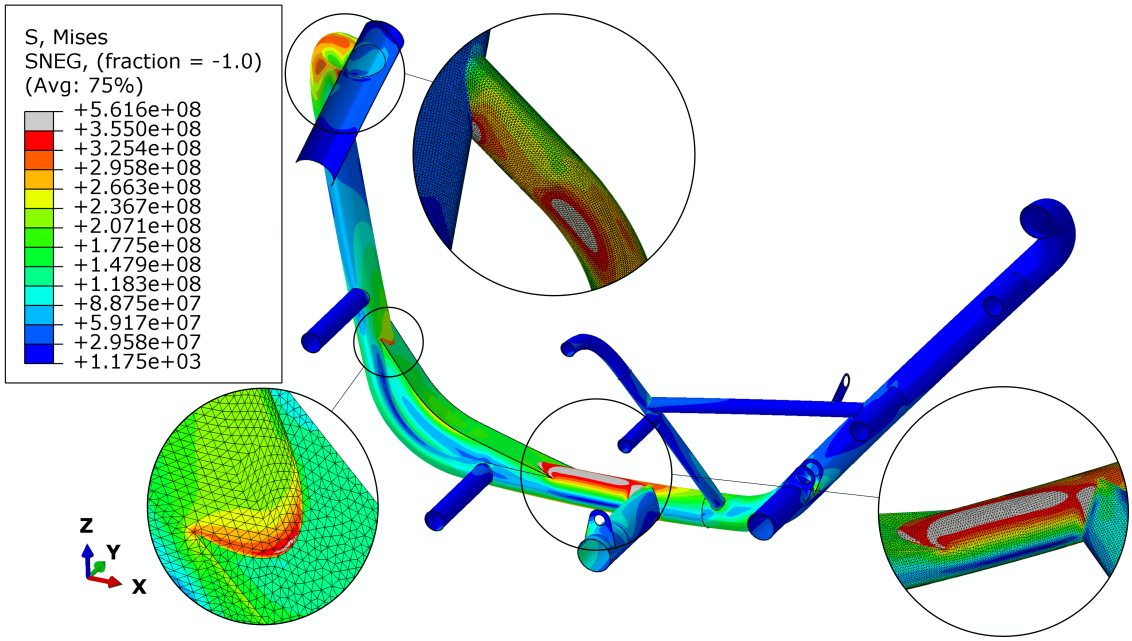


Figure 5.76: von Mises stress obtained by the simulation with the change in the reinforcement [Pa].

With the adjustment of the reinforcement it was possible to obtain better results, both in zone 1 and zone 3, where the area affected by the highest stresses decreased. Despite the improvements, stresses were added at the connection of the reinforcement with the chassis tube. The next step was to extend the reinforcement until after the intermediate tube, as this carries the eye where very high forces are applied. The following figure shows the new design of the reinforcement in zone 1.

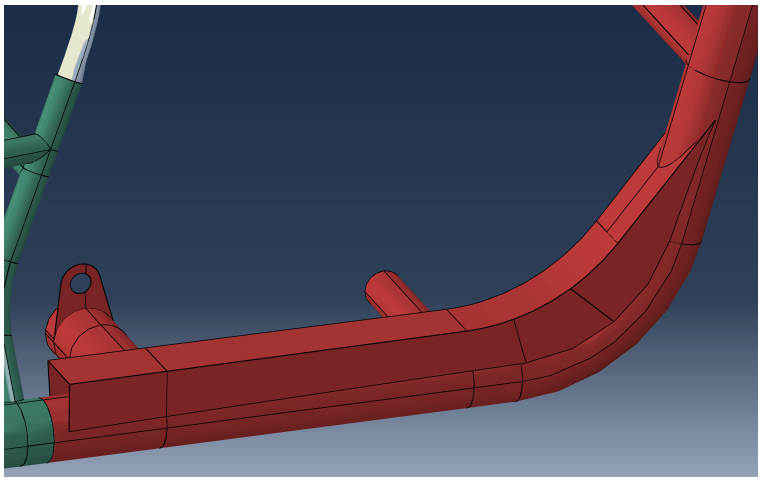


Figure 5.77: New design of the reinforcement in zone 1.

The following figure shows the result of the simulation described.

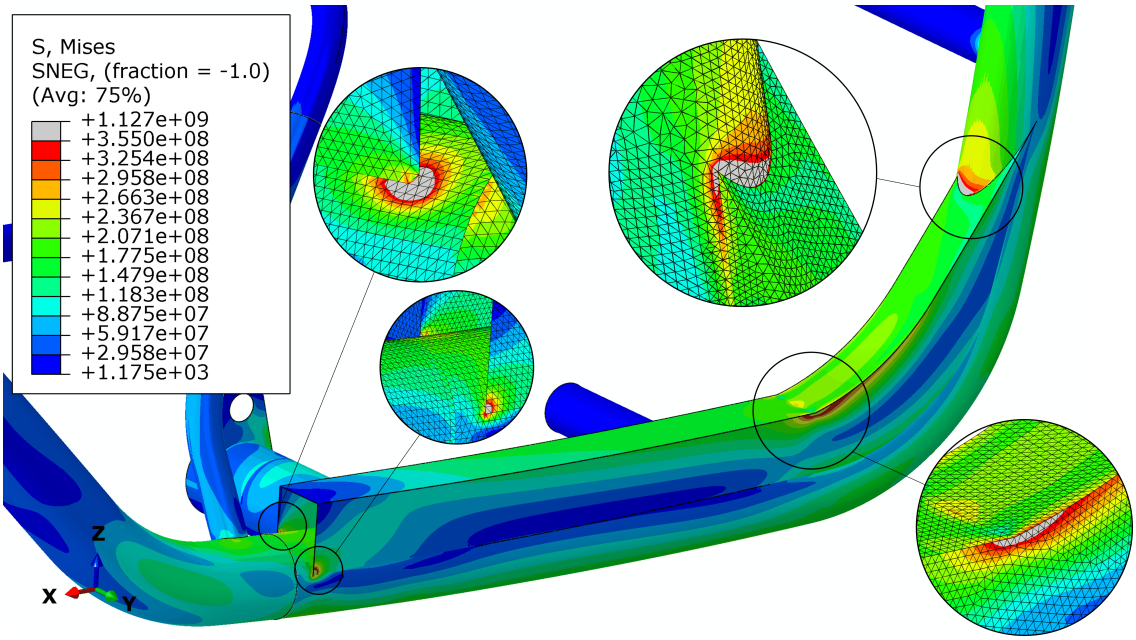


Figure 5.78: von Mises stress obtained with the new design of the reinforcement in zone 1 [Pa].

From the results presented, it can be seen that there was a significant improvement with the extension of the reinforcement. The area that presented extremely high tensions was eliminated, presenting now only a few points of high tensions, mainly at the connection with the main tube. In order to eliminate the stress points created at the end of the reinforcement, it was cut in a triangular shape, as shown in figure 5.79.

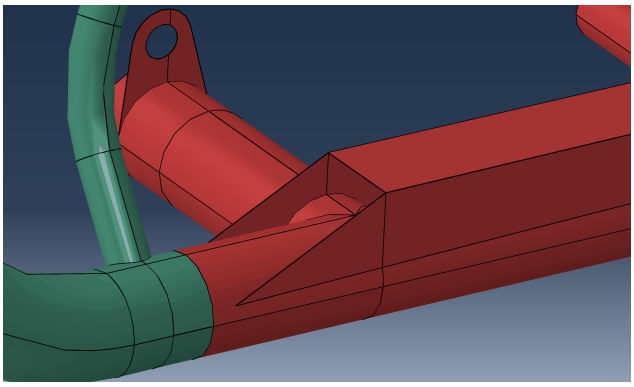


Figure 5.79: Detail added to the reinforcement.

The result of changing the end of the reinforcement is shown in the following figure.

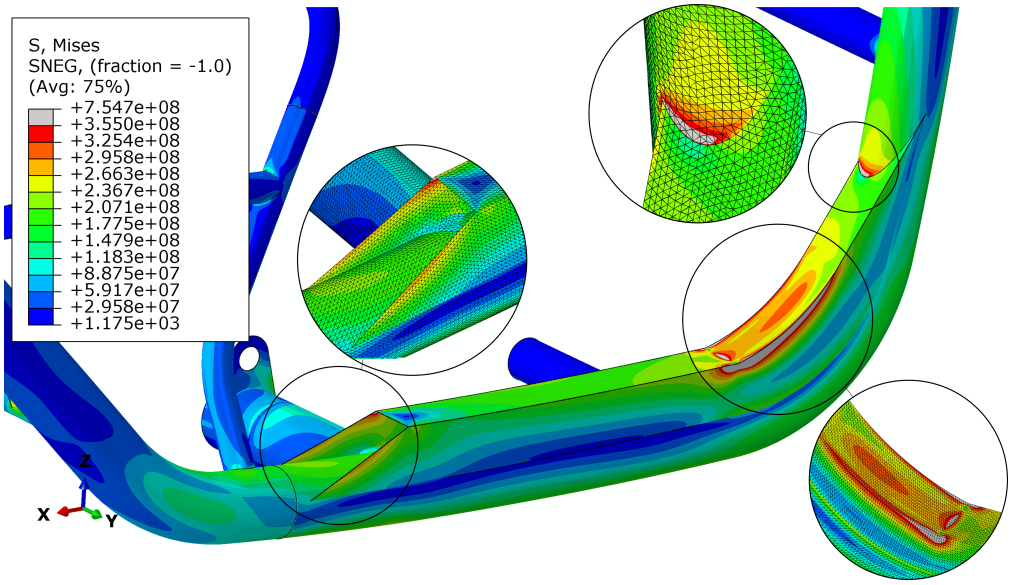


Figure 5.80: von Mises stress obtained with the change of the reinforcement [Pa].

In figure 5.80 it is possible to observe that the high stress points were eliminated with this adjustment of the end of the reinforcement. As already mentioned, Abaqus is very influenced by the details of the solutions, knowing this, the reinforcement was redesigned so that there is tangent between the extension of the reinforcement and the curvature zone of this. This way, it was possible to obtain the following result.

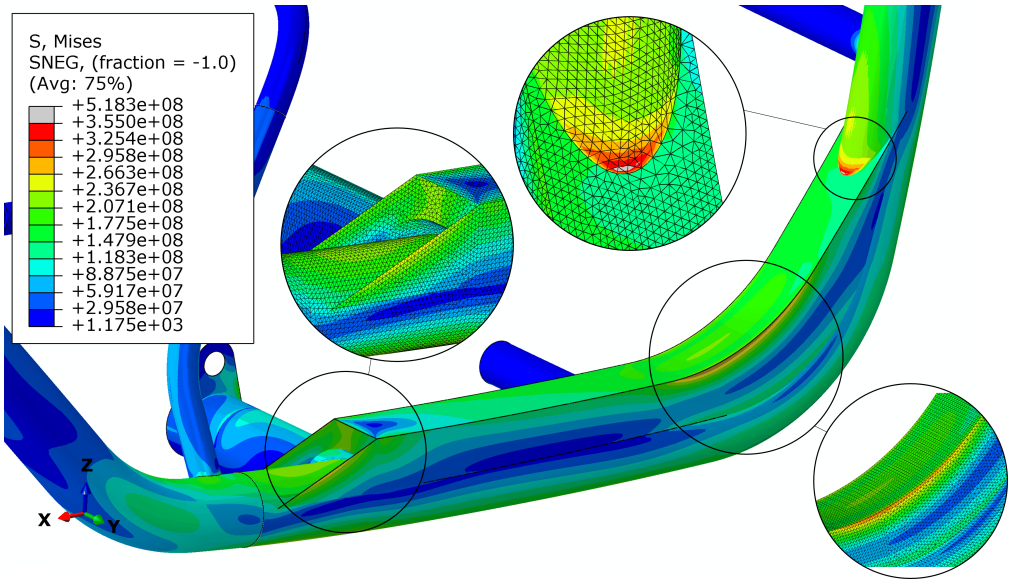


Figure 5.81: Final results of von Mises stress of the zone 1 with the reinforcement design improved [Pa].

With the adjustment of the tangency it was then possible to eliminate the tensions present in the reinforcement curvature, leaving only the upper area of the reinforcement with high tensions. This location of tensions is not very important since it is in an area where the reinforcement will be welded to the tube, placing material and increasing the resistance of the reinforcement.

5.2.4 Extra zone

After reinforcing zone 2 and improving the reinforcement in zone 1, it was possible to find another zone that also presented high stresses, as can be seen in figure 5.82. This figure is a more general representation of the results presented in figure 5.81.

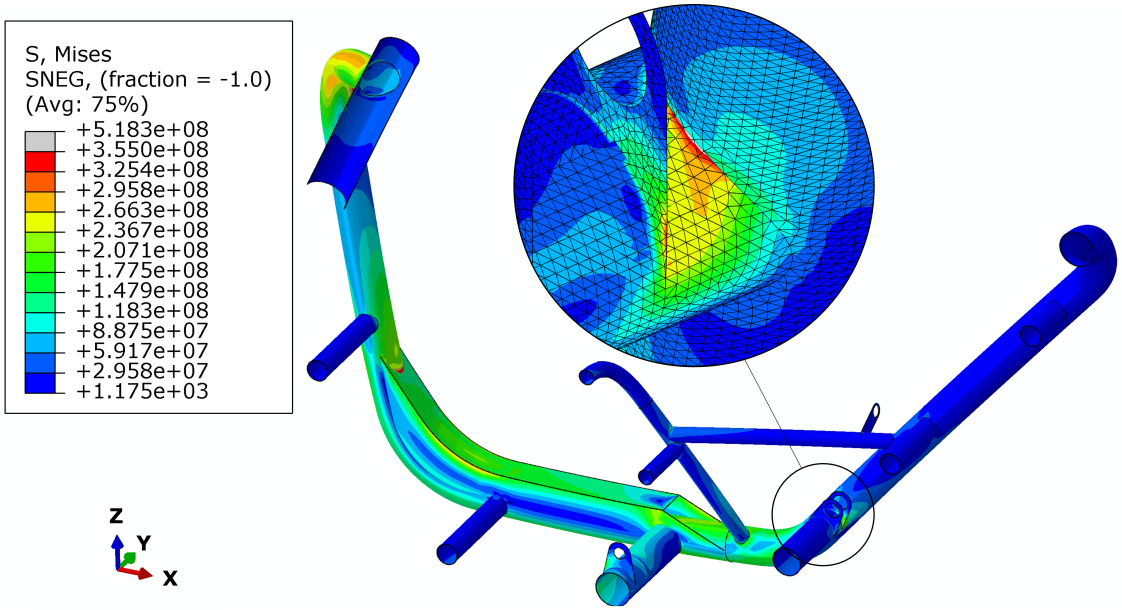


Figure 5.82: Detail in the results obtained in the last simulation [Pa].

The procedure for improving this area was to increase the thickness of the intermediate tube from 2 mm to 3 mm. This change is also important because this intermediate tube contains the eyebolt that connects the swing arm to the chassis. The result of the alteration is shown in the following figure.

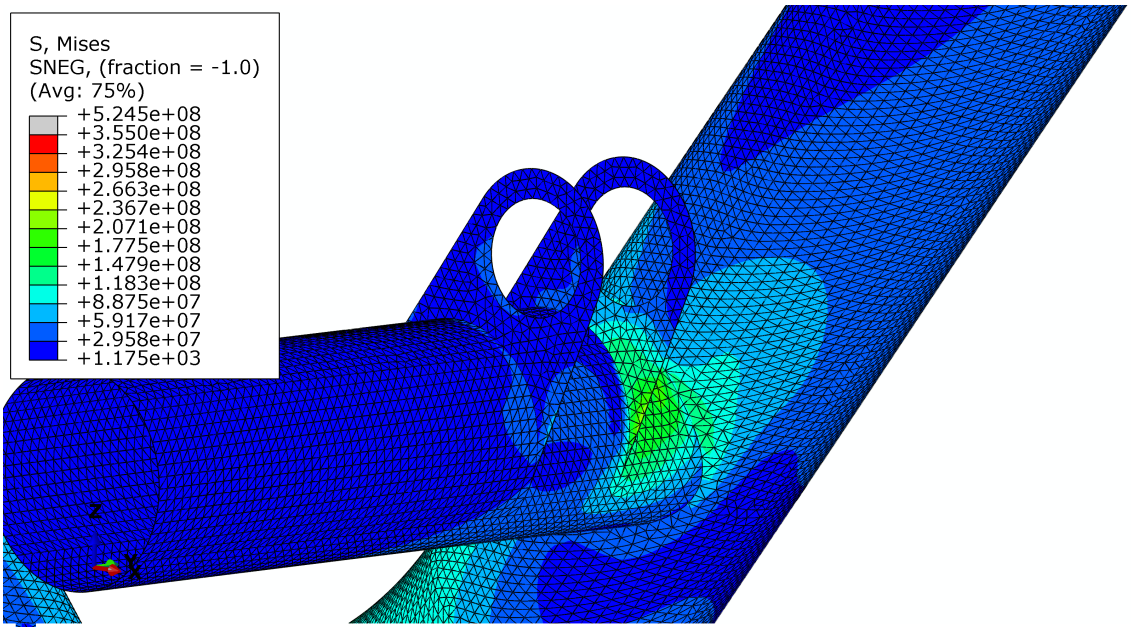


Figure 5.83: von Mises stress obtained with the improvement in the intermediate tube [Pa].

As can be seen in the figure above, the stress concentration was corrected by increasing the thickness.

5.2.5 Zone 3 - Modification on Boundary Conditions

Before proceeding to the reinforcement necessary to improve the stresses in zone 3, highlighted in figure 5.26, it was decided to reassess the boundary conditions. After re-evaluation, they were changed in order to try to better represent the real-life situation.

Regarding the steering column, it was decided to change the embedding condition of the column internal faces, since it is a very rough boundary condition that does not represent the reality. A cylindrical coordinate system was then added to the structure so that the z-axis was coincident with the axis of rotation of the column, as presented in figure 5.84a. In addition, two reference points were added associated by a coupling constraint with the column's lower and upper edge, as the figures 5.84a and 5.84b try to present. In order to approximate the simulation to reality, without detailing the simulation too much, it was assumed that the bottom edge of the column could not move, but that the top edge could move further away or closer and also rotate around the rotation axis. This is intended to assume that the steering column can stretch or shrink with the applied forces and can also rotate around its axis of rotation. Thus in relation to the constraints of the reference points with the edges, a kinematic coupling was used, with all degrees of freedom locked. Besides these constraints, another was added between the two reference points, associated to the created coordinate

system, which allows the displacement in z-axis and rotation around this axis also. Besides this, the lower reference point was applied an embedded boundary condition.



(a) between the reference point and the lower edge.

(b) between the reference point and the upper edge.

Figure 5.84: Tie constraints,

The boundary condition was also re-evaluated regarding the support associated with the swing arm, marked by C in figure 4.8. Thus, a cylindrical coordinate system was added to the eyebolt, as shown in figure 5.85, so that the z-axis coincided with the axis created between the center of the two eyebolts' holes. Subsequently, with a reference point connected to the inner edges of the eyebolts, all degrees of freedom, except U2 and UR3, were blocked by a coupling constraint. These degrees represent the radius variation that the eye can present and the rotation of the edges around the z-axis of the new coordinate system. At the reference point, a displacement boundary condition was applied to block all directions except the x-displacement, which intends to demonstrate that the frame can shrink or stretch with the applied forces.

The conditions used in the following simulations will be with the boundary conditions described above.

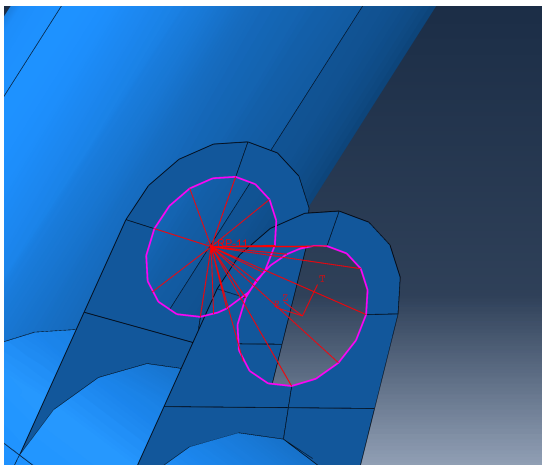


Figure 5.85: Tie constraint between the reference point and the inner edges of the eyebolts.

In this way, it is believed to represent reality in a more correct way, without going into too much detail.

Therefore, solution six was simulated without any type of reinforcement in order to observe the influence that the new boundary conditions have on the structure. The results of this simulation are shown in figure 5.86 and can be compared with the results of figure 5.72.

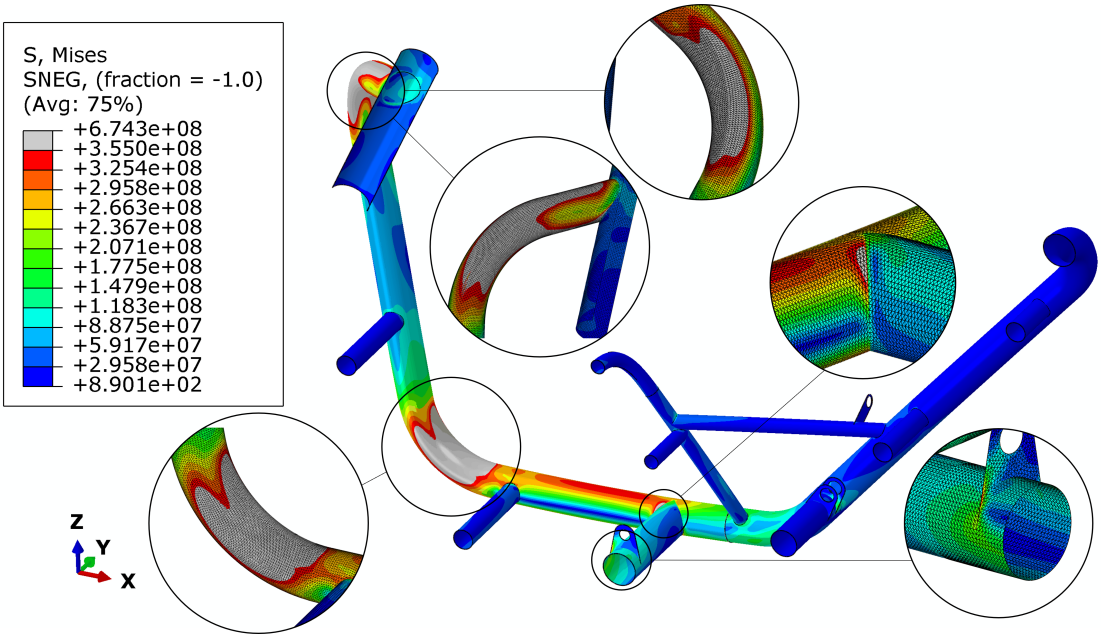


Figure 5.86: von Mises stress obtained by the simulation with the new boundary conditions [Pa].

Comparing the two results that only differ in the boundary conditions, it is possible to see that in terms of areas affected with high stresses there was no improvement, since they are very similar mainly in zones 1 and 3. However, using the new boundary conditions the maximum resulting stress is lower, which can be an indicator of an improvement.

Next, it was advanced to solution six with all the reinforcements, that is, in zone 1, zone 2, and the extra zone. This solution was simulated and the result obtained is shown in figure 5.87.

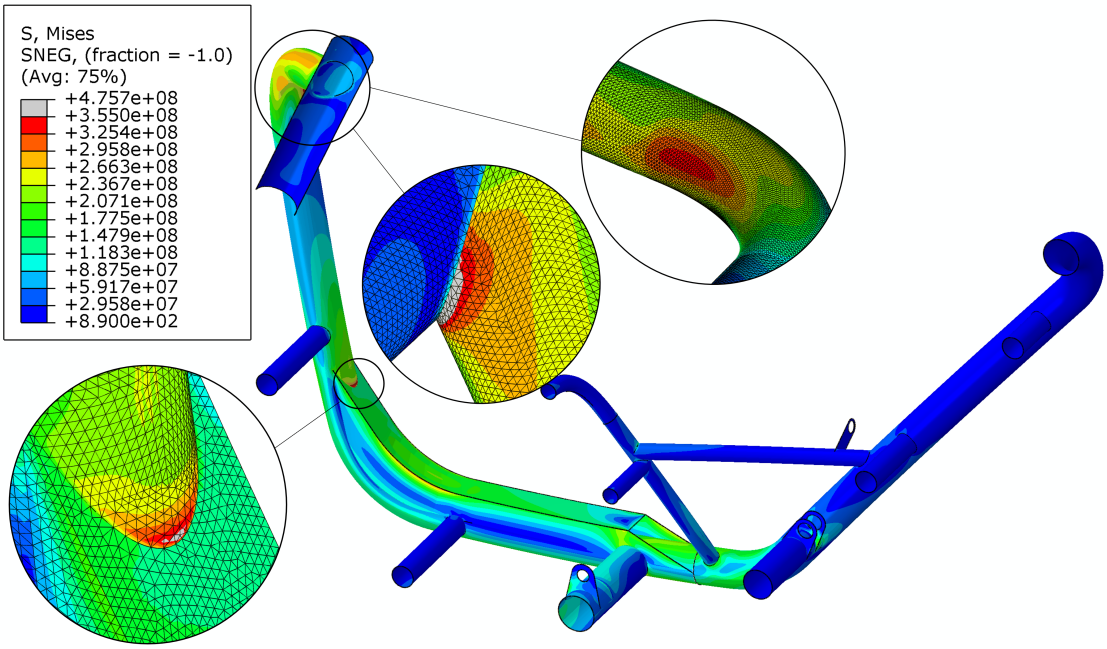


Figure 5.87: von Mises stress of solution six with the reinforcements applied [Pa].

As can be seen from the results, with the reinforcements applied, the structure of solution six is extremely improved, with an evolution either in the most affected areas or in the resulting maximum. Analysing the results, it can be seen that the reinforcements in zones 1, 2 and in the extra zone completely reduce the stresses obtained.

In zone 1, it is possible to observe a small area with slightly higher stresses, but it is reasonable to think that as the welding cord would be in that zone, connecting the reinforcement to the tube, these stresses would disappear as it would give more material and rigidity to the place.

Regarding the zone 3 of the solution six, a small grey area can be observed between the connection of the frame tube and the steering column. In this situation, it was also assumed that with a welding seam, or even a double seam, these tensions would not be originated since the connection would be much stiffer. This concludes the analysis of the structural reinforcements of solution six.

For comparison, the simulation presented has a total number of nodes of 521689 and, as explained in subchapter 4.4, consists of STRI65 quadratic triangular elements.

5.2.6 Final Mesh

This subchapter has as single objective to present a comparison of results between simulations with quadratic triangular elements and linear quadrilateral elements. In this way, the last simulation presented was improved in the whole mesh, so that all areas present

a structured mesh. In the following figure, it is represented an example of the code of green colour, that the program uses for when the surface, to be meshed, presents the necessary conditions to apply a structured mesh.

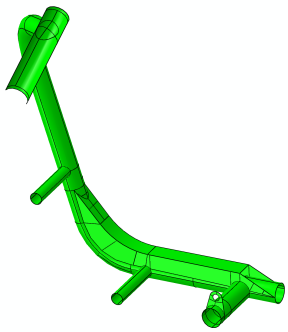


Figure 5.88: Colour code used by Abaqus software to identify that the surfaces that is able to create a structured mesh.

As it is possible to verify, the whole front structure presents good conditions for the application of a structured mesh. The simulation results are presented in the figure below.

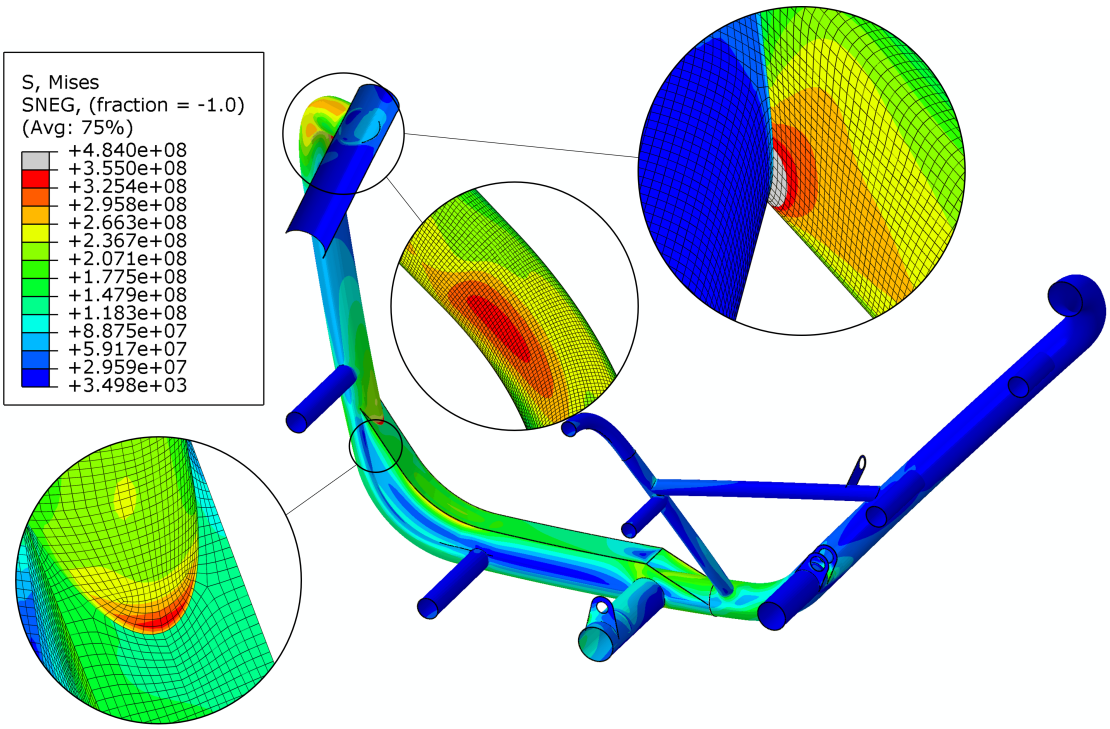


Figure 5.89: von Mises stress of the simulation of the solution six with a structured mesh [Pa].

Observing the figure 5.89 it can be seen from the zoom-in views that the mesh is

structured, symmetrical and with relatively similar elements in terms of size. Furthermore, it is also possible to observe that in zone 1 the highlighted zone is better compared to the one shown in the previous results, because it does not present any stresses above the yield limit. However, it is important to highlight that as the connection between the reinforcement and the structure is made with a weld cord, this would further reinforce this area.

Regarding zone 1, we can see that the affected area is more localised and smaller. Thus, it is again possible to assume that the double welding bead would be a good solution to avoid problems at this location.

This simulation has 137613 nodes and consists of linear quadrilateral elements of the S4R type.

To conclude the extensive analysis of solution six, it is important to note that the final mass of this chassis is 12,608 kg and also look at the deformation of the structure, presented in figure 5.90.

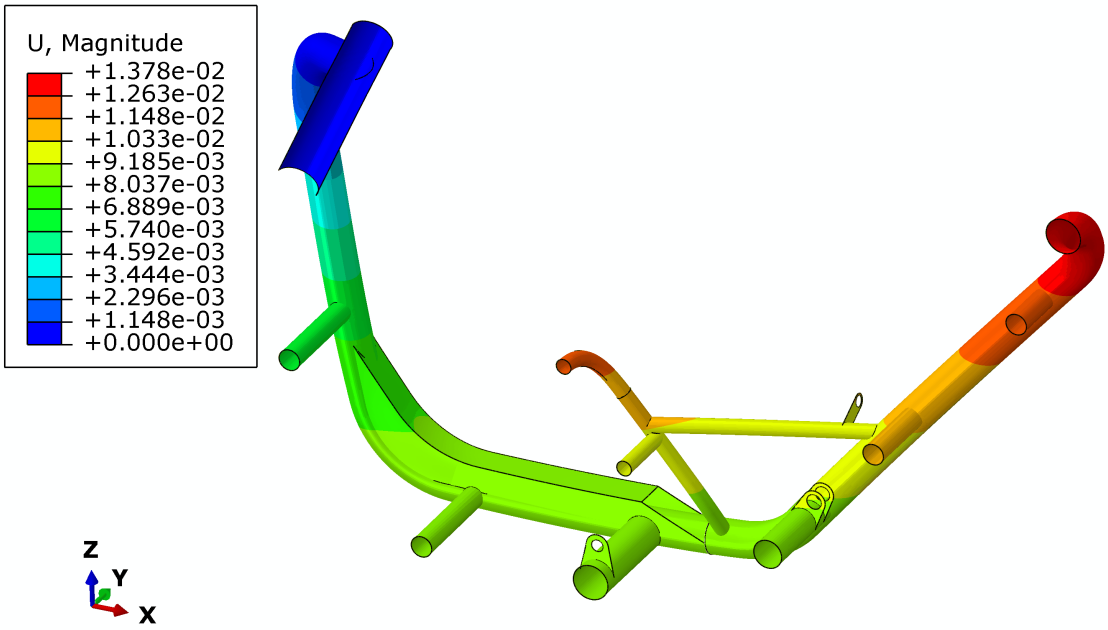


Figure 5.90: Displacement results, in meters of the sixth solution simulation.

5.3 Structural reinforcements in solution seven

This subchapter is focused on the development of the reinforcements for the solution seven. After the complete analysis of solution six, the analysis of solution seven starts again by making some changes to the structure itself, using SolidWorks software:

- alteration of the diameter and thickness of the main pipes to 50 mm and a thickness of 3 mm;
- change of the diameter of the intermediate tube where the eyebolt that serves as a connection to the shock absorber belongs;
- modification of the radius of curvature of the lower part of the chassis from 100 mm to 125 mm;
- alteration of the thickness to 3 mm of the intermediate tube where the eyebolt that serves as a connection to the swing arm belongs to;
- increase the height of the chassis in order to create more space between the exterior design of the scooter and the frame;
- change of the direction of the pipe connecting to the steering column.

Despite the modification to the direction of the connecting tube, it is important to note that with the increase to 50 mm diameter it was extremely complicated to find a way to connect the frame to the column, without intersecting with the scooter body. As can be seen in the picture below, with the steering column at the angle and height provided in the first assembly, the tube overlaps the outer design by a few millimetres. It is therefore necessary to mention that if at the end of all the analysis, this solution is the most suitable, it will be necessary to change the exterior design of the scooter by a few millimetres.

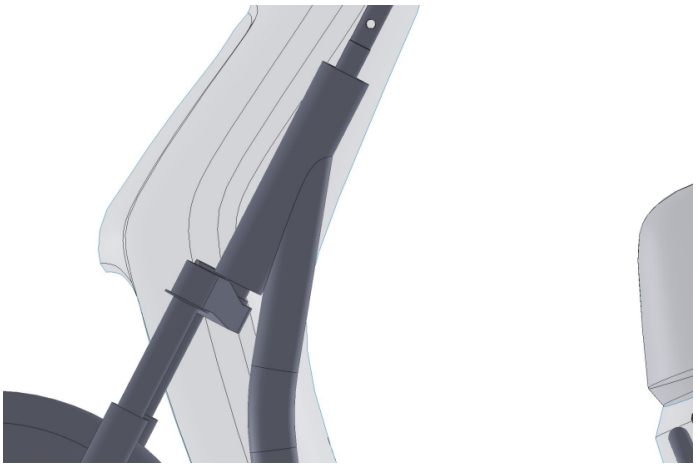


Figure 5.91: New modifications intersect the external body of the scooter.

The following figure shows solution seven, already converted to Abaqus, with the changes mentioned above.

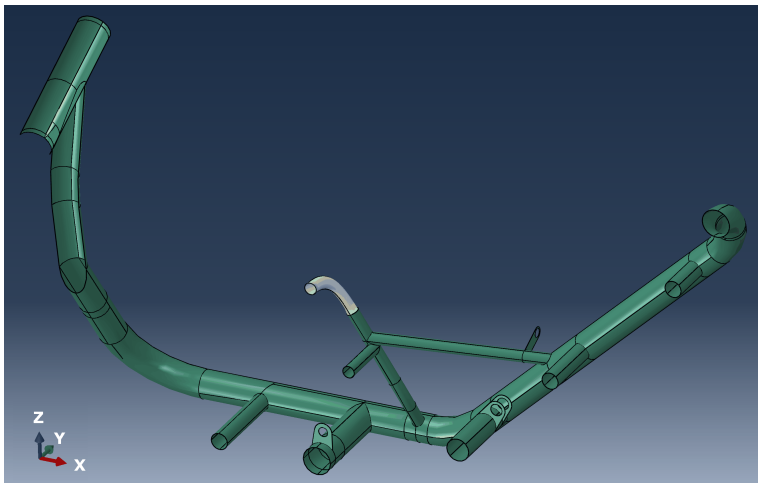


Figure 5.92: Frame of the seventh solution with new the modifications.

In figure 5.93 is presented the simulation results of solution seven with the modifications mentioned, but without any type of reinforcement. This result can be compared with the result presented in figure 5.25, since they present different changes in the structure and also different boundary conditions.

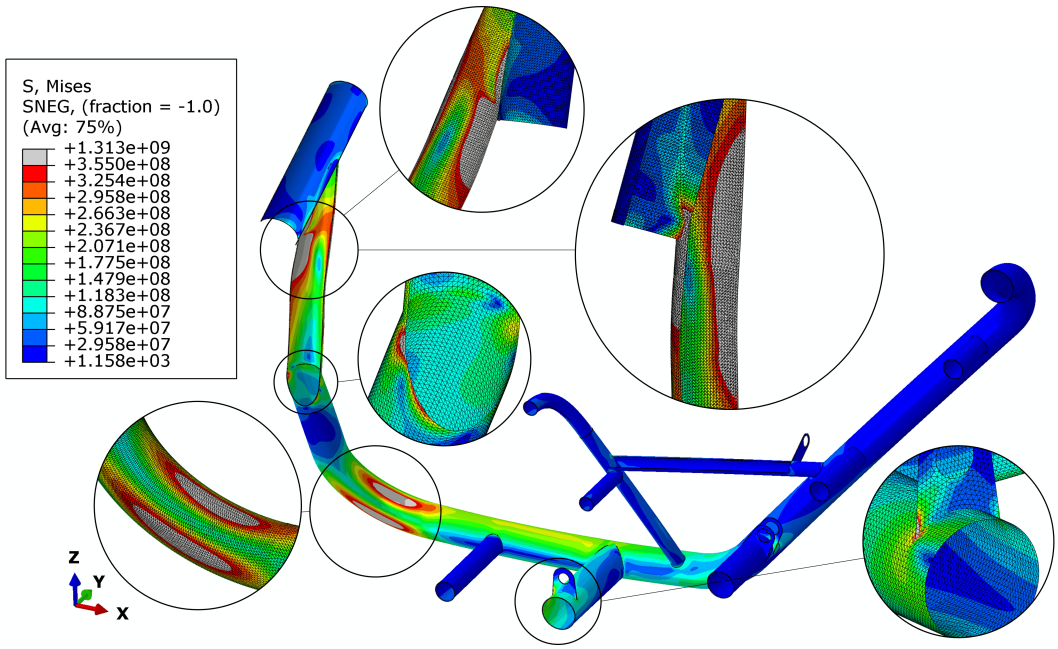


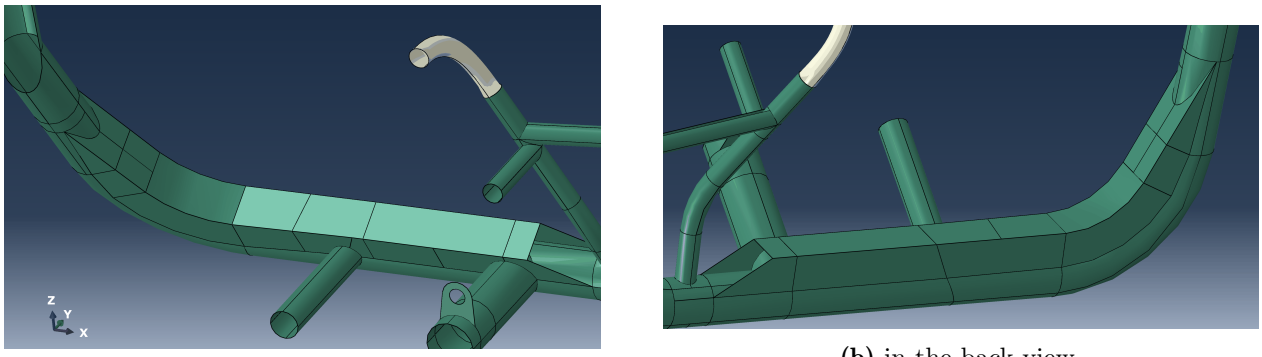
Figure 5.93: von Mises stress of the simulation of the seven solution, without any reinforcement [Pa].

As it is possible to compare between the two results, the maximum stresses decreased,

but the areas where the stresses are higher than the yield stress remained similar, except in zone 2 where the stresses were extremely reduced.

A zone that presents slight differences is zone 1, where the affected area compared to the previous result is slightly reduced. This reduction is due to the fact that the radius of curvature in zone 1 has been increased. In addition, a small reduction can also be seen in zone 3, at the connection to the steering column. Overall, it can be said that the maximum von Mises stress has decreased and some of the modifications to the structure have brought positive results.

After analysing the structure without any reinforcement, the two developed for solution six were introduced. Thus, as it is possible to observe in the figure 5.94 it was developed a reinforcement for the zone 1, constituted by a bent u-shaped sheet that follow the direction of the frame. In addition, the reinforcement plate for zone 2 was also added, as shown in figure 5.95



(a) in front view.

(b) in the back view.

Figure 5.94: Reinforcement of the zone 1,

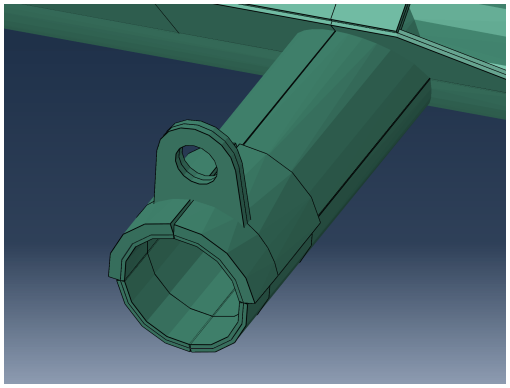


Figure 5.95: Reinforcement of the zone 2.

The simulation result of solution seven, with the reinforcements similar to those used in solution six, is shown in the following figure.

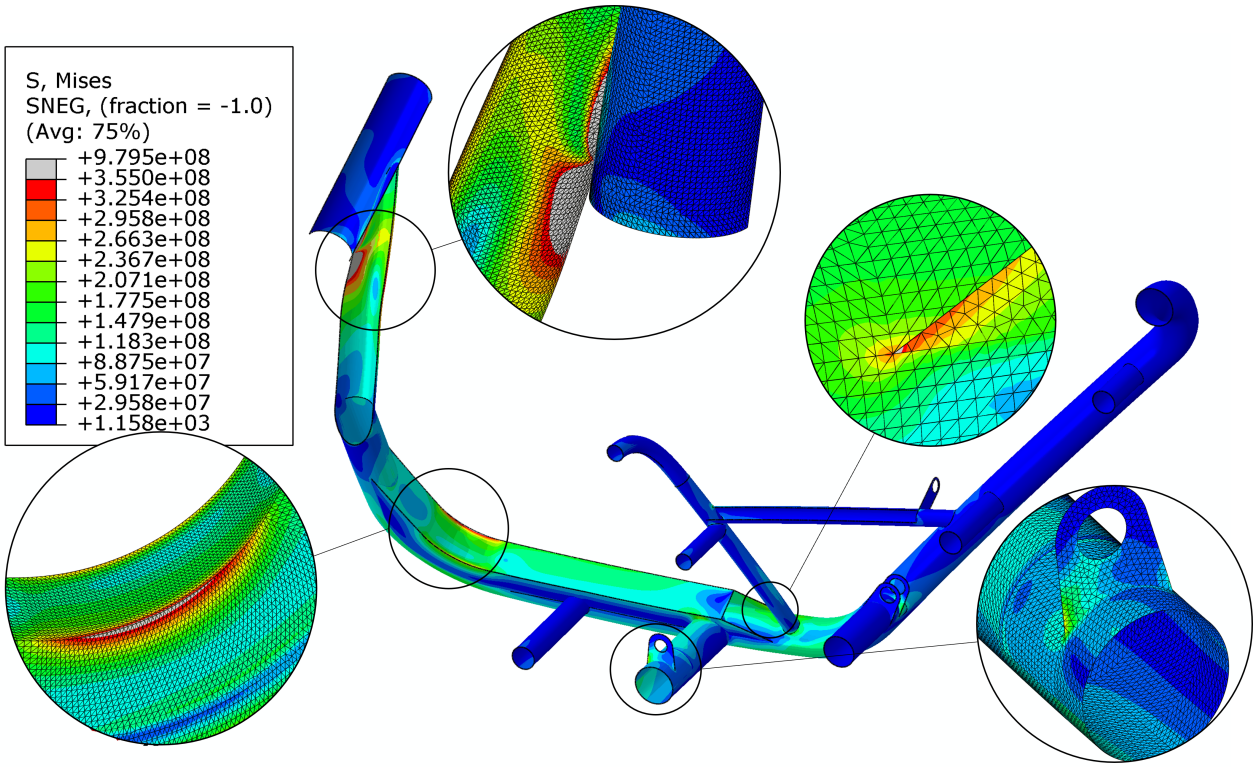


Figure 5.96: von Mises stress of the simulation with the reinforcements applied [Pa].

Analysing the results with and without reinforcement it can be observed a great evolution in the stresses. The highest stresses were significantly reduced and the stresses in the reinforced areas were exponentially reduced.

In zone 1, with the reinforcement of the U-shaped bent plate, there is only a small grey area, but it is not a concern for two main reasons. The first, as already mentioned, the Abaqus software is very sensitive to details and so these high stresses can occur from the design of the sheets and from not having performed this design in the best way for the software. In addition, it is wise to ignore these stresses because in reality when bending the sheet, it will always present a radius of concordance in the bend and not a 90 degree angle as the design in the drawing. Several attempts were made to change the design in order to represent the radius of concordance. However, due to the curvature of the faces, no valid solution could be found.

Also in the reinforcement applied to zone 1, it is possible to find a singularity that will be ignored in the analysis. This situation appears as a singularity since the stresses above the yield stress are found in only one node, and this node serves as a connection to the frame tube. Again, it may be the design details of the reinforcement itself that are causing these stresses.

In zone 2, it is easy to see that the solution of the sheet reinforcement completely solves

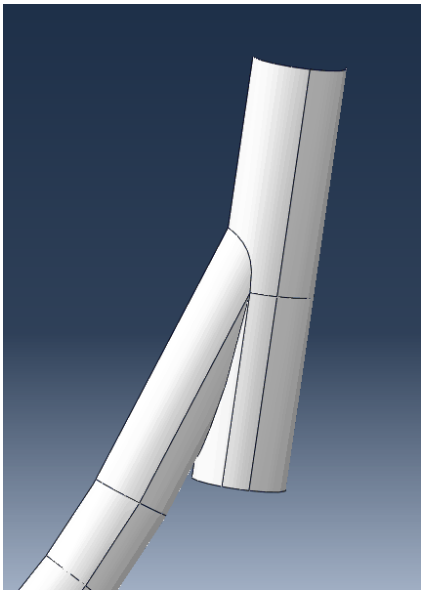
any stresses obtained.

In zone 3, as no reinforcement was applied yet, it is possible to observe a zone with high stresses in a relatively significant area. Therefore, the next subchapter will be dedicated to the development of the best reinforcement for this area.

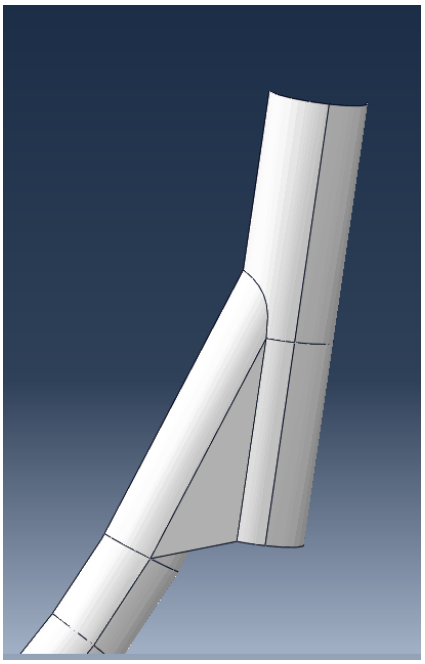
5.3.1 Zone 3

Even after the reinforcements added to zones 1 and 2 of solution seven, zone 3 is still under very high stresses. This can be explained by the fact that in solution six there were two tubes connecting to the steering column, while in solution seven only one tube is the connector. Thus, it was necessary to carefully evaluate zone 3 of solution seven.

The first iteration of reinforcement was based on the chassis used in the market, presented in subchapter 2.2.7. Figure 5.97a shows the frame connection to the steering column, without any reinforcement. While in figure 5.97b is a view of the first reinforcement solution consisting of a 3 mm triangular plate that connects to both the tube and the steering column.



(a) Initial view.



(b) Final view.

Figure 5.97: Reinforcement of the zone 3 of the solution seven.

The results obtained for this change are shown in the figure below. This presents a more detailed view on the area under study, rather than the whole structure.

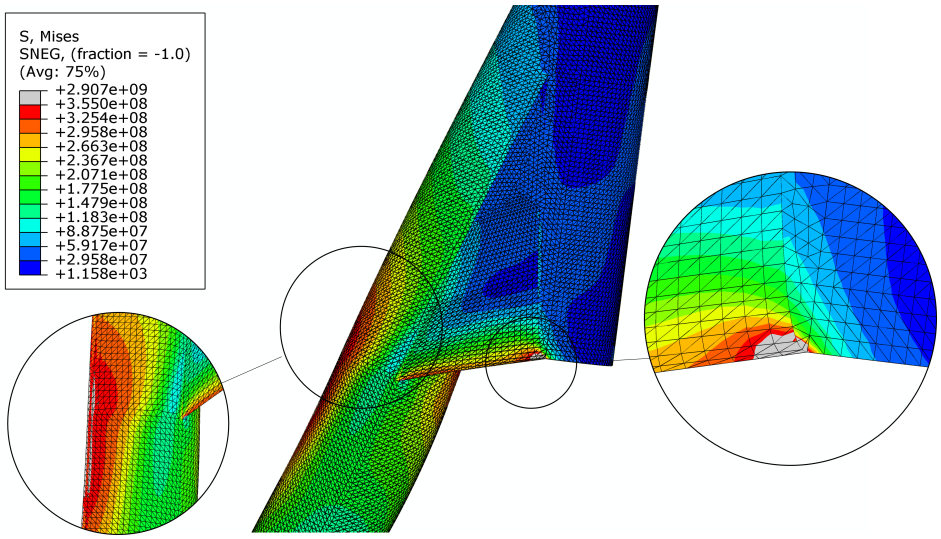


Figure 5.98: von Mises stress of the solution seven with the added reinforcement in zone 2 [Pa].

Observing the results we can see two issues. The first is the lack of rigidity that the tube presents to support all the stresses applied on it. The second is the small area of the plate that presents stresses above the yield stress. This area is concentrated mainly in the connection of the plate to the steering column and it is possible to consider that these stresses can be a result of the details when creating the plate.

Another perspective was analysed in order to reinforce zone 3. In the picture 5.99 is the frame connection, divided by various colours. In the red tube, the thickness was changed from 3mm to 4mm, and the outer diameter of 50mm remained unchanged. The goal is to give more rigidity to the tube itself in order to understand if it is possible to solve this area with this simple solution.

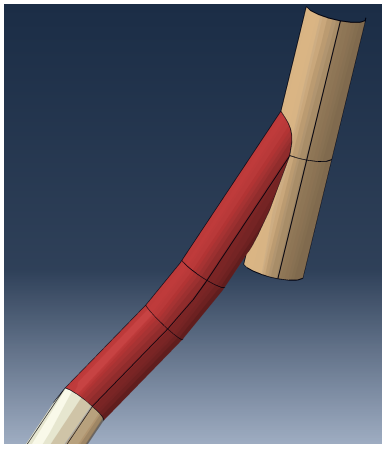


Figure 5.99: View of the tubes that suffered a change in the thickness.

The results obtained for the simulation presented are shown in the figure below.

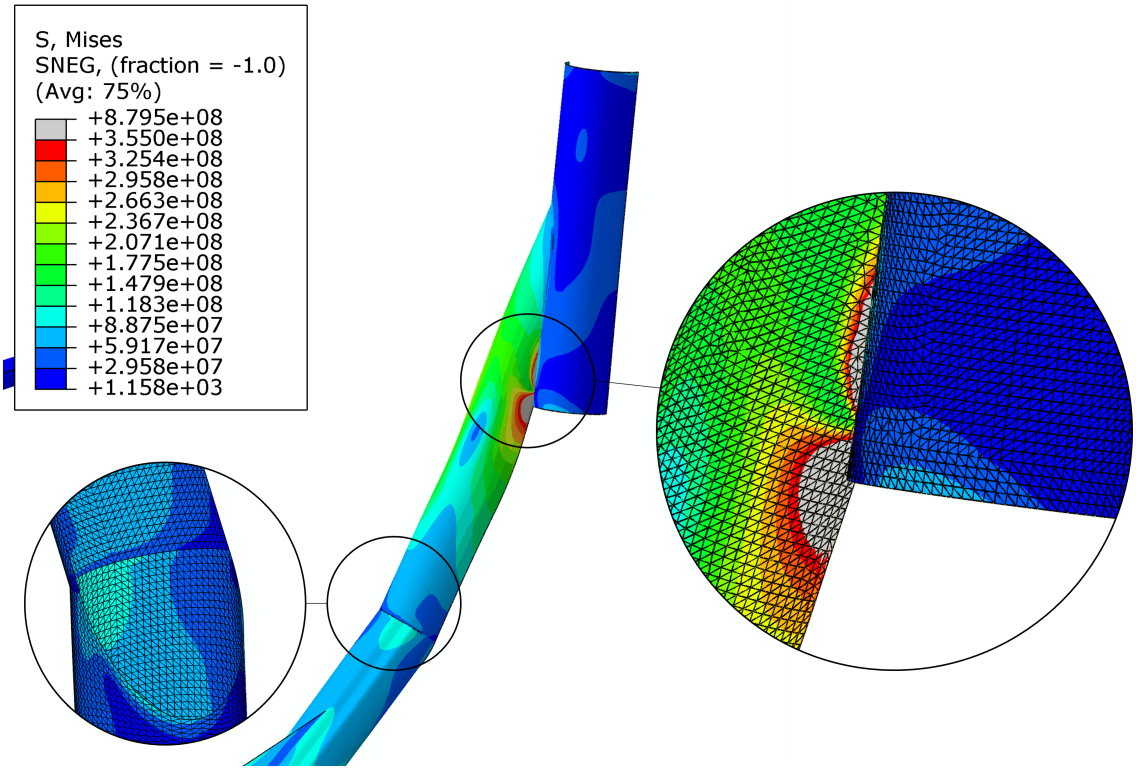


Figure 5.100: von Mises stress of the simulation with the change of thickness in the main tube [Pa].

Comparing the results obtained with previous ones, it can be seen that in terms of stresses in the pipe itself there was a great evolution. However, the problem of stresses near the connection was not solved yet. In this way, the two solutions presented were combined, namely: the increase of the thickness to 4 mm and the application of the triangular plate, in order to reinforce zone 1. The result of the simulation of solution seven is shown in figure 5.101.

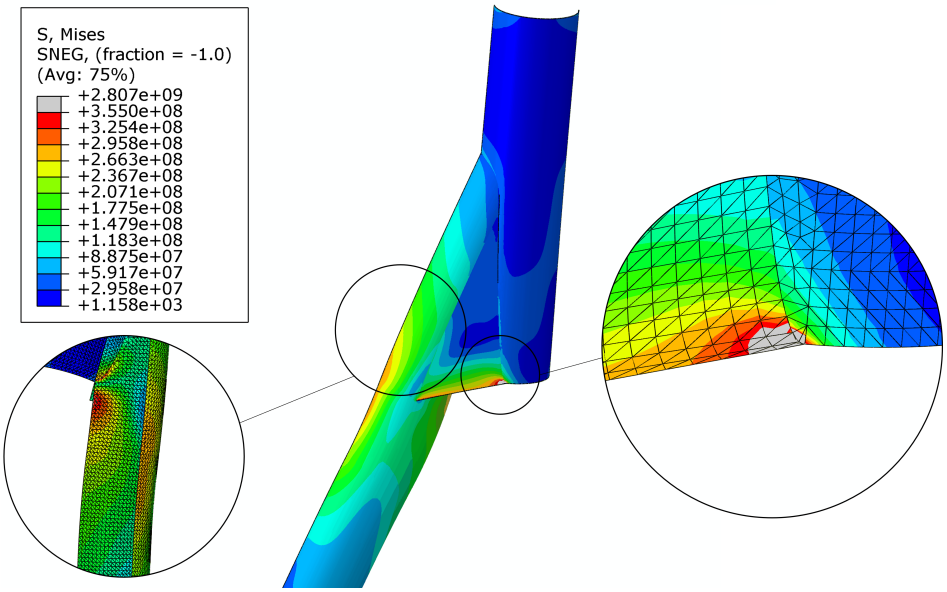


Figure 5.101: Final result of von Mises stress of the solution seven with the reinforcements in zone 2 [Pa].

With the changes applied it can be seen that the stresses in the tube have improved significantly, but that the connection point between the reinforcement and the steering column still has very high stresses. Apart from the fact that the problem of these stresses could be from the design details, it is also possible to considerate that with the weld joint at this location the resulting stresses would no longer be so high.

One more iteration was developed in order to check if the area presenting the high stresses is possible to reduce. For this, a part of the triangular plate was removed so that it does not concentrate all the stresses in the connection area. The iteration is presented in the figure below.

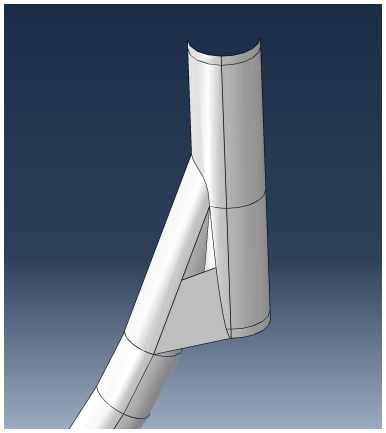


Figure 5.102: New iteration of the reinforcement on zone 2.

The simulation result with the change in the reinforcement of zone 2 is shown in the following figure.

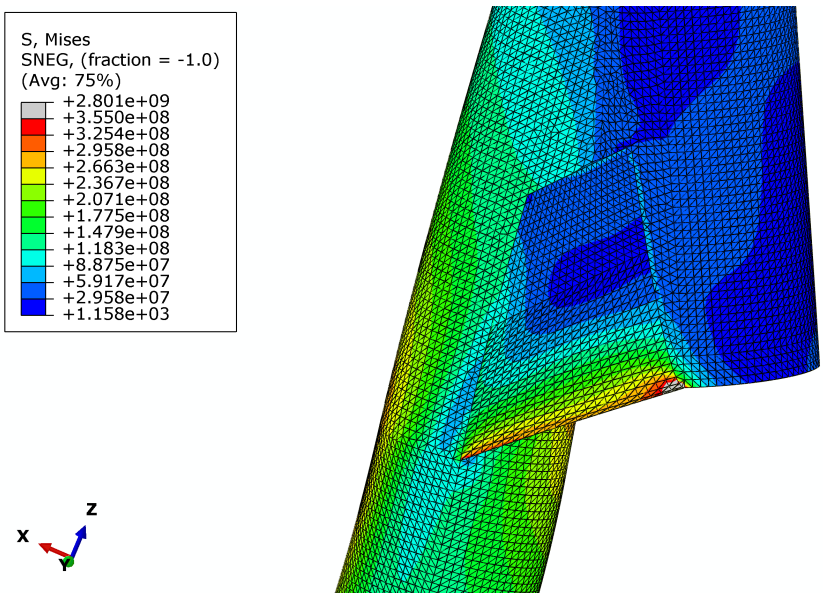


Figure 5.103: von Mises stress of the new iteration of the reinforcement on zone 2 [Pa].

As it is possible to observe the new iteration did not change significantly the stresses obtained, so it was considered that this area may be influenced by defects in the design or even by a singularity in the connection point. Thus, the result obtained is presented next, but with a more general view of the structure to verify the stresses along the entire structure.

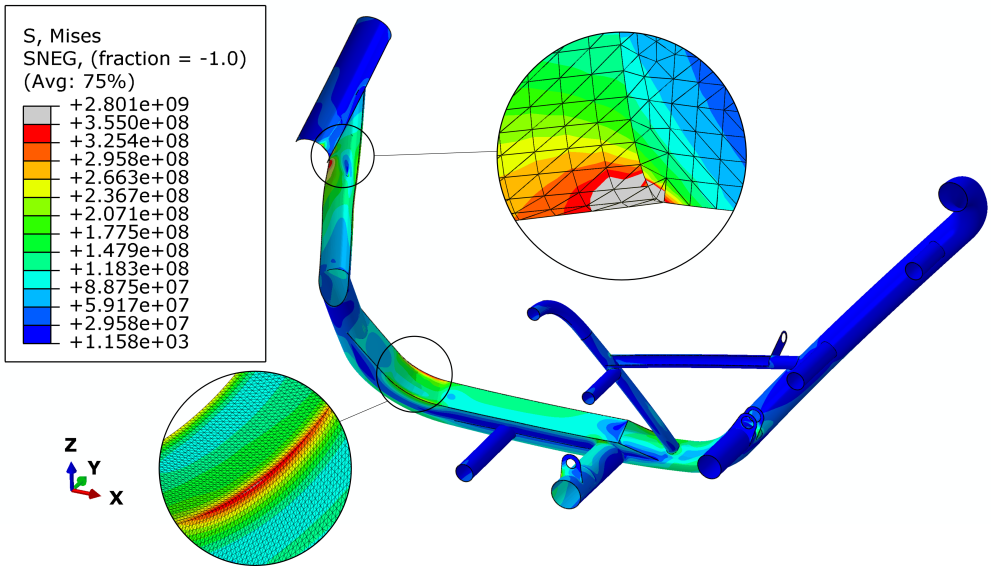


Figure 5.104: General result of von Mises stress of the new iteration of the reinforcement on zone 2 [Pa].

The analysis of structure seven is considered concluded since it would not bring significant changes to the improvement of the mesh, as it was possible to observe in the example of solution six, and it would be too big an investment of time to improve the mesh in order to present it all structured. However, it is important to note that the final mass of solution seven is of 11,568 kg and the final deformations are presented in the following figure.

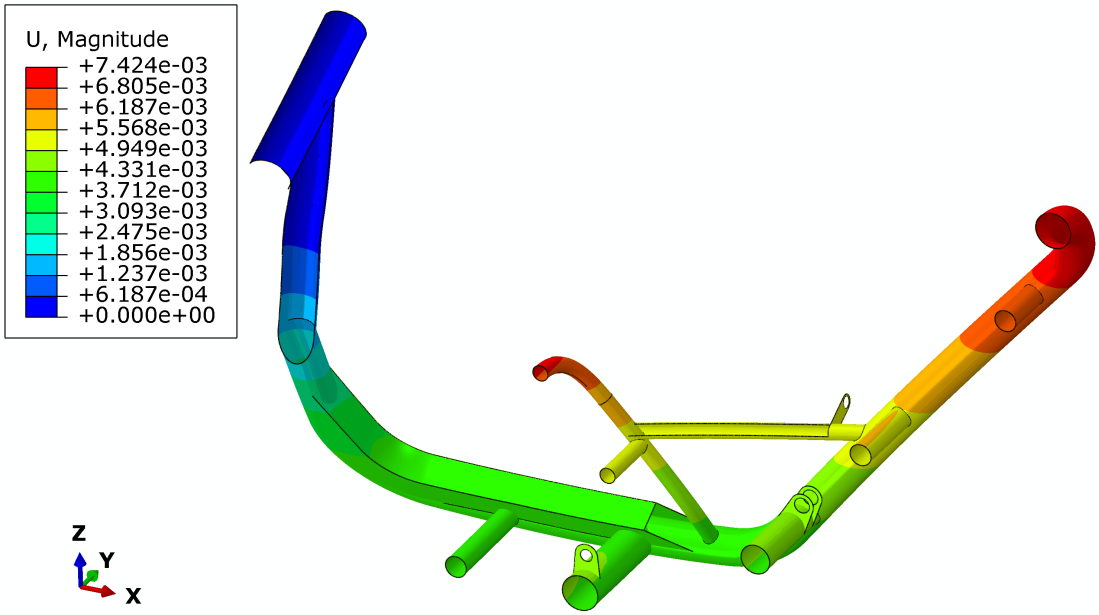


Figure 5.105: Displacement results, in meters, of the simulation of the solution seven.

5.4 Structural reinforcements in solution eight

This subchapter aims to develop the reinforcements for solution eight. After the complete analysis of solutions six and seven, the analysis of solution eight proceeds by making some changes, in SolidWorks software, in the structure itself, as occurred in the other solutions. These changes were:

- alteration of the diameter and thickness of the side pipes to 50 mm and a thickness of 3 mm, as the tube connecting to the steering column already had a diameter of 50 mm;
- change in the radius of curvature of the lower part of the chassis from 80 mm to 125 mm;
- alteration in the direction of the pipe connecting to the steering column;
- increased the height of the chassis in order to create more space between the exterior design of the scooter and the frame;
- modification of the thickness, to 3 mm, of the intermediate tube, where the eyebolt that serves as a connection to the oscillating arm belongs to;
- change of the diameter of the intermediate tube where the eyebolt connects with the shock absorber.

As mentioned in solution seven, solution eight presents the same issue of exceeding the limits of the scooter's exterior design by a few millimetres. Despite this situation, if this chassis is really the most suitable for the imposed conditions, it will be necessary to correct this detail in the body of the scooter.

With the changes applied and the conversion made to Abaqus, solution eight is presented below, with the various colours representing each constituent part.

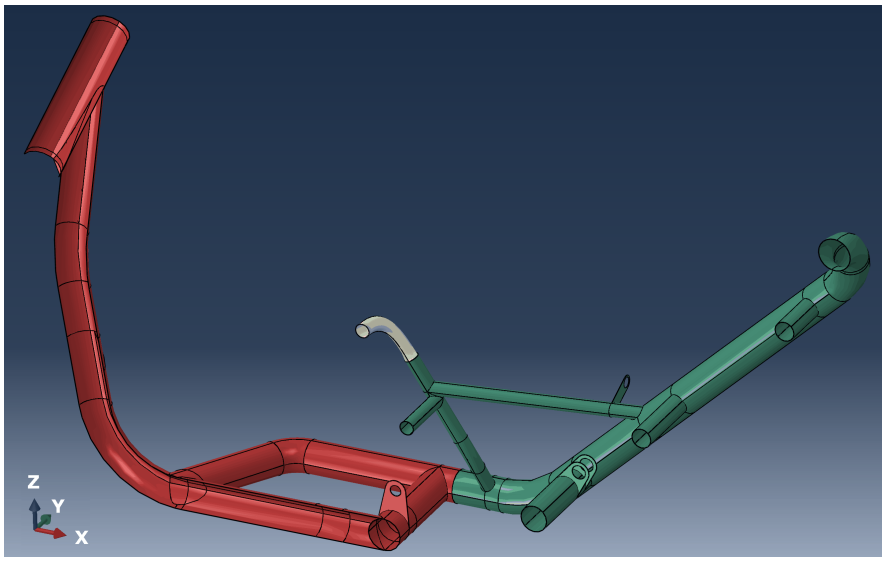


Figure 5.106: Frame part of solution eight with the new modifications.

As performed for the other solutions, the figure 5.107 shows the simulation results of solution eight without any type of reinforcement applied. This result could be compared with the result presented in figure 5.18, but at the stage of this simulation the material had not been changed from S235 to S355. In this way, the grey areas are under different conditions.

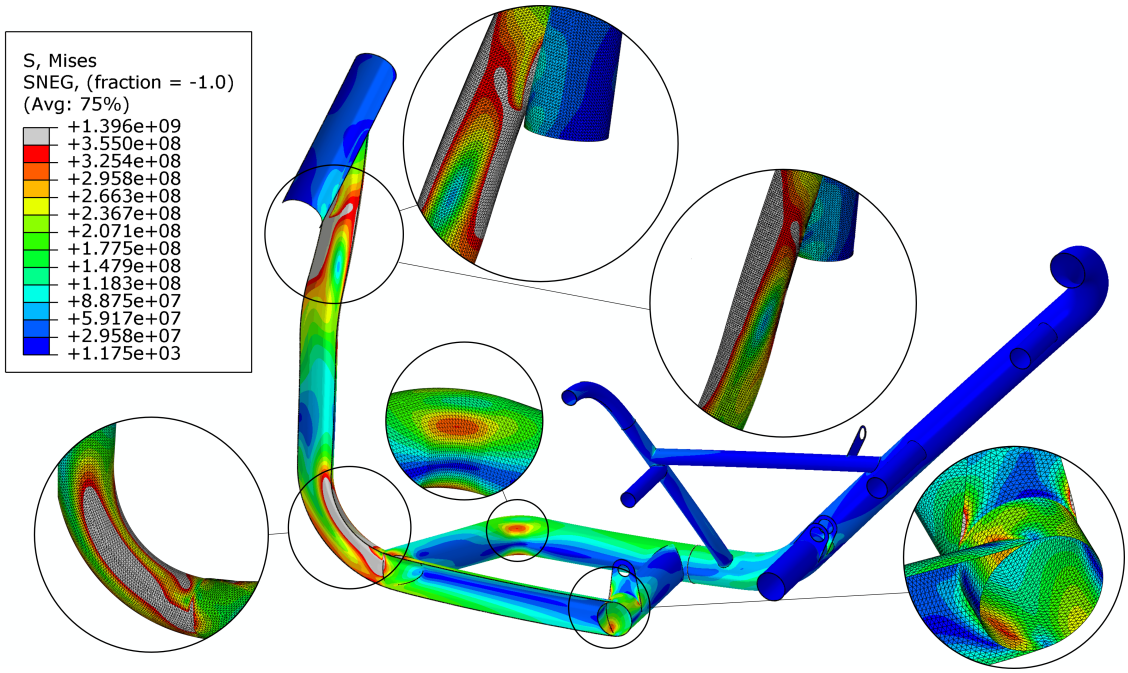
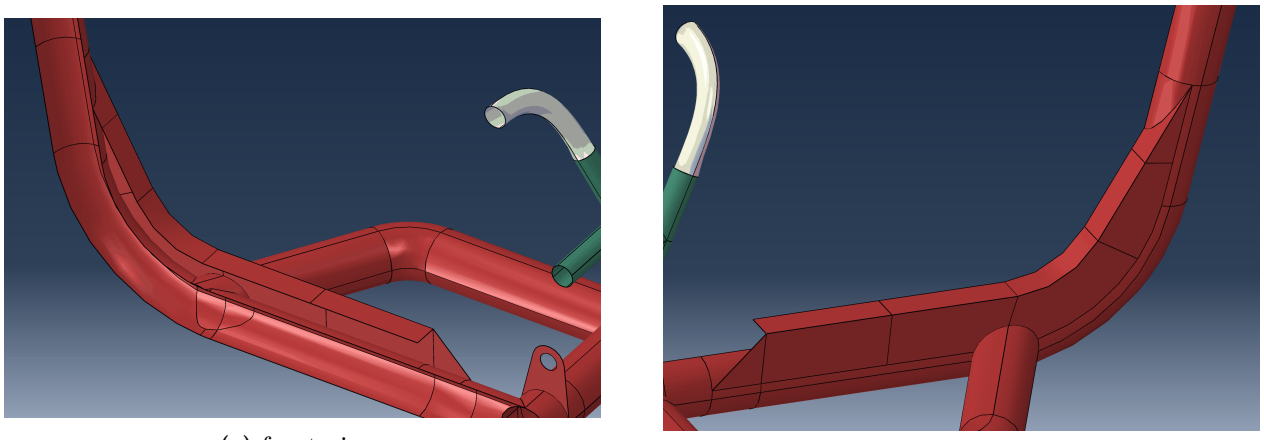


Figure 5.107: von Mises stress of the solution eight without any reinforcements [Pa].

Analysing the result, it can be seen that zones 1 and 3 present significant stresses, but zone 2 and the side tube curve present reasonable results since they do not have any type of reinforcement. Similar reinforcements to those used in solution 8 were then applied , namely:

- a U-shaped bent plate for zone 1, represented in figure 5.108;
- a reinforcement plate for zone 2;
- increase in thickness to 4 mm, maintaining the outer diameter of 50 mm, on the pipe connecting to the steering column;
- application of a triangular plate, of 3 mm, which connects to the pipe and the steering column, shown in figure 5.109.



(a) front view.

(b) back view.

Figure 5.108: Reinforcement of the zone 1 in the solution eight,

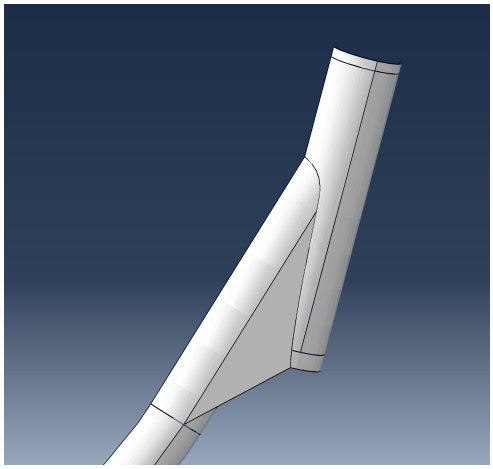


Figure 5.109: Reinforcement of the zone 3 in the solution eight.

Solution eight, with all reinforcements applied, was simulated and in figure 5.110 is the result obtained.

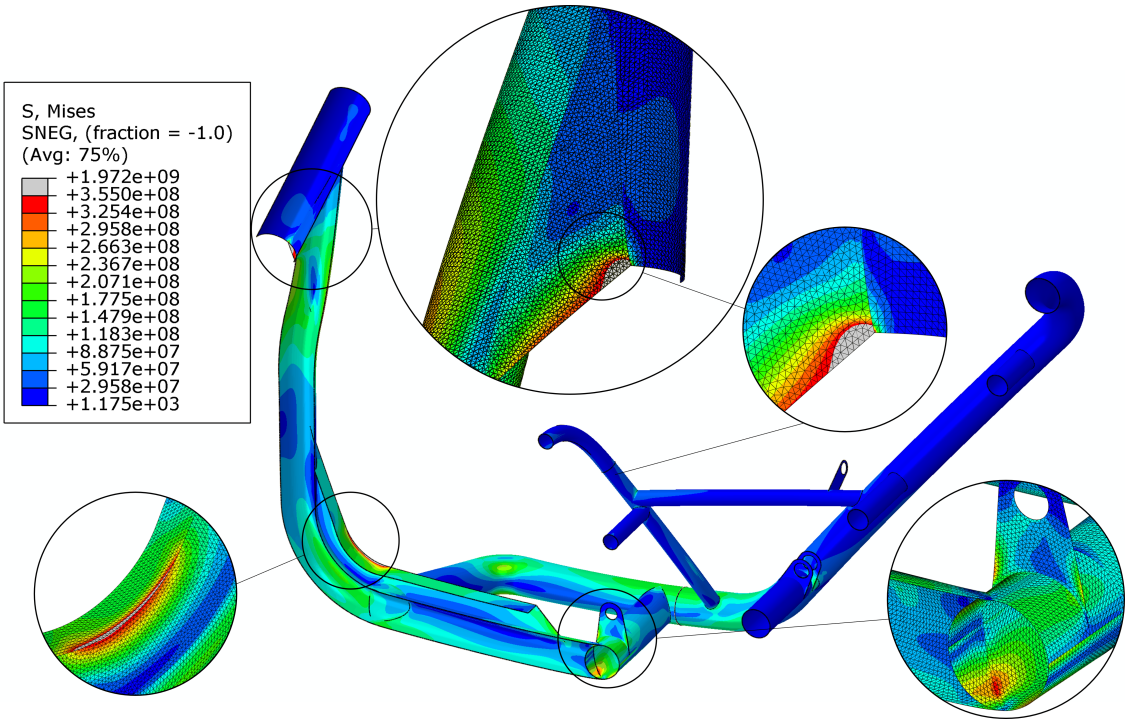


Figure 5.110: von Mises stress obtained with the simulation of the solution eight with all the reinforcement applied [Pa].

Analysing the final result of the simulation of solution eight, it is possible to comment that, similarly to solution seven, it presents stresses in zone 2, in the U-shaped bent plate, which may be due to the aggressive representation of a 90 degree angle between the faces, while in reality a concordance radius will appear. In addition, an area of high stresses is also visible in zone 3, most likely due to poorly designed details during the development of the reinforcement. The Abaqus software is too sensitive to this type of detail.

The reinforcement plate of zone 3 was not cut, as occurred in solution eight, because it was not observed a significant improvement with this change.

This concludes the analysis of solution eight, which has a final mass of 11.258 kg and the deformations obtained are presented in the following figure.

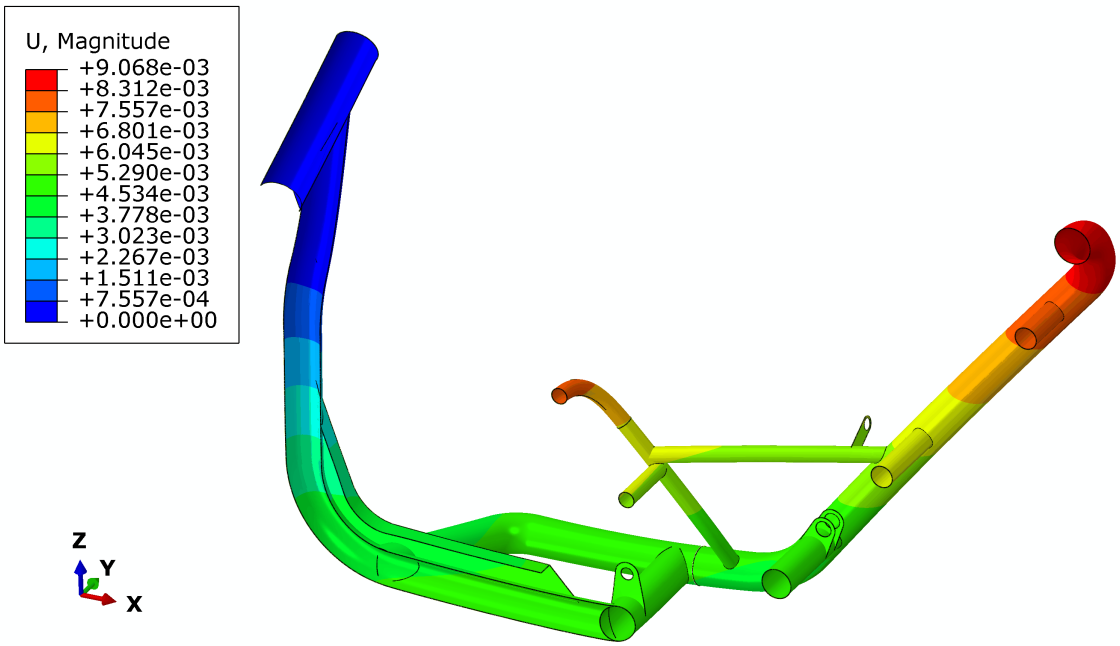


Figure 5.111: Displacement results, in meters, of the eighth solution simulation.

5.5 Weight Requirement

In order to simplify the process of transporting the scooters between the respective parks, the desired mass of the scooter is 80 kg, including the mass of the batteries, which in total is 25 kg.

In this subchapter one of the initial requirements that AJP set for the project is analysed. As explained, this project aims to enter the world of sharing, for that it was defined that the ideal mass would be 80 kg to facilitate the transportation. In the table 5.1 is an estimate of the masses of the main components of the scooter, except the chassis.

Table 5.1: Table of the masses of the principal components of the scooter

Component	**Mass / kg**
Motor	22
Front Wheel	4
Back Wheel	4,2
Front fork	7,5
Shock Absorber	4
Oscillating Arm	4 - 5
Batteries	25
Wires	2
Plastic Panels	3 - 4
Handlebar	4
Back structure	3 - 5

As mentioned, the table presents an estimate of the mass corresponding to each component. Thus, to add up all the mass referred to in the previous table, the upper values of each range were used to be as conservative as possible. Thus, a value of 86,7 kg is obtained only with the main components of the scooter, which is already higher than the stipulated value of 80 kg.

In the table 5.2 the values of each solution and the total mass of the scooter with each frame are presented.

Table 5.2: Table with each frame' mass and the total mass of the scooter for each solution

Frame Solution	**Frame' Mass / kg**	**Total Mass / kg**
Six	12,608	99,308
Seven	11,568	98,268
Eight	11,258	97,958

As can be concluded, if the estimates are correct, it will not be possible to develop a scooter under 80 kg without carrying out a major change in the main components.

Chapter 6

Conclusions and Future Works

6.1 Conclusions

The process of designing and developing a product is iterative and incremental. There is essential information that can lead to new design solutions and initial requirements that must always be considered. This thesis aimed at designing and analysing a chassis numerically for a motorcycle scooter. As there are always different shapes and new ideas for a product, a total of six solutions for the chassis were developed, of which only three are significantly valid to proceed with the analysis process.

Regarding the numerical analysis of the three selected solutions, it is important to mention the influence that some design details may have on the final result. This dissertation has examples in which varying how to create the same plate and the result obtained was different. This shows how necessary it is to always pay attention to details and know the Abaqus software well, which this author only acquired knowledge during the last year of her master's degree.

Considering the results obtained from the simulations of the selected chassis, several parameters must be considered when comparing which is the best solution. Parameters such as weight, production difficulty and interference with possible external components.

In terms of mass, the three solutions have a relatively similar mass. Solution six with 12,608 kg and solutions seven and eight with 11,568 kg and 11,258 kg, respectively. As can be seen, the gap between the three is relatively low, and comparing the seventh and eighth solutions we can even say that they are almost equal. This slight difference between solution six and solutions seven and eight is due to the fact that the first solution uses two connecting pipes for the steering column, while in the others, only one pipe is used. If it were necessary to choose only based on weight, solution eight would be the one selected.

Analysing in terms of difficulty of production, it is possible to conclude advantages and disadvantages of each solution. The sixth solution is made up of two connecting tubes that have a very specific direction and curves that are very complicated to manufacture. However, the seventh and eighth solutions have the U-shaped reinforcement which leads to a bending of a sheet and also the adjustment of the sheet to the curvature of the frame. The back of the three solutions is the same which leads to the same manufacturing effort.

Comparing in terms of interference with other scooter components, it can be seen that no chassis presents major problems, and all connections, such as the swingarm and shock absorber, are well designed and reinforced. However, as mentioned, as the single tube connection needs to have room to connect with the steering column, solutions seven and eight impose a minimal change in the exterior design of the scooter. Considering this aspect alone, solution six would be the most suitable for the project.

Another parameter to consider would be the displacement of each structure under the forces applied. It is important for structures to have their displacement to adapt to the conditions, but these cannot be large. With the photos presented in the previous chapter and focusing more on the lower part of the structure, which is the most important part of the chassis, we can see that solutions six, seven, and eight have an average displacement of 5.90, 5.105, and 5.111, respectively. That way, based only on this parameter, solution eighth would be the selected solution.

After comparing the solutions through various aspects, it is left to AJP Motos to select the best solution that fits the vision they present in the project, since all solutions are relatively good, each with advantages and disadvantages.

6.2 Future Work

After completing this dissertation, it would be necessary to carry out several questions to perform a more detailed analysis of the selected solutions.

From a dynamic structural evaluation in Abaqus software, taking into account all the dynamic loads of the system, to the realisation of an experimental evaluation of both static and dynamic design. The experimental analysis could be carried out during the production of the second dynamic prototype AJP has committed to producing for the MobiNext project.

Other aspects that could be considered would be the evolution of the boundary conditions to those that reflect more the reality and the analysis of ways to reduce the mass of the chassis and the reinforcements. Besides, a more detailed analysis of the areas that still present high stresses would be interesting, and also the experimentation with new types of reinforcements that could lead to better results than the ones presented.

Bibliography

1. Maioglou, D. *Motorcycle Design : defining a new typology and form for the electric motorcycle of the 21st century* Accessed: August 12, 2022. 2017. http://hdl.handle.net/11544/15253.
2. Chou, J. R. & Hsiao, S. W. Product design and prototype making for an electric scooter. *Materials Design 26,* 439–449. ISSN: 0261-3069 (5 Aug. 2005).
3. Institute, G. G. G. Promoting Green Mobility Through Electric Motorcycles in Cambodia (Jan. 2021).
4. *AJP Motos Official Website* Last accessed 18 April 2022. 2022. https://ajpmotos.com/.
5. W3Techs. *PR7 2021 – AJP Motorcycle Company* Last accessed 16 April 2022. 2017. https://ajpmotos.com/pt-pt/collections/adventure/products/pr7-2021.
6. *Consórcio | Mobinext* Last accessed 16 April 2022. 2022. https://mobinext.wixsite.com/projeto/cons%C3%B3rcio.
7. Mayne, K. Smarter Cycling Series: Data from bike-share, for bike-share. *European Cyclists' Federation.* Last accessed 29 May 2022. https://ecf.com/news-and-events/news/smarter-cycling-series-data-bike-share-bike-share (Aug. 2015).
8. Bruxo, M. Bolt launches electric scooter-sharing system in Faro - Portugal Resident. *Portugal Resident.* Last accessed 29 May 2022. https://www.portugalresident.com/bolt-launches-electric-scooter-sharing-system-in-faro/ (Jan. 2020).
9. Wu, C. F., Toman, D., Lin, T. & Tseng, S. Over 10K Shared e-Scooters: Why Is Japan Seeking Knowhow from Taiwan? *CommonWealth Magazine.* Last accessed 29 May 2022. https://english.cw.com.tw/article/article.action?id=2617 (2019).
10. GIBBS, N. BMW expands car-sharing program to China | Automotive News Europe. *Automotive News Europe.* Last accessed 29 May 2022. https://europe.autonews.com/article/20171124/ANE/171129861/bmw-expands-car-sharing-program-to-china (Nov. 2017).
11. Zheng, Z. *et al.* Extreme unbalanced mobility network in bike sharing system. *Physica A: Statistical Mechanics and its Applications 563.* ISSN: 0378-4371 (Oct. 2020).
12. Li, A. *et al.* Comprehensive comparison of e-scooter sharing mobility: Evidence from 30 European cities. *Transportation Research Part D: Transport and Environment 105,* 103229. ISSN: 1361-9209 (Mar. 2022).

13. Ushijima, H., Helinyi, P., Aoki, S., Nishiyama, Y. & Sezaki, K. An Unsupervised Learning-based Approach for User Mobility Analysis of E-Scooter Sharing Systems. *IEEE Conference on Intelligent Transportation Systems, Proceedings, ITSC,* 1425–1430 (Sept. 2021).
14. Ly, B. Mobility sharing economy in Shanghai. *Cogent Business and Management 7.* ISSN: 23311975 (1 June 2020).
15. *Home | Mobinext* Accessed: August 12, 2022. 2021. `https://mobinext.wixsite.com/projeto`.
16. Global, H. *Lexmoto E-Lex 1500* Last accessed 29 May 2022. 2018. `https://global.honda/newsroom/news/2018/2181129eng-pcx-electric.html`.
17. Motorcycles, L. & Scooters. *Lexmoto LX08* Last accessed 29 May 2022. 2020. `https://www.lexmoto.co.uk/models/LX08MAX-E5`.
18. Motorcycles, L. & Scooters. *Lexmoto LX06* Last accessed 29 May 2022. 2020. `https://www.lexmoto.co.uk/models/LX06MAX-E5`.
19. Motorcycles, L. & Scooters. *Honda to Begin Lease Sales of Electric Scooter "PCX ELECTRIC"* Last accessed 29 May 2022. 2020. `https://www.lexmoto.co.uk/models/YD3000D-03-E5`.
20. Global, H. *Catalogue EK3 L3e 2020* Aug. 2020.
21. Innovation, S. *Catálogo CPx* 2020.
22. Interconnect, T. P. M. *Catalogue Muvi* Nov. 2017.
23. Yongfan, L., Shuai, Z. & Jing, W. Research on the Optimization Design of Motorcycle Engine Based on DOE Methodology. *Procedia Engineering 174,* 740–747. ISSN: 18777058 (2017).
24. Delgado Ojeda, R. J. *Motorcycle frame design and optimization* Accessed: August 12, 2022. 2016. `http://hdl.handle.net/2117/96944`.
25. Livesey, A. *Motorcycle Engineering* 1st ed. ISBN: 9780367816858. `https://www.taylorfrancis.com/books/mono/10.1201/9780367816858/motorcycle-engineering-andrew-livesey` (Routledge, Apr. 2021).
26. Cossalter, V., Lot, R. & Massaro, M. Motorcycle Dynamics. *Modelling, Simulation and Control of Two-Wheeled Vehicles,* 1–42. `https://onlinelibrary.wiley.com/doi/abs/10.1002/9781118536391.ch1` (Mar. 2014).
27. Tony, F. *Motorcycle Handling and Chassis Design: The Art and Science* (Tony Foale Designs, 2003).
28. Seeley, A. *The Scooter Book* ISBN: 1844250954 (Haynes Publishing, Sept. 2004).
29. Hsu, C.-H., Liu, B.-S., Jhuang, S.-L. & Li, Y.-C. The study of ergonomic evaluation and critical design factors for electric scooter, 1–4 (2016).

30. Rogacki, I., Rusiński, E. & Sawicki, M. Structural analysis of composite scooter monocoque. *Lecture Notes in Mechanical Engineering - Proceedings of the 14th International Scientific Conference: Computer Aided Engineering,* 599–610. ISSN: 21954364 (2019).

31. Gilera, P. V. *Frame for VESPA 50 - Online Genuine Spare Parts Catalog* Accessed: August 12, 2022. https://www.parts-piaggio.com/vespa-scooters/50-VESPA-SCOOTER/VESPA/Other-year/50-4T/Chassis/Frame/1296/19/11142/2842.

32. Noce, D. The Engineering Process for the Design of a Motorcycle Chassis and Suspension. *PhD Dissertations and Master's Theses.* https://commons.erau.edu/edt/112 (May 2012).

33. VerticalScope. *Inc. Midual motorcycles type 1* Accessed: August 12, 2022. https://www.motorcycle.com/.

34. *HELMET SIZE CHART - Speed and Strength* 2020. https://www.ssgear.com/helmet-size-chart/.

35. *Liberty - Piaggio - OLX Portugal* Accessed: September 25, 2022. 2021. https://www.olx.pt/d/carros-motos-e-barcos/motociclos-scooters/piaggio/q-liberty/.

36. EduPack, A. G. *Structural Steel, S235J* Last accessed 29 May 2022. 2021.

Chapter 7

Attachments

7.1 Technical specifications of PR7 [5]

	PR7
ENGINE	Single cylinder, 4 stroke, 4 valves - DOHC, liquid cooled
BORE X STROKE	100 x 76.4 mm
DISPLACEMENT	600 cc
FEEDING	Athena fuel injection system Ø45 mm
STARTER	Electric
CLUTCH	Oil bath, multi-disc
TRANSMISSION	6 speed
FRAME	Composite - aluminum / steel
SEAT HEIGHT	920 mm
WHEELBASE	1540 mm
GROUND CLEARANCE	310 mm
FUEL TANK	17 L
FRONT TYRE	90/90 - 21''
REAR TYRE	140/80 - 18''
FRONT SUSPENSION	ZF Sachs Ø48 mm close-circuit – 300 mm stroke – fully adjustable
REAR SUSPENSION	ZF Sachs prog. system with reser. - 280 mm stroke - fully adjustable
FRONT BRAKES	2 piston BREMBO caliper - Disc Ø300 mm
REAR BRAKES	Single piston BREMBO caliper - Disc Ø240 mm

7.2 Technical specifications of PCx electric of Honda [16]

Specifications

Name		PCX ELECTRIC
Type		Honda ZAD-EF01
Length x Width x Height (mm)		1,960×740×1,095
Wheelbase (mm)		1,380
Minimum ground clearance (mm)★		132
Seat height (mm)★		760
Curb weight (kg)		144
Occupants (persons)		2
Travel distance on single charge*5(km)	As reported to Ministry of Land、Infrastructure and Transport	41（60km/h steady state test）< 1 passenger >
Minimum turning circle (m)		2.1
Power unit / type		EF01M / AC motor
Output (kw)		0.98
Maximum output (kW[PS]/rpm)		4.2[5.7]/5,500
Maximum torque (N·m[kgf·m]/rpm)		18 [1.8]/500
Battery type		Lithium ion
Main battery voltage / capacity		50.4V/20.8Ah×2
Battery charger		AC100V（single phase）
Tires	Front	100/80-14M/C 48P
	Rear	120/70-14M/C 55P
Brakes	Front	Hydraulic disc
	Reat	Mechanical leading / trailing
Suspension	Front	Telescopic
	Rear	Unit-swing

7.3 Technical specifications of LX08 of Lexmoto [17]



Specifications

OVERVIEW

Model Name	Lexmoto LX08
Model Code	LX08MAX-E5

PERFORMANCE

Max Power	(5.4 hp) 4.0kW
Max Speed	47 MPH (75 KMH)

ENGINE

Engine Type	Electric Motor
Gear Type	Twist and Go

WHEELS

Front Brake	Hydraulic Disc
Rear Brake	Hydraulic Disc
Front Tyre	120/70-12
Rear Tyre	120/70-12
Tyre Model	Tubeless
Front Suspension	Telescopic Forks
Rear Suspension	Twin Shock Absorber

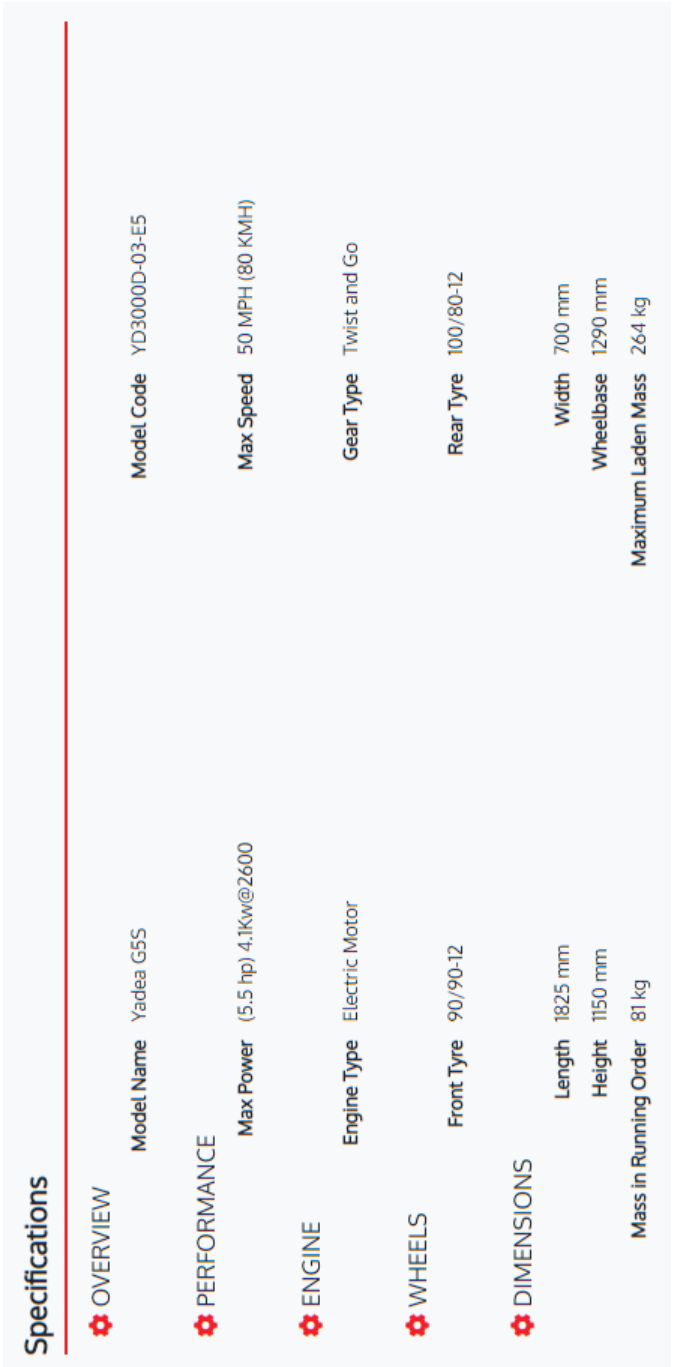
DIMENSIONS

Length	1895 mm
Width	700 mm
Height	1180 mm
Wheelbase	1345 mm
Mass in Running Order	84 kg
Maximum Laden Mass	255 kg

7.4 Technical specifications of LX06 of Lexmoto [18]



7.5 Technical specifications of Yadea G5S of Lexmoto [19]



Specifications

OVERVIEW

Model Name	Yadea G5S	Model Code	YD3000D-03-E5

PERFORMANCE

Max Power	(5.5 hp) 4.1Kw@2600	Max Speed	50 MPH (80 KMH)

ENGINE

Engine Type	Electric Motor	Gear Type	Twist and Go

WHEELS

Front Tyre	90/90-12	Rear Tyre	100/80-12

DIMENSIONS

Length	1825 mm	Width	700 mm
Height	1150 mm	Wheelbase	1290 mm
Mass in Running Order	81 kg	Maximum Laden Mass	264 kg

7.6 Technical specifications and battery details of EK3 of Horwin [20]

DIMENSIONS





Length: 1900mm
Width: 690mm
Height: 1130mm
Seat height: 780mm

Motor Type	Central Motor
Controller	FOC
Battery	72V, 40AH (optionally 80 AH with second battery)

MEASUREMENTS

Front hub	MT2.5×14	Net weight without battery	95 KG
Rear hub	MT3.0×13	Technically permissible	
Front tire size	100/80-14	maximum laden mass	284 KG
Rear tire size	110/70-13	Wheel hub	Aluminium alloy
Wheel base	1320 mm		
Minimum ground clearance	125 mm		

SPECIFICATION

Rated Power	3.5 KW	Range	100 KM (AT 45 KM/H WITH
Max Power	6.2 KW		75 KG DRIVER)
Rated RPM	6365 R/min	Charging Times	⩾1000 times
Rear wheel Max. torque	195 Nm	Tire	Front 14''/ Rear 13''
Top Speed	95 km/h	Brake System	CBS oil brake
Reduction Ratio	1:7.8	Charging	10A
		Charging Time	4h (0-100%)

FEATURES

Lights	LED (front, rear, flashing)
Swipe screen to start	YES

BATTERY

BATTERY WITH ITS OWN MANAGEMENT

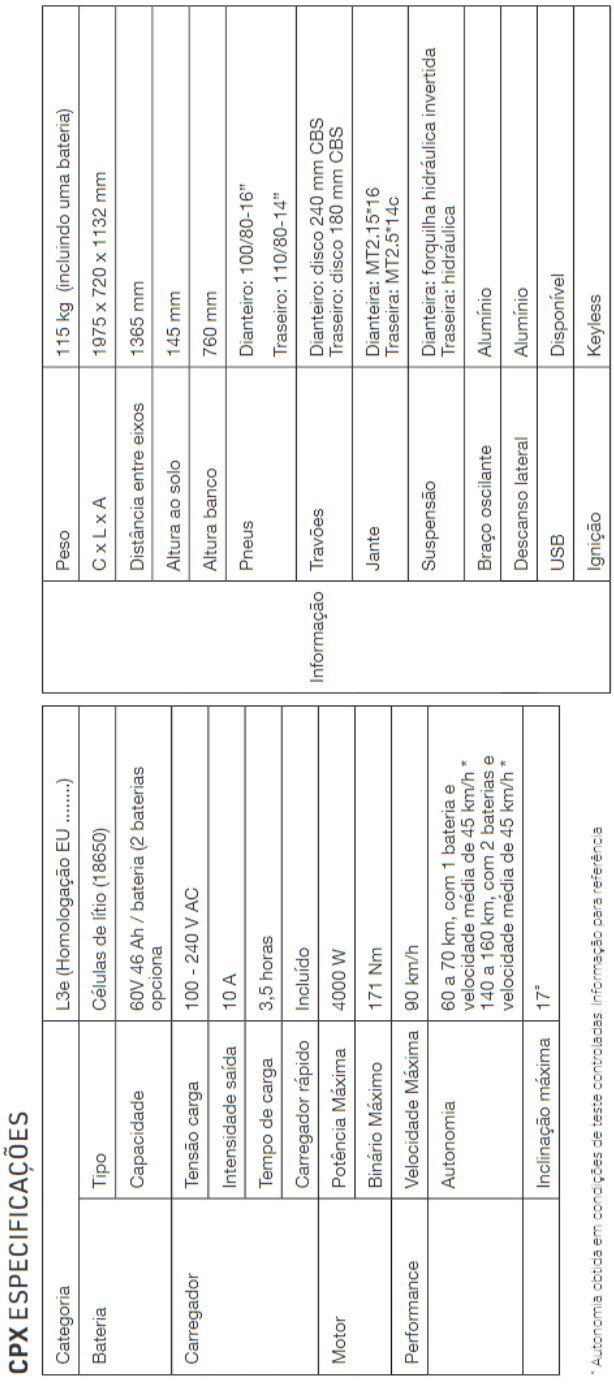
The EK3 scooter can be equipped with two lithium-ion batteries that are easily removable.
The battery is supplied with efficient 18650 lithium-ion battery cells. The SOC monitoring system and the modern battery management system can prevent malfunctions.

Among other things, they provide protection against over-charging, discharging, over-voltage, short circuit and monitor the temperature of the batteries. One battery cell has a capacity of 10.44Wh, the whole battery has 2.88kWh. The battery life is over 1000 cycles. The standard charging current is 10A. The charging time of one battery is 4 hours.

An intelligent charger is used for this.

40 AH	100 KM	4 H
BATTERY & TWO BATTERIES	MAX. RANGE (45 KM/H)	CHARGING TIME (ONE BATTERY)

7.7 Technical specifications of CPx of Super Soco [21]



CPX ESPECIFICAÇÕES

Categoria		L3e (Homologação EU .....)
Bateria	Tipo	Células de lítio (18650)
	Capacidade	60V 46 Ah / bateria (2 baterias opciona
Carregador	Tensão carga	100 - 240 V AC
	Intensidade saída	10 A
	Tempo de carga	3,5 horas
	Carregador rápido	Incluído
Motor	Potência Máxima	4000 W
	Binário Máximo	171 Nm
Performance	Velocidade Máxima	90 km/h
	Autonomia	60 a 70 km, com 1 bateria e velocidade média de 45 km/h * 140 a 160 km, com 2 baterias e velocidade média de 45 km/h *
	Inclinação máxima	17°

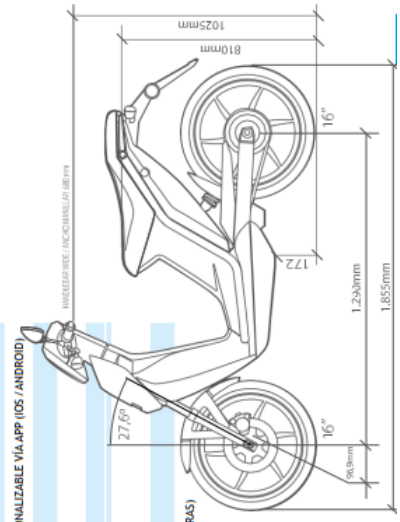
Informação	Peso	115 kg (incluindo uma bateria)
	C x L x A	1975 x 720 x 1132 mm
	Distância entre eixos	1365 mm
	Altura ao solo	145 mm
	Altura banco	760 mm
	Pneus	Dianteiro: 100/80-16" Traseiro: 110/80-14"
	Travões	Dianteiro: disco 240 mm CBS Traseiro: disco 180 mm CBS
	Jante	Dianteira: MT2.15*16 Traseira: MT2.5*14c
	Suspensão	Dianteira: forquilha hidráulica invertida Traseira: hidráulica
	Braço oscilante	Alumínio
	Descanso lateral	Alumínio
	USB	Disponível
	Ignição	Keyless

* Autonomia obtida em condições de teste controladas. Informação para referência

7.8 Technical specifications of Muvi of Torrot [22]

TECHNICAL SPECIFICATIONS
ESPECIFICACIONES TÉCNICAS

FRAME /CHASIS	**TUBULAR STEEL FRAME** /TUBULAR DE ACERO
FRONT SUSPENSION /SUSP. DELANTERA	**HYDRAULIC TELESCOPIC FORK** /HORQUILLA TELESCÓPICA HIDRÁULICA
REAR SUSPENSION /SUSP. TRASERA	**SIDE MONOSHOCK WITH PRELOAD ADJUSTMENT** /MONOAMORTIGUADOR LATERAL CON AJUSTE EN PRECARGA
BRAKES /FRENOS	**HYDRAULIC COMBINED SYSTEM (CBS) FRONT-REAR** /SISTEMA HIDRAULICO COMBINADO DELANTE-DETRÁS: 220MM-200MM
TRANSMISSION /TRANSMISIÓN	**TOOTHED BELT HTD 1:5** /CORREA DENTADA HTD 1:5
ENGINE /MOTOR	**TORROT BRUSHLESS 48V**
POWER /POTENCIA	2,65 KW / 35 NM (L1E-B) 3 kW / 35 NM (L3E-A1)
MAX SPEED /VELOCIDAD MÁX.	45 KM/H (L1E-B) 60 KM/H (L3E-A1)
BATTERIES /BATERÍAS	**REMOVABLE 2X48V 31,9 Ah LI-ION RANGE UP TO:** /EXTRAÍBLES 2X48V 31,9 Ah LI-ION AUTONOMÍA: **103 KM***
DIAGNOSTICS - COMMUNICATIONS / DIAGNOSIS - COMUNICACIONES	ECU (ELECTRONIC CONTROL UNIT) CAN-BUS / BLUETOOTH
DASHBOARD	**INTELIGENT, LCD 4" 320X240 CUSTOMIZABLE VIA APP** /LCD INTELIGENTE 4" 320X240 PERSONALIZABLE VÍA APP (IOS / ANDROID)
RIMS /LLANTAS	**ALUMINIUM 16" X 2.15** /ALUMINIO 16" X 2.15
TIRES /NEUMÁTICOS	90/80-R16
WEIGHT /MASA EN ORDEN DE MARCHA	**93 KG BATTERIES INCLUDED** /93KG BATERÍAS INCLUIDAS
MAX WEIGHT AUTHORIZED / PESO MÁXIMO AUTORIZADO	235 KG
CHARGER /CARGADOR	**54.6V 5A DOUBLE BATTERY CHARGER (5 HOURS)** /54.6V 5A CARGADOR DOBLE (5 HORAS)
OPTIONAL /OPCIONAL	**54.6V 10A DOUBLE BATTERY CHARGER (2,5 HOURS)** /54.6V 10A CARGADOR DOBLE (2,5 HORAS)



***L3e-A1 approved up to 81 km in accordance with WMTC-2** /L3e-A1 homologados 81 km según WMTC-2
L1e-B approved up to 83 km in accordance with CEPE R47 /L1e-B homologados 83 km según CEPE R47
L1e-B 25 Km/h approved up to 103 km in accordance with CEPE R47 /L1e-B 25 Km/h homologados 103 km según CEPE R47

7.9 Properties of S235 Steel [36]

Ansys GRANTA EDUPACK

Structural steel, S235J

General information

Ansys Name	Structural steel, S235J

Designation

Structural steel, S235J, wrought

Condition	Hot rolled
EN name	S235JR, S235J0, S235J2
EN number	1.0038, 1.0114, 1.0117

Typical uses

Welded non-critical structures, general mechanical engineering, automotive components, construction, automotive, tools, axles, gears, springs, ships, rolling stocks, petroleum storage tanks, containers, open die forgings, frames for presses, heating plates for presses

Included in Materials Data for Simulation	✓

Composition overview

Compositional summary

Fe98-100 (impurities: Mn<1.4, Cu<0.55, C<0.2, P<0.035, S<0.035, N<0.012)

Material family	Metal (ferrous)
Base material	Fe (Iron)

Composition detail (metals, ceramics and glasses)

C (carbon)	0	-	0.2	%
Cu (copper)	0	-	0.55	%
Fe (iron)	* 97.8	-	100	%
Mn (manganese)	0	-	1.4	%
N (nitrogen)	0	-	0.012	%
P (phosphorus)	0	-	0.035	%
S (sulfur)	0	-	0.035	%

Price

Price	* 0.581	-	0.645	GBP/kg
Price per unit volume	* 4.54e3	-	5.09e3	GBP/m^3

Physical properties

Density	7.81e3	-	7.89e3	kg/m^3

Mechanical properties

Young's modulus	205	-	215	GPa
Specific stiffness	* 26.1	-	27.4	MN.m/kg
Yield strength (elastic limit)	235	-	274	MPa

Notes
These values are applicable for minimum thickness for this grade.

Tensile strength	360	-	510	MPa

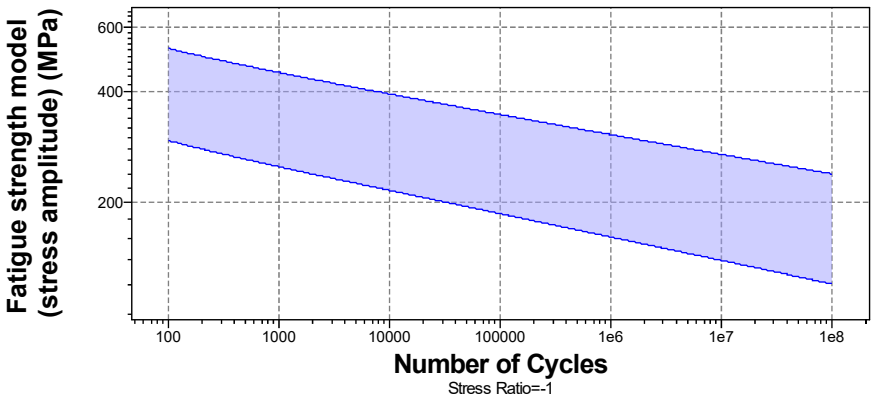
Notes
These values are applicable for minimum thickness for this grade.

Specific strength	* 29.9	-	34.9	kN.m/kg

Values marked * are estimates.
Ansys Granta provides no warranty for this data.

Elongation	17	-	26	% strain
Tangent modulus	1.18e3			MPa
Compressive modulus	* 205	-	215	GPa
Compressive strength	* 235	-	274	MPa
Flexural modulus	* 205	-	215	GPa
Flexural strength (modulus of rupture)	* 225	-	319	MPa
Shear modulus	* 78.9	-	82.7	GPa
Shear strength	* 136	-	158	MPa
Bulk modulus	* 171	-	179	GPa
Poisson's ratio	0.3			
Shape factor	63			
Hardness - Vickers	* 107	-	152	HV
Hardness - Brinell	100	-	154	HB
Elastic stored energy (springs)	* 132	-	178	kJ/m^3
Fatigue strength at 10^7 cycles	* 180	-	210	MPa
Fatigue strength model (stress amplitude)	* 140	-	271	MPa

Parameters: Stress Ratio = -1, Number of Cycles = 1e7cycles



Impact & fracture properties

Fracture toughness	* 45.5	-	55	MPa.m^0.5
Toughness (G)	* 9.93	-	14.3	kJ/m^2

Thermal properties

Melting point	1.48e3	-	1.53e3	°C
Maximum service temperature	* 473	-	519	°C
Minimum service temperature	* -56.8	-	-46.8	°C
Thermal conductivity	40	-	57.4	W/m.°C
Specific heat capacity	460	-	480	J/kg.°C
Thermal expansion coefficient	11.5	-	12.5	µstrain/°C

Values marked * are estimates.
Ansys Granta provides no warranty for this data.

7.10 Properties of S355 Steel [36]

GRANTA EduPack

Structural steel, S355J

General information

Designation

Structural steel, S355J, wrought

Condition	Hot rolled
US name	A572 Grade 50
EN name	S355JR, S355J0, S355J2
EN number	1.0045, 1.0553, 1.0577

Typical uses

Welded, bolted and riverted structures, construction, power plants, yellow goods, oil rigs, offshore structures, tanks, rail, energy, mining, wind tower components.

Included in Materials Data for Simulation	✓

Composition overview

Compositional summary

Fe97-100 (impurities: Mn<1.6, Cu<0.55, C<0.24, P<0.035, S<0.035, N<0.012)

Material family	Metal (ferrous)
Base material	Fe (Iron)

Composition detail (metals, ceramics and glasses)

Al (aluminum)	0	-	0,02	%
C (carbon)	0	-	0,24	%
Cu (copper)	0	-	0,55	%
Fe (iron)	* 97	-	100	%
Mn (manganese)	0	-	1,6	%
N (nitrogen)	0	-	0,012	%
P (phosphorus)	0	-	0,035	%
S (sulfur)	0	-	0,035	%
Si (silicon)	0	-	0,55	%

Price

Price	* 0,722	-	0,8	EUR/kg
Price per unit volume	* 5,66e3	-	6,27e3	EUR/m^3

Physical properties

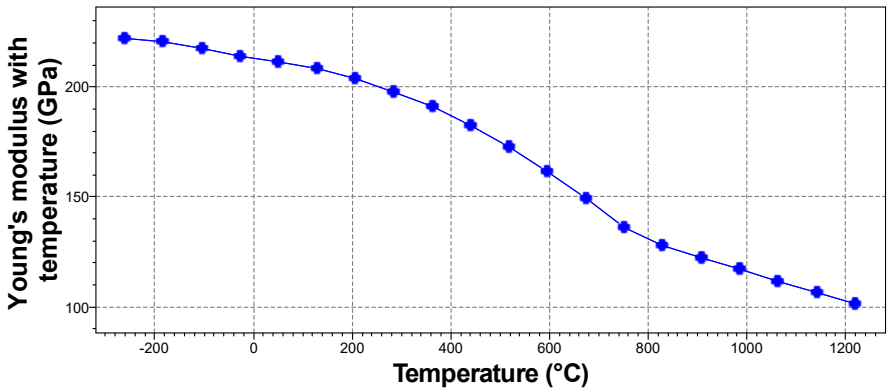
Density	7,83e3	-	7,84e3	kg/m^3

Mechanical properties

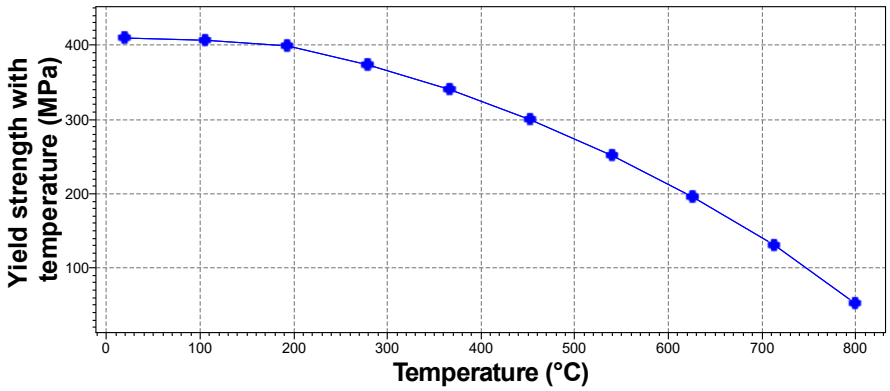
Young's modulus	205	-	215	GPa
Young's modulus with temperature	212	-	212	GPa

Parameters: Temperature = 23°C

Values marked * are estimates.
ANSYS Granta provides no warranty for this data.



Specific stiffness	* 26,2	-	27,4	MN.m/kg
Yield strength (elastic limit)	355	-	414	MPa
Notes: These values are applicable for minimum thickness for this grade.				
Yield strength with temperature	409	-	409	MPa
Parameters: Temperature = 23°C				



Tensile strength	470	-	680	MPa
Notes: These values are applicable for minimum thickness for this grade.				
Specific strength	* 45,3	-	52,8	kN.m/kg
Elongation	14	-	22	% strain
Tangent modulus	1,48e3			MPa
Compressive modulus	* 205	-	215	GPa
Compressive strength	* 355	-	414	MPa
Flexural modulus	* 205	-	215	GPa
Flexural strength (modulus of rupture)	* 315	-	455	MPa
Shear modulus	* 78,9	-	82,7	GPa

Values marked * are estimates.
ANSYS Granta provides no warranty for this data.